Prognostics of Proton-exchange Membrane Fuel Cell

Remaining useful life prediction of proton-exchange membrane fuel cell tested under static and quasi-dynamic operating conditions

Matthew Georgio Dekkers

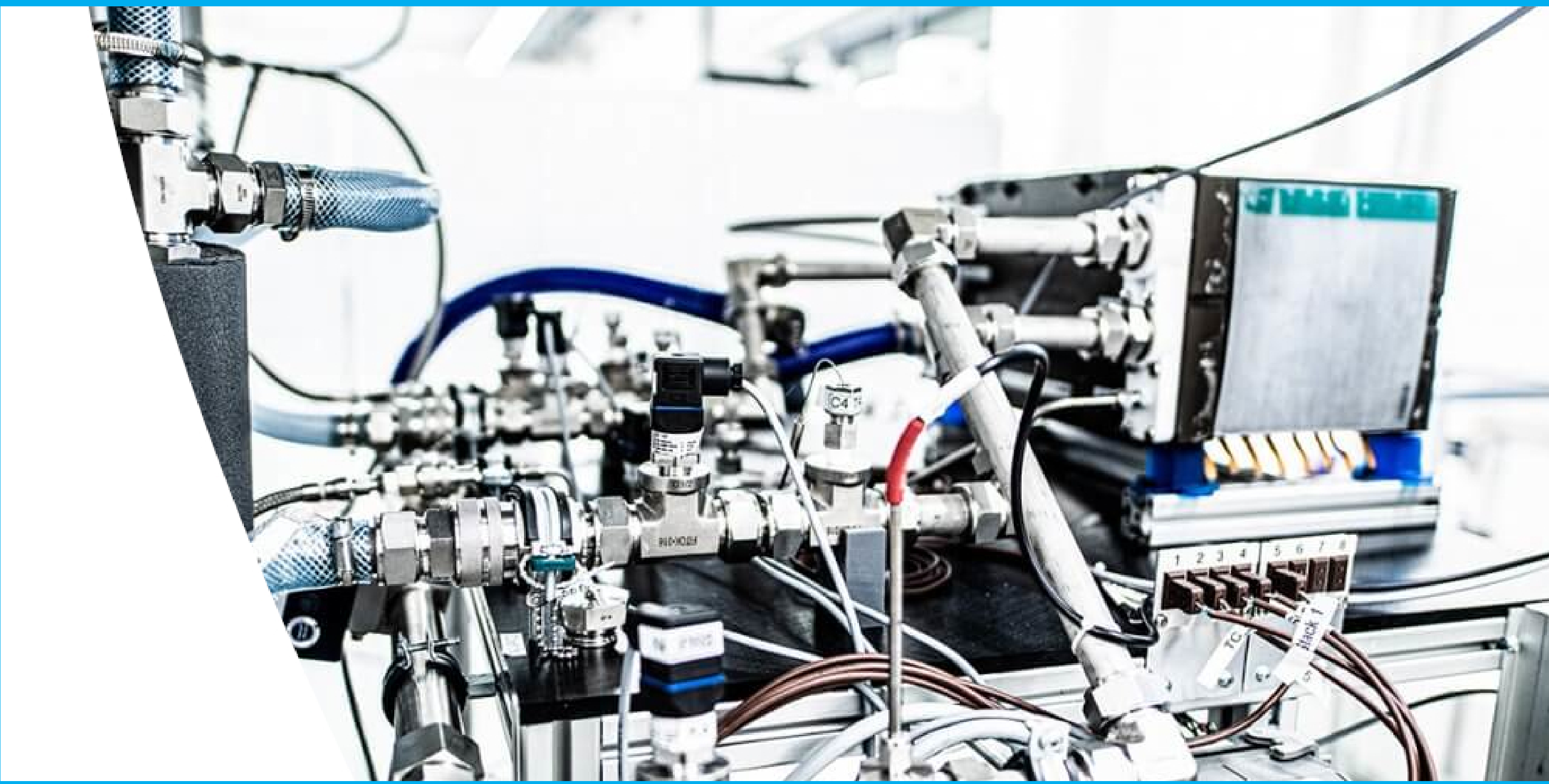

TUDelft

Prognostics of Proton-exchange Membrane Fuel Cell

Remaining useful life prediction of proton-exchange membrane fuel cell tested under static and quasi-dynamic operating conditions

by

Matthew Georgio Dekkers

to obtain the degree of Master of Science

at Delft University of Technology,

to be defended publicly on the 19th of August.

Student number:	4533860
Project duration:	01-11-2023 – 19-08-2024
Thesis supervisors:	Dr. Márcia L. Baptista
	Dr. Holger Kuhn
Chair:	Dr. Arvind G. Rao
External examiner:	Dr. Alexei Sharpans'kykh
Faculty:	Aerospace Engineering

TU Delft

Acknowledgements

I would like to thank Hendrie Derking from Cryoworld for connecting me with ZAL Center of Applied Aeronautical Research GmbH. Additionally, I am grateful to my daily supervisor, Márcia Baptista from Delft University of Technology, for her guidance and encouragement. I am also deeply thankful to Holger Kuhn, Sebastian Altmann, Leonid Lichtenstein, and Roland Gerhards for the opportunity and support to conduct this research at ZAL. Furthermore, I would like to thank my colleagues, Tuan Nguyen, Louis-Marie Audoin, Sai Vijay Siva Prasad, Fynn Schroeder, Tobias Riedel, and Soeren Huss, for their valuable discussions and assistance with various experiments related to my research.

I would also like to express my gratitude to my parents for their support during my educational journey. They have shown me how to push myself to work hard and the importance of perseverance. Their encouragement has given me the opportunity to become the first person in our family to attend university. Lastly, I want to thank my girlfriend, Lyana Usa, for her unconditional love and support. I will never forget her ability to lift my moods and stand by me during my toughest moments.

M.G. Dekkers
Delft, July 2024

Contents

List of Figures

List of Tables

Nomenclature

Abbreviations and Acronyms

ANOVA	Analysis of Variance
CNN	Convolutional Neural Network
DI	Double-input
DWT	Discrete Wavelet Transform
EESN	Ensemble Echo State Network
EIS	Electrochemical Impedance Spectroscopy
ESN	Echo State Network
ESP	Echo State Property
GA	Genetic Algorithm
GRU	Gated Recurrent Unit
KF	Kalman Filter
LSTM	Long Short-term Memory
MEA	Membrane Electrode Assembly
MISMO	Multiple-input Several Multiple-outputs
ML	Machine Learning
OCV	Open Circuit Voltage
PEMFC	Proton Exchange Membrane Fuel Cell
PF	Particle Filter
PFSA	Perfluorosulfonic Acid
PH	Prediction Horizon
PROPICE	Prognostic and Health Management of PEM Fuel Cell Systems
Pt	Platinum
QD	Quasi Dynamic
RNN	Recurrent Neural Network
RPLR	Relative Power-loss Rate
RUL	Remaining Useful Life
SI	Single-input
SS	Steady State

Roman Symbols

α	Leaking rate
β	Regularisation parameter
ΔG	Variation of free Gibbs energy [J]

ρ	Spectral radius
f_t	Forget gate
i_t	Input gate
K	Dimension input signal
L	Dimension output signal
N_n	Number of neurons
o_t	Output gate
R_{ct}	Charge transfer coefficient
W	Internal weight matrix
W_{fb}	Feedback weight matrix
W_{in}	Input weight matrix
W_{out}	Output matrix
hr	hour
s	seconds

Introduction

Predicting the degradation and Remaining Useful Life (RUL) of Proton-exchange Membrane (PEM) fuel cells is essential for ensuring their reliability and efficiency in various applications. As PEM fuel cells play a role in clean energy technologies, understanding their degradation mechanisms and accurately forecast their performance can enhance their operational lifetime and ensure safe operations.

This thesis explores advanced prognostic methodologies for PEM fuel cells, focusing on the integration of data-driven techniques and empirical modelling to predict PEM fuel cell degradation and RUL. The study leverages comprehensive datasets provided by the FCLAB Research Federation, which include experimental data from durability tests conducted during the IEEE PHM 2014 Data Challenge. Specifically, the *FC1 Dataset* consists of 1154 hr of static operational data, while the *FC2 Dataset* includes 1020 hr of data from quasi-dynamic operational conditions. These datasets are crucial for developing and validating predictive models.

The proposed prognostic method employs Seasonal and Trend decomposition via LOESS (STL) to decompose current and voltage time-series data into trend, seasonal, and residual components. This decomposition facilitates a more nuanced understanding of the underlying patterns and variations in the data. The study then compares the performance of Long Short-Term Memory (LSTM) networks and Echo State Networks (ESNs) in predicting the decomposed current time-series components. Notably, an ESN, optimised via Bayesian optimisation with Optuna, is utilised to iteratively forecast voltage components based on the predicted current and previous voltage data. This approach is specifically tailored to achieve a Prognostic Horizon (PH) of 125 hr.

Additionally, empirical and semi-empirical models are used to assess membrane thickness degradation, using linear regression to minimise reliance on experimental data and refine the degradation predictions. The integration of predicted voltage and membrane thickness data enables accurate RUL forecast, providing insights into medium-term performance trends.

The results underscore the versatility and effectiveness of the proposed methods, demonstrating their capability to handle complex time-series data and deliver precise forecasts of PEM fuel cell degradation. This thesis contributes to the field by offering prognostic tools and methodologies that can be applied to various operating conditions, thereby advancing the understanding and management of PEM fuel cell performance.

This thesis report is organised as follows: In Part I, the scientific paper is presented. Part II contains the relevant Literature Study that supports the research.

Part I

Scientific Paper

Highlights

Remaining useful life prediction of proton-exchange membrane fuel cell tested under static and quasi-dynamic operating conditions

Matthew Georgio Dekkers

- An Echo State Network (ESN) is proposed for iteratively predicting stack voltage degradation of Proton-exchange Membrane (PEM) fuel cells, using current and voltage data from the previous time step. Seasonal and Trend decomposition using LOESS (STL) is applied to decompose these time-series into trend, seasonal, and residual components.
- The proposed ESN-based method for predicting stack voltage degradation is utilised to forecast the Remaining Useful Life (RUL) of PEM fuel cells, achieving a Prognostic Horizon of 125 hr. This method meets the $\alpha - \lambda$ accuracy metric, demonstrating its effectiveness in medium-term RUL prediction.
- The research applies models for membrane thickness degradation using empirical and semi-empirical approaches, revealing that averaging thickness across cells can lead to RUL overestimation.

Remaining useful life prediction of proton-exchange membrane fuel cell tested under static and quasi-dynamic operating conditions

Matthew Georgio Dekkers[a]

[a] Faculty of Aerospace Engineering, Delft University of Technology, Delft, The Netherlands

ARTICLE INFO

Keywords:
Proton-exchange membrane fuel cell
Prognostics and health management
Degradation voltage and current
Degradation membrane
Remaining useful life
Prognostic horizon
Static conditions
Quasi-dynamic conditions
Echo state network
Long short-term memory network
Semi-empirical model
Empirical model

ABSTRACT

Proton-exchange Membrane (PEM) fuel cells are essential systems for hydrogen-electric powertrains in aviation, aiming to meet climate-neutral goals. However, their integration faces challenges, particularly regarding power density, reliability, and durability. This research addresses PEM fuel cell durability through Prognostics and Health Management to predict Remaining Useful Life (RUL) under static and quasi-dynamic conditions. We propose a prognostic method utilising Echo State Networks (ESNs) to manage the chaotic time-series data of PEM fuel cells, extending the Prognostic Horizon (PH) to 125 hours. Our approach involves decomposing stack voltage and current time-series data into trend, seasonal, and residual components via Seasonal and Trend decomposition using LOESS, and predicting these iteratively with ESNs optimised through Bayesian optimisation using Optuna. A comparative study found that ESNs perform best at predicting trends in single-input, single-output forecasts of current time-series, while Long Short-Term Memory networks are better at capturing seasonality and residuals. Additionally, while empirical and semi-empirical models assessed PEM fuel cell membrane health, their effectiveness in predicting RUL in combination with predicted stack voltage was limited by average degradation across cells. This study presents a robust and universal prognostic approach for PEM fuel cells, facilitating their reliable integration into aviation applications.

1. Introduction

In the aviation industry, Proton-exchange Membrane (PEM) fuel cells are considered a key system in hydrogen-electric powertrains to meet climate-neutral goals [1, 2]. These PEM fuel cells are as essential to future aircraft as conventional aircraft engines are to current aircraft. Their integration is proposed for regional aircraft configurations [3, 4, 5]. However, the implementation of PEM fuel cells in regional aircraft faces challenges, particularly in achieving required power density, reliability, and durability [6, 7, 8]. The durability of PEM fuel cells is a significant concern, as their limited operational lifetime can pose economical risks for aircraft operators [9]. Currently, PEM fuel cells have an operational lifetime of 20,000 hr, without performing maintenance activities [10]. This contrasts with traditional aircraft engines, where maintenance activities play a crucial role in extending their operational lifetime. For instance, the Rolls-Royce AE 3007A engine, integrated into the Embraer ERJ 135 regional aircraft, has an operational lifetime of 53 million hr due to regular maintenance [11]. Operational data from aircraft engines are regularly analysed to assess the health of the system and its critical components. Prognostics and Health Management (PHM) is an important framework that assists in predicting degradation, the Remaining Useful Life (RUL) and maintenance activities of aircraft engines [12, 13]. PHM plays an essential role in extending the operational lifetime of aircraft engines, preventing catastrophic failures, and avoiding the use of components beyond repair. Similarly, PHM has the potential to extend the operational lifetime of PEM fuel cells through degradation and RUL predictions on operational data and assist in scheduling maintenance activities [14, 15].

Before a prognostic method can be applied to determine the RUL of a PEM fuel cell, an appropriate health indicator needs to be selected. This health indicator quantifies the level of degradation of the system or an individual component within the PEM fuel cell. For PEM fuel cells, the choice of health indicator is influenced by the operating conditions, which affect the observability of degradation [8]. These operating conditions depend on the current demanded by the load and can be categorised into three types: (1) static, (2) quasi-dynamic, and (3) dynamic. Due to limited data availability, this work focuses on static and quasi-dynamic operating conditions, which represent stationary and variable load conditions of an electric motor, respectively [16]. For these conditions, the voltage of all individual cells combined, known as the stack voltage, is generally used as the health indicator on system-level.

However, a system-level health indicator provides limited information to the operator regarding the causes of degradation. Therefore, an additional health indicator on component-level is required, especially for the most critical component within a PEM fuel cell. According to Jouin et al. [14], the membrane is the most critical component within a PEM fuel cell, and its health can be assessed by analysing the reduction in membrane thickness. Currently, degradation of membrane thickness cannot be directly obtained by monitoring a sensor's output. However, a prognostic method can be applied to analyse its degradation.

Generally, there are three types of prognostic methods for degradation predictions of PEM fuel cells and its components: (1) physics-based, (2) data-driven, and (3) hybrid [15, 17]. Physics-based methods are limited to a specific PEM fuel cell and require detailed specifications from the manufacturer, limiting their universality for different PEM fuel cells. Contrary, data-driven methods, leverage Artificial

Intelligence (AI) techniques, particularly Recurrent Neural Networks (RNNs), and experimental time-series data. This time-series data, consisting of operational conditions over time such as voltage, current, and air humidity, captures the dynamic behaviour and degradation trends of PEM fuel cells. Since these time-series data are universal for PEM fuel cells and can be predicted by RNNs without requiring physical laws, RNNs can be deployed across various PEM fuel cells. Therefore, data-driven methods offer the potential for a universal prognostic approach for PEM fuel cells.

Once an appropriate health indicator is selected, a threshold must be defined to identify the critical point at which the PEM fuel cell's degradation becomes severe [18]. This threshold can represent the moment when the PEM fuel cell can no longer generate sufficient power, potentially preventing a regional aircraft from taking off or leading to unsafe operations. The point in time when the health indicator crosses this threshold is considered the End of Life (EoL) of the PEM fuel cell.

Prior to reaching the EoL, a PEM fuel cell remains functional, requiring the prediction of the degradation of the health indicator to estimate the RUL of the PEM fuel cell. This approach is standard within PHM. However, previous studies on the PHM of PEM fuel cells have often overlooked this step [19, 20, 21]. Instead, they focus on predicting the system-level health indicator up to a threshold and then compare this predicted RUL to the actual RUL at EoL. There is a need to understand, for each predicted time step of the health indicator, how long the PEM fuel cell can continue to operate. This understanding enables more accurate and actionable RUL predictions, thereby ensuring operational safety and enhancing maintenance planning.

The ability to accurately predict RUL over an extended period is referred to as the Prognostic Horizon (PH) of a prediction method. The RUL predictions must meet a predefined limit to be considered accurate [22, 23]. Within PHM, $\alpha - \lambda$ accuracy is considered as a reliable evaluation metric, which incorporates an error bound around the actual RUL which narrows as the PEM fuel cell approaches its EoL. RUL predictions can be categorised by PH into short-term (up to 24 hr), medium-term (24 to 168 hr), and long-term (beyond 168 hr) [15]. Although some studies claim to offer long-term RUL predictions, they often rely on experimental data during the prediction phase, which limits their actual prediction horizon to the short-term category [20, 21, 24, 25]. This reliance undermines their ability to provide true long-term forecasts. Extending the PH into the medium-term range presents challenges due to the chaotic time-series behaviour of the system-level health indicator. To address this, an RNN capable of handling such chaotic behaviour is required.

This research aims to investigate how Echo State Networks (ESNs) can handle chaotic time-series data from durability datasets of PEM fuel cells and extend the PH into the medium-term range. ESNs, first introduced in 2001 by Jaeger [26], belong to the field of Reservoir Computing, and have shown exceptional capabilities to generate accurate predictions from chaotic time-series data. They have been applied in Quantum Neuromorphic Computing [27], Neuromorphic Hardware [28, 29], and Speech Recognition [30, 31]. Their application to PHM of PEM fuel cells is emerging and an active area of research [32, 33, 34]. In addition, this research will combine existing empirical and semi-empirical membrane degradation models to identify membrane health with minimal use of experimental data [35, 36]. While applying these physics-based models provides valuable insights, their application is constrained to PEM fuel cells that meet specific model requirements, limiting their universality.

Our methodology focuses on developing an ESN to iteratively predict the degradation of stack voltage. By "iteratively," we mean that the ESN reuses its previous stack voltage prediction to forecast the next time step. To enhance the accuracy of these predictions, we incorporate two key approaches. First, we decompose the stack voltage and current time-series into three components: trend, seasonal, and residual, using Seasonal and Trend decomposition via LOESS (STL) [37]. This decomposition method is commonly used in chaotic time-series predictions [38, 39, 40]. Second, the decomposed current signals are predicted by an RNN. The previous current prediction is combined with the previous stack voltage prediction to forecast the next stack voltage time step using the ESN. The current provides essential information about the degradation pattern of the stack voltage, as the stack voltage multiplied by the current represents the stack's power. We conduct a comparative study of current time-series predictions between the ESN and another RNN, specifically an existing Long Short-Term Memory (LSTM) Network [41]. The decomposed voltage signals are then predicted by the ESN, and the original voltage signal is reconstructed by combining the three components. The hyperparameters of the ESN are optimised using Bayesian optimisation with Optuna [42]. Finally, the predicted stack voltage degradation and membrane thickness are used to predict the RUL of the PEM fuel cell using linear regression.

Our research is focused on answering the following primary research question:

R1 How to quantify, assess, and forecast the medium-term health of PEM fuel cells and their most critical component tested under static and quasi-dynamic operating conditions?

Our hypothesis for the primary research question is as follows:

H1 Voltage degradation and membrane thickness can quantify the health of a PEM fuel cell and its most critical component, the membrane, under static and quasi-dynamic conditions. A physics-based model can assess the membrane's health, and voltage degradation can be forecast with an RNN.

The sub-questions that support the main research question are:

R1.1 How to model medium-term degradation of the membrane within PEM fuel cells?

R1.2 How to enhance the PH of a PEM fuel cell's RUL into the medium-term range?

Our hypothesis for the sub-questions are:

H1.1 A physics-based model can be applied to investigate the impact of hydroxyl radical attack on the membrane which can lead to a reduction in membrane thickness.

H1.2 An RNN with a high temporal memory capacity, e.g. an ESN, can generate medium-term predictions on voltage degradation based on previous information of voltage and current. These medium-term predictions can enhance the PH of RUL predictions.

The principal contributions of this work are outlined as follows:

1. Utilised Seasonal and Trend decomposition via LOESS to decompose current and voltage time-series data into trend, seasonal, and residual components.
2. Evaluated and compared the performance of LSTM and ESN models for predicting the decomposed current time-series components.
3. Applied an ESN, optimised through Bayesian optimisation with Optuna, to iteratively predict voltage components based on previous time step predictions of current and voltage.
4. Implemented both empirical and semi-empirical models to assess membrane thickness degradation, incorporating linear regression to minimise reliance on experimental data.
5. Integrated predicted voltage and membrane thickness data to forecast RUL, achieving a 125 hr Prognostic Horizon by focusing on voltage degradation predictions, thus enabling medium-term forecasts.

This paper is structured as follows. Section 2 provides an overview of data-driven prognostic methods, ESNs for time-series prediction, and membrane degradation modeling. In section 3, we clarify the methodology by detailing the durability datasets, health indicators, and the ESN architecture. This section also explores the impact and optimisation of ESN hyperparameters, comparing them with an existing LSTM. Additionally, the decomposition techniques used and the application of ESN and LSTM for predicting current and stack voltage are discussed. The empirical and semi-empirical membrane degradation models and prediction techniques are presented, followed by the prediction of the RUL. Section 4 presents the results of the study, accompanied by a discussion of the findings. Finally, section 5 provides a summary of the conclusions drawn from the research, and section 6 outlines recommendations for future research directions.

2. Related Work

This section reviews data-driven prognostic methods for PEM fuel cells, as detailed in subsection 2.1. It covers the use of Echo State Networks for time-series forecasting in subsection 2.2. Finally, subsection 2.3 addresses models for membrane degradation.

2.1. Data-driven prognostics for PEM fuel cells

Data-driven prognostic methods rely on the availability of durability datasets to train AI models that learn the dynamic behaviour of health indicators. Significant progress in this field has been made using two datasets from the FCLAB Research Federation (FR CNRS 3539), obtained during IEEE PHM 2014 Data Challenge, which contain experimental ageing data [16]. These two datasets have been used in the field of PHM to extend the PH by tackling the difficulties of predicting chaotic time-series behaviour of health indicators. This requires RNNs capable of handling such complexity. Various RNNs have been applied to address this issue, including Gated Recurrent Units (GRUs) [24, 43, 44], Long Short-term Memory (LSTMs) Networks [45, 46, 47], Convolutional Neural Networks (CNNs) [20, 48], Transformers [49, 50, 51], Echo State Networks (ESNs) [8, 52, 53], and fusion models combining different RNNs [19, 21, 25].

Zhang et al. [24] explored the use of GRUs in various configurations, incorporating bidirectional elements and stacked architectures, to predict long-term degradation and RUL based on datasets from the IEEE PHM 2014 Data Challenge. Despite being labeled as long-term, these predictions rely on short-term operational data, thus not truly achieving long-term forecasting. They applied thresholds of 97% and 95% of the initial stack voltage to determine the EoL under static and quasi-dynamic operating conditions, respectively, with stack voltage predictions made one hr in advance. Similarly, Zuo et al. [43] introduced an attention-based GRU optimised via grid search for hyperparameter tuning to predict long-term voltage degradation. However, their approach also predominantly utilises short-term data.

Liu et al. [45] developed a LSTM using short-term data to predict the voltage degradation. Wang et al. [54] created a fusion prognostic strategy by incorporating a physics-based approach to extract a PEM fuel cell's health indicator and to predict its degradation with an Adaptive Brownian Bridge-based Aggregation (ABBA) LSTM, which expresses the original data with reduced dimensionality. RUL predictions were generated at 50 hr intervals, achieving a relative error of 11.4%. Liu et al. [47] developed a residual-CNN-LSTM to generate medium-term degradation predictions and achieved a prediction horizon of 80 hr for quasi-dynamic operating conditions.

Peng et al. [48] combined a CNN with an LSTM, limited to short-term predictions. Benaggoune et al. [20] proposed a dilated and conditional CNN with a multi-step ahead prediction method, achieving significant accuracy for a 24 hr prediction horizon of stack voltage degradation.

Lv et al. [49] applied a Transformer model for PHM of a PEM fuel cell for the first time, achieving a prediction horizon of 13.5 hr for degradation prediction, without generating RUL predictions. They reapled the self-attention mechanism in the Vanilla Transformer by a series-attention mechanism. Although the work mentions long-term prognostics, its prediction horizon stays within the short-term range. Tang et al. [50] proposed a Transfer Learning Transformer Neural Network with multiple input parameters, using only short-term data to predict degradation and lacking RUL predictions. Fu et al. [51] demonstrated the use of a Non-stationary Transformer with one-step, three-step, and five-step ahead degradation prediction and RUL prediction. However, they found that the Transformer's ability to handle multiple time steps ahead predictions was limited.

Morando et al. [52] proposed a decomposition framework using a wavelet filter to separate cell voltae data into an approximation component, representing the degradation trend, and a detailed component, capturing seasonality and residuals. Both components were iteratively predicted by an ESN. While the cell voltage's trend was accurately predicted over a prediction horizon of 1400 hr, the ESN presented relatively large errors in predicting voltage recovery and seasonality. Their ESN was tested on a 1700 hr durability test with a dynamic mission profile.Vichard et al. [53] conducted an open cathode durability test of 5000 hr under variable temperature conditions. They proposed an ESN with three input parameters: ambient temperature, operating time, and output voltage from the previous prediction stage. Although the model iteratively predicted voltage, it relied on short-term ambient temperature data. Hua et al. [8] developed an ESN with a single input iterative structure, which faced difficulties in capturing the time-series dynamics. They also created an ESN with a double input, incorporating a scheduled stack current based on seasonal requirements. This approach improved degradation trend accuracy and RUL prediction, achieving a PH of 250 hr. However, its applicability to non-stationary systems like aircraft is limited due to the non-schedulable nature of the stack current.

Li et al. [19] developed a fusion model integrating bidirectional LSTM-GRU with an ESN for voltage predictions, using a Particle Swarm Optimisation (PSO) algorithm for feature extraction. They achieved a prediction horizon of 100 hr with a sliding-window approach, resulting in an RUL prediction error of up to 3% after 200 hours of training, which represents 20% of the dataset. However, their fusion model lacked RUL predictions for each predicted voltage time step.Sahajpal et al. [21] tested six deep learning techniques, including LSTMs, GRUs, and their combinations with 1-D CNNs and bidirectional elements, using fuel cell stack data from the IEEE PHM 2014 Data Challenge datasets. The stack voltage was predicted 1 hr ahead, and a 96% initial stack voltage threshold was used to determine the RUL, aligning with thresholds used by Benaggoune et al. [20], Xia et al. [25], and Li et al. [19]. Xia et al. [25] decomposed the voltage signal into calendar aging and reversible aging components using locally weighted regression (LOESS). They predicted these components iteratively with an Adaptive Extended Kalman Filter (AEKF) and an LSTM with a sliding window of 20, achieving a PH of 1 hr with a maximum RUL error of 26 hr, without considering a RUL prediction for each predicted stack voltage step. A Genetic Algorithm (GA) optimised the hyperparameters of the LSTM.

2.2. *Echo state networks for time-series*

Echo State Networks have emerged as a powerful tool for time-series prediction, leveraging their intrinsic memory capabilities to model complex temporal patterns [55]. ESNs have found applications across various fields, including voltage prediction, where they couple with Markov chains to provide current profiles [56], enhancing prediction accuracy.

ESNs can extend their predictive horizons by iterating over multiple steps. However, this iterative approach introduces challenges, particularly in hyperparameter selection, as the performance is highly sensitive to the chosen values [57]. To address this, Valencia et al. [58] proposed an ESN optimised with a Genetic Algorithm (GA) and a Separation Ratio Graph (SRG) for multi-step time-series forecasting. This model successfully identified the most suitable reservoir topology, demonstrating high performance on benchmark datasets from the NN3 and M3 Forecasting Competitions, with predictions spanning six, eight, and eighteen steps.

To boost ESN capabilities, Mezzi et al. [59] introduced a Multi-Reservoir ESN for predicting the RUL of PEM fuel cells. By coupling multiple reservoirs, each with different hyperparameters, the model encapsulates crucial characteristics of chaotic time-series data. Similarly, Mezzi et al. [56] utilised Markov chains to replicate PEM fuel cell load profiles, enhancing predictions of voltage degradation and RUL.

Genetic Algorithms have been selected to optimise ESN configurations further. Zhong et al. [60] developed a double-reservoir ESN optimised with a GA for one-step ahead turbofan engine time-series predictions. Deng et al. [33] proposed a stacked ESN optimised via GA, leveraging short-term data for degradation predictions.

Hyperparameter tuning remains critical for ESN performance. Hua et al. [8] conducted a sensitivity analysis using ANOVA to understand the influence of parameters like leaking rate α, spectral radius ρ, and regularisation parameter β. They found optimal performance with a high leaking rate, medium spectral radius, and medium regularization parameter.

For enhancing prediction accuracy, Hua et al. [61] applied Discrete Wavelet Transform (DWT) to decompose health indicators into multiple signals. Each decomposed signal was then predicted by independent ESNs, which were ensembled to provide final predictions. Additionally, Hua et al. [62] integrated GA with DWT in ESNs, optimising key parameters and demonstrating that the approximation component coefficient sufficiently represents the original signal for accurate predictions.

Innovative ESN architectures continue to push the boundaries of time-series prediction. Jin et al. [34] developed an ESN with a Cycle Reservoir with Jump (CRJ) and an Adaptive Fuzzy Sampler (AFS), though it exhibited high error in stack voltage degradation predictions. González-Zapata et al. [63] optimised an ESN with Hindmarsh-Rose neurons and Particle Swarm Optimisation (PSO), achieving accurate predictions for up to 10,000 steps on chaotic time-series datasets. Ando and Chang [64] demonstrated the application of ESNs for road traffic forecasting, achieving accurate predictions 600 steps ahead.

The literature underscores the versatility of ESNs in generating accurate iterative predictions over extended horizons. Key to their success are preprocessing steps to reduce the complexity of chaotic time-series and careful hyperparameter optimisation.

2.3. Membrane degradation modelling

Understanding and modelling of membrane degradation in PEM fuel cells is essential for effective health management and predictions on RUL. Membrane degradation can be classified into five main categories: (1) chemical, (2) mechanical, (3) thermal, (4) shorting, and (5) contamination [14].

Chemical degradation, the primary cause of limited membrane life, involves membrane decomposition due to chemical reactions and contamination [65]. Indicators include gas crossover rate and fluoride release rate, with degradation characterised by membrane thinning and the release of HF, CO_2, and H_2SO_4 [14, 66]. Recent advancements include a semi-empirical model proposed by Chandesris et al. [36], which links membrane thickness degradation to fluoride release caused by hydroxyl radicals. This model highlights how reactions with hydroxyl radicals and peroxide species contribute to membrane thinning, influenced by factors such as cell voltage and metal impurities [67].

Mechanical degradation results from stresses, swelling, and contraction due to operating conditions, leading to micro-holes, tears, perforations, and blisters [68]. This type of degradation is often caused by manufacturing defects and prolonged operation [69]. Stress cycling and improper humidity conditions during operation may aggravate these effects, causing membrane shrinkage or swelling, which influences cell performance and durability [70, 71]. A comprehensive review by Qiu et al. [72] provides an in-depth analysis of mechanical failure mechanisms, offering insights into mitigation strategies and material properties to improve membrane durability across its lifespan.

Thermal degradation is generally controlled by thermal management systems within the PEM fuel cell stack, maintaining temperatures between 60-80 °C [66]. However, damage from freeze/thaw cycles can still occur. Kim et al. [73] studied how diffusion media properties, such as stiffness and thickness, affect Membrane Electrode Assembly (MEA) damage during freeze/thaw cycles. The study revealed that while stiffer diffusion media can reduce surface cracks, it may also increase damage if not managed correctly.

Membrane shorting, considered a form of mechanical degradation, is caused by direct electron movement from the anode to the cathode, leading to micro-holes and membrane melting [65].

Contamination occurs due to foreign species, often from catalyst degradation or impurities in gases and humidifiers [14, 74]. This can significantly reduce membrane conductivity.

Membrane thickness is a key indicator of membrane degradation, as it correlates with gas crossover and fluoride release rates. Decreases in membrane thickness can lead to increased hydrogen crossover and potential cell failure [35, 36]. A semi-empirical model developed by Karpenko-Jereb et al. [35] integrates physico-chemical properties to analyse degradation rates, while a Computational Fluid Dynamics (CFD) model simulates 3D cell performance. This model demonstrates non-uniform in-plane degradation and highlights the impact of relative humidity and temperature on cell current density.

Recent modelling advancements have introduced complex frameworks. Singh et al. [75] presented a transient 2D model simulating hydroxyl radical attacks and membrane degradation, validated against experimental data for accuracy. Macauley et al. [76] developed an empirical model for predicting membrane lifetime in heavy-duty fuel cells, considering factors like cell voltage and temperature. Furthermore, Frühwirt et al. [77] proposed a zero-dimensional kinetic framework that uses coupled chemical equations to predict membrane lifetime based on fluoride emission rates, also addressing the impact of metal impurities.

In summary, advances in modelling membrane degradation provide valuable insights into the various degradation mechanisms and their impact on fuel cell performance. By integrating different modelling approaches and empirical research, the durability and reliability of PEM fuel cells can be enhanced.

3. Methodology

This section outlines the methodology used in this study. In subsection 3.1, the durability datasets are explained. The health indicators utilised in this work are discussed in subsection 3.2. The fundamentals of the Echo State Network are presented in subsection 3.3, followed by an explanation of the applied Long Short-term Memory Network in subsection 3.4. All steps of the prediction method are discussed in subsection 3.5. The models for modelling membrane degradation are elaborated in subsection 3.6. Finally, the method for predicting the Remaining Useful Life is described in subsection 3.7.

3.1. Data PEM fuel cell durability

The availability of data is an essential element for enabling this work on predicting PEM fuel cell degradation and RUL. Within this study, two datasets from FCLAB Research Federation (FR CNRS 3539) are used which were obtained during IEEE PHM 2014 Data Challenge and contain experimental ageing data [16]. Both durability tests are performed with a five-cell stack module of Proton Motor Fuel Cell GmbH which have an active surface area of 100

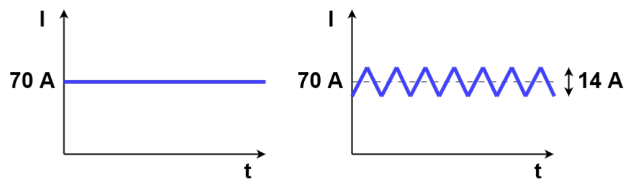

Figure 1: Static and quasi-dynamic operating conditions in terms of current setting of *FC1 Dataset* and *FC2 Dataset*, respectively.

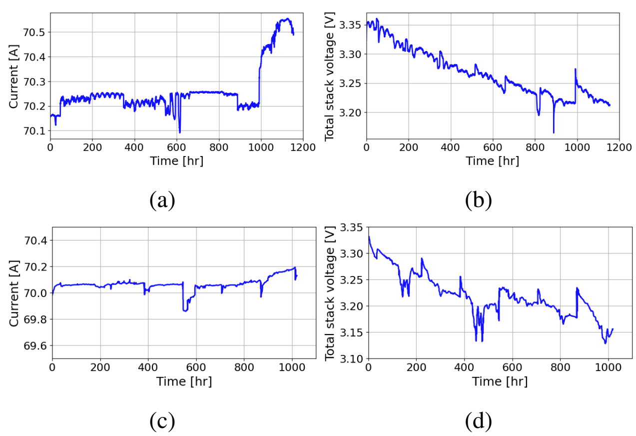

Figure 2: Mission profiles in terms of current and the associated voltage response: (a) static current, (b) static voltage, (c) quasi-dynamic current, (d) quasi-dynamic voltage.

cm^2. The first fuel cell is operated under static operating conditions at a current setting of 70 A and is denoted as *FC1 Dataset*. The *FC1 Dataset* contains 1154 hr of experimental data. The second fuel cell is operated under quasi-dynamic operating conditions at a current setting of 70 A with a triangular ripple current of 14 A oscillating at a frequency of 5 kHz, and is denoted as *FC2 Dataset*. The *FC2 Dataset* contains 1020 hr of experimental data. The static and quasi-dynamic operating conditions are presented in Figure 1 and the mission profiles in terms of current and voltage response of *FC1 Dataset* and *FC2 Dataset* are provided in Figure 2.

FC1 Dataset and *FC2 Dataset* contain measurements of various parameters, e.g. cell voltage, total stack voltage, current, humidity, and incoming and outcoming pressure of hydrogen. An overview of all measured parameters is provided in Table 1 and the specifications of the PEM fuel cell in combination with operating settings are presented in Table 2. Throughout the durability test, the PEM fuel cell's condition was analysed multiple times by performing a characterisation test and Electrochemical Impedance Spectra (EIS).

3.2. Health indicators

The purpose of using a health indicator for a PEM fuel cell is to express the health in a parameter that can clearly be communicated to the end user, and it can assist in the scheduling of maintenance tasks. At the system-level, the health indicator for the *FC1 Dataset* and *FC2 Dataset* is

Table 1
Measured parameters within *FC1 Dataset* and *FC2 Dataset* with their physical description [8, 16, 21].

Parameter	Physical description
U_1 - U_5	Single cell voltage (V)
U_{tot}	Total stack voltage (V)
I	Current (A)
J	Current density (A/cm^2)
$T_{in}H_2$ / $T_{out}H_2$	Inlet/Outlet temperatures of H_2 (°C)
T_{in}Air / T_{out}Air	Inlet/Outlet temperatures of air (°C)
T_{in}Wat / T_{out}Wat	Inlet/Outlet temperatures of water (°C)
$P_{in}H_2$ / $P_{out}H_2$	Inlet/Outlet pressure of H_2 (mBar)
P_{in}Air / P_{out}Air	Inlet/Outlet pressure of air (mBar)
$D_{in}H_2$ / $D_{out}H_2$	Inlet/Outlet flow rate of H_2 (L/min)
D_{in}Air / D_{out}Air	Inlet/Outlet flow rate of air (L/min)
DWat	Flow rate of cooling water (L/min)
HrAIRFC	Inlet humidity of air (%)

Table 2
Characteristics and experimental operating parameters of PEM fuel cell from IEEE PHM 2014 Data Challenge [16, 66, 78].

Parameter	Value
Gas diffusion layers thickness	400 μm
Membrane thickness	15 μm
Cell active area	100 cm^2
Membrane Electrode Assemblies type	GORE PRIMEA 5761
Membrane type	GORE-SELECT®
Open circuit voltage	1 V
Nominal voltage	0.6 V
Rated power	30 W
Cell number	5
Manufacturer	Proton Motor Fuel Cell GmbH
Relative humidity of anode and cathode	50%
Temperature	60 °C
Absolute pressure of anode and cathode	1.5 bar
Stochiometry ratio of anode and cathode	1.5-2 bar
Inlet Pressure of anode and cathode	1.3 bar

the total stack voltage. This parameter is monitored during the operations of the PEM fuel cell. On the component-level, only the membrane is analysed because it is identified as the most critical component within the PEM fuel cell [14]. The health indicator used on component-level is the membrane thickness, assessed by an empirical and semi-empirical model based on data from the *FC1 Dataset* and *FC2 Dataset*.

3.3. Echo state network

This subsection introduces the Echo State Network, a key element for predicting performance degradation within this work. The ESN is a brain-inspired Recurrent Neural Network, with the hidden layer being replaced by a large randomly generated reservoir of neurons which are sparsely connected that imitates the topology of a brain-like system [8, 55]. These type of brain-inspired RNNs are called Reservoir Computing (RC) methods. Within this section, the architecture of an ESN is discussed in subsubsection 3.3.1.

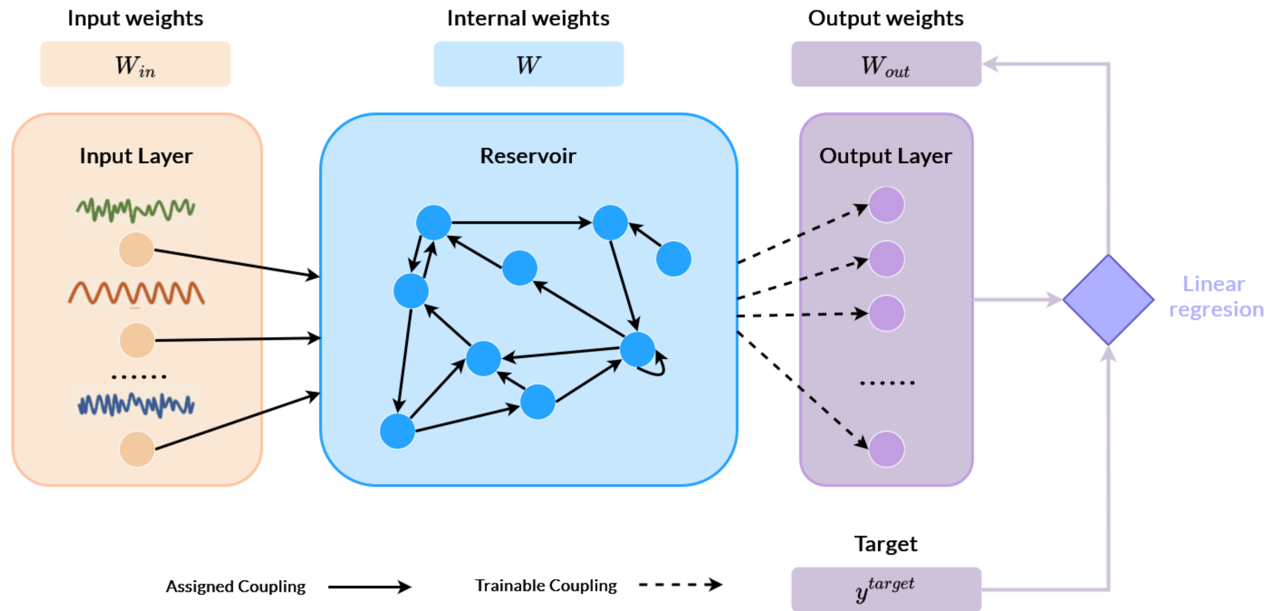

Figure 3: Architecture of Echo State Network.

Furthermore, an optimisation method is proposed in subsubsection 3.3.2 for optimising ESN hyperparameters based on Bayesian optimisation with Optuna [42].

3.3.1. Architecture of ESN

The architecture of an ESN consists of three distinct layers. First, a sensing layer, which receives the input signals and acts as a form of signal preprocessing. Second, the reservoir, which is composed of sparsely connected neurons, and preserves the dynamics of a chaotic time-series. Third, the output layer, which integrates all the signals from the reservoir to produce the network's output. A visual representation of this architecture is provided in Figure 3.

This architecture is a type of Reservoir Computing, as defined by Verstraeten et al. [79]. Within the field of machine learning and computational neuroscience, two RC techniques were introduced which consisted of a different neuron definition. Jaeger [26] introduced Echo State Networks with sigmoidal neurons for machine learning, while Maass et al. [80] introduced Liquid State Machines (LSMs) with Leaky Integrate-and-Fire (LIF) neurons, which are derived from spiking neural networks used in computational neuroscience. ESNs are particularly effective at learning chaotic time-series data by only training the output weights, as demonstrated by Schiller and Steil [81], who noted that dominant weight changes occur in the output weights. ESNs take advantage of this phenomenon by randomly generating the input and internal weight matrices, and keeping these weight matrices fixed, while training the output weight matrix using linear regression or ridge regression.

Key hyperparameters of an ESN include the number of neurons N_n in the dynamic reservoir, spectral radius ρ which represents the maximum eigenvalue of internal weight matrix W, leaking rate α which represents dynamic performance of the reservoir, regularisation parameter β, and coefficients of input and internal weight matrices W_{in} and W. Lukoševičius [57] has provided a detailed guide on manual parameter settings of an Echo State Network. For this study, the ESN was implemented using ReservoirPy [82], a specialised library for developing and experimenting with reservoir computing models.

The dynamics of the neurons inside the reservoir needs to be optimised to obtain a balance between the stability of the network and the computational complexity of the output weights [8]. An optimal reservoir should preserve fading memory and result in neurons with a considerable level of dynamics. The level of dynamics of the reservoir is expressed by the Echo State Property (ESP), and needs to be considered carefully to obtain the aforementioned balance in an Echo State Network. *Jaeger* [26] states that a leaky integrator ESN has the Echo State Property if the initial conditions are washed out at a rate that is independent from the input. In practice, ESP is obtained when the effective spectral radius $|\lambda|_{max}(\hat{W})$ is smaller than 1 for zero inputs and larger or equal to 1 for non-zero inputs [83]. This is not the only condition to obtain ESP because the spectral radius is depending on the characteristics of the input signal and expected output signal [61]. Therefore, a spectral radius larger than 1 could still maintain Echo State Property of the reservoir in an ESN.

Several studies have identified that the leaking rate α, spectral radius ρ, and regularisation parameter β, are the most influential hyperparameters for the ESN performance [32, 58, 84]. Therefore, other hyperparameters are kept fixed. The hyperparameter settings are based on practical guidelines provided by Lukoševičius [57] and other works [8, 19, 56]. In this study, the number of neurons N_n is set to 500. The input scaling is fixed at 1.0, meaning the input is not further scaled. Neuron connectivity is set to 0.1 to maintain a sparsely connected reservoir, while input connectivity is set to 0.2 to ensure that not all neurons in the reservoir are constantly connected to the input. A random seed value of 2307 is used to ensure that all randomly generated input and internal weights are consistent across the study.

3.3.2. Optimisation of ESN hyperparameters

Bayesian optimisation considers the past results of the hyperparameters and their impact on the objective function that is to be minimised. Thereby, an informed decision is made and part of the search space that cannot lead to improvements are ignored. Calls to the objective function are limited by use of a surrogate function which analyses the past objective function results and selected hyperparameters values. The surrogate function maps the hyperparameters in a high-dimensional space to the objective function's probability score. Therefore, the surrogate function can be considered as an approximation of the objective function. The selected surrogate function is Tree Parzen Estimator (TPE). Exploration and exploitation are balanced by the TPE algorithm, presented in Equation 1, during optimisation of hyperparameter performance [85]. The acquisition function guides the selection of the next set of hyperparameters to test, with the median pruner being applied to eliminate less promising candidates based on past performance. Optuna is chosen for implementing Bayesian optimisation due to its user-friendly integration and effective handling of complex optimisation tasks. The algorithm of Bayesian optimisation is explained step by step in Table 3.

$$\text{TPE:} \quad l(\mathbf{x}) = \frac{p(f(\mathbf{x}) < \gamma \mid \mathbf{x})}{p(f(\mathbf{x}) \geq \gamma \mid \mathbf{x})} \tag{1}$$

3.4. Long short-term memory network

The LSTM architecture presented by Jakob Aungiers and Christian Clauss [41] has been chosen for its effectiveness in forecasting chaotic time-series data, particularly in the financial market, where it demonstrated high accuracy in predicting 50 to 80 steps ahead. This LSTM framework is optimised for multi-step ahead predictions, making it suited for handling complex and dynamic time-series datasets. Given its performance in similar applications, this LSTM model serves as a baseline for generating predictions from the decomposed current time-series data of PEM fuel cells.

The selected LSTM consists of six layers, each chosen to enhance the model's ability to capture long-term dependencies and manage sequential data effectively. The initial layer of the LSTM network is an LSTM layer with 100 neurons configured to return sequences. This design allows the network to output a sequence of data points, maintaining the temporal structure of the input data. By preserving sequence information, this layer enables the model to learn and capture the dynamics and patterns in time-series data. The first layer is followed by a dropout layer with a dropout rate of 0.2. Dropout serves as a regularisation technique that randomly deactivates a fraction of the neurons during training. This helps prevent overfitting by ensuring that the model does not become overly reliant on any specific neuron. The third layer is an LSTM layer, also consisting of 100 neurons, that continues to return sequences. The fourth layer is an LSTM layer, featuring 100 neurons, which is configured to return only the final output rather than sequences. This layer fuses the information from the preceding layers into a fixed-size representation. An additional dropout layer with a dropout rate of 0.2 is introduced after the final LSTM layer. The final layer of the network is a dense layer with a single neuron and a linear activation function. This layer generates the final prediction.

Table 3
Bayesian optimisation implementation.

Algorithm: Bayesian optimisation
Input: Search space, objective function, number of iterations
Output: Optimal hyperparameters α, ρ, β
Step 1: Initialise the search space
Leaking Rate (α): Range from 0.0001 to 0.2
Spectral Radius (ρ): Range from 0.6 to 1.5
Regularisation Parameter (β): Range from 1×10^{-5} to 1×10^{-1}
Step 2: Select a random value of each hyperparameter
Sample initial hyperparameters
Step 3: Define the objective function
Define mean-squared error between predicted and true time-series data to be minimised
Step 4: Choose a surrogate function
Use Tree Parzen Estimator (TPE) to approximate the objective function presented in Equation 1
Step 5: Select optimal hyperparameters
For $n = 1$ to $N_{iter} = 100$
Based on exploration-exploitation trade-off, select $\mathbf{x}_n$ from S using TPE
Step 6: Evaluate the objective function
Train the model and evaluate $f(\mathbf{x}_n)$
Step 7: Update the surrogate function
Update the TPE model with the new results $(\mathbf{x}_n, f(\mathbf{x}_n))$
Prune unpromising trials using the Median pruner function:
$m_{best} = \text{median}(\{f(\mathbf{x}_i) \mid i < n\})$
Prune trial if $f(\mathbf{x}_n) > m_{best}$
Step 8: Output the optimal hyperparameters
$\mathbf{x}_{opt} = \arg\min f(\mathbf{x})$

The model applies the Adam optimiser, known for its efficiency and adaptive learning rates. Adam helps in faster convergence and improved performance by dynamically adjusting the learning rates based on the gradients [86]. Mean Squared Error (MSE) is utilised as the loss function, which measures the average squared difference between predicted and true values.

For each decomposed current time-series component, an individual trained LSTM is used. For the *FC1 Dataset*, the LSTM is trained on 525 hr of data to capture the dynamics of the trend, seasonal, and residual components. For the *FC2 Dataset*, the LSTMs initially trained on the *FC1 Dataset* current components are re-used to assess their ability to perform predictions on a different dataset without additional training, effectively implementing transfer learning. During training, the LSTM receives sequences of 125 data points to learn how to predict the next 125 steps. In the prediction phase, the LSTM receives the past 125 hr of experimental data to predict the next 125 hr, and this process is repeated until the end of the durability dataset is reached.

3.5. Method for predicting performance degradation

This subsection outlines the method to predict total stack voltage degradation. The process consists of four main stages. First, data preprocessing is discussed in subsubsection 3.5.1. The data is initially downsampled and filtered using a Savitzky-Golay filter to smooth out noise. The current and total stack voltage time-series data from the *FC1 Dataset* and *FC2 Dataset* are then normalised to prepare them for decomposition. Second, Seasonal and Trend decomposition via LOESS (STL) is discussed in subsubsection 3.5.2. This step separates the trend, seasonal, and residual components of the time-series data. Third, in subsubsection 3.5.3, we explain the prediction method for the current time-series components using LSTM and ESN. Fourth, subsubsection 3.5.4 describes how the total stack voltage components are iteratively predicted by utilising the predicted components from the previous time step of the current and total stack voltage.

3.5.1. Data preprocessing

The *FC1 Dataset* and *FC2 Dataset* contain varying sampling rates and noise. To standardise the time steps across the time-series and ensure compatability with the LSTM and ESN models, we first downsampled the datasets. This adjustment aligned the current time-series data to 1 hr intervals, facilitating predictions of at least 100 hr ahead, which corresponds to around 100 time steps—well within the LSTM's predictive capabilities. Following downsampling, we applied a Savitzky-Golay filter with a window length of 5 time steps to reduce noise while preserving essential signal features. The filtered data was then normalised to a range between 0 and 1 to prepare it for model training and prediction. After the prediction phase of the current time-series components, the current time-series components were upsampled to a 15 min intervals. This upsampling was necessary to match the sampling rate of the voltage time-series, which was downsampled to 15 min to maintain critical information. The decision to use a 15 min sampling rate for the voltage data was informed by an analysis of information gain, as shown in Figure 4. This analysis indicated that significant information loss occurs with longer sampling intervals beyond 15 min. Although downsampling the current time-series to 1 hr may result in some information loss, this trade-off is considered acceptable as the current predictions are primarily used to support the total stack voltage predictions. The impact of various downsampling rates on the total stack voltage is illustrated in Figure 5, which shows that downsampling beyond 15 min intervals leads to a loss of critical information.

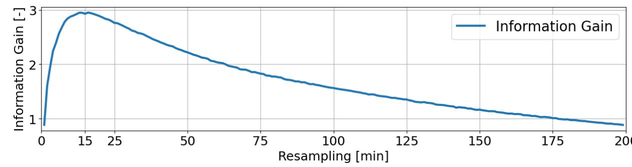

Figure 4: Impact of resampling rate on information gain of total stack voltage of the *FC1 Dataset*.

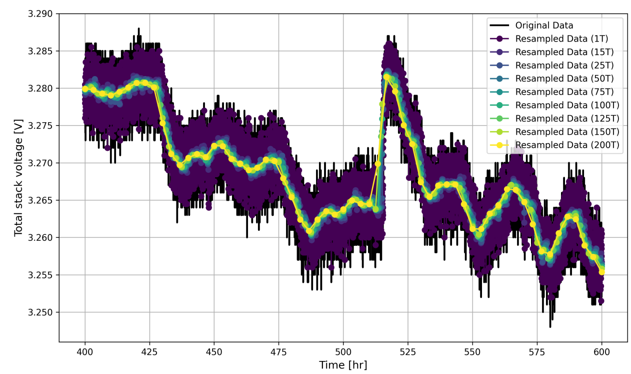

Figure 5: Impact of resampling rate on total stack voltage of the *FC1 Dataset* between 400 and 600 hr.

3.5.2. Data decomposition

Time-series decomposition using Seasonal and Trend decomposition via LOESS, first introduced by R. Cleveland et al. [37], plays an essential role in the proposed method. STL utilises Locally Weighted Scatterplot Smooting (LOESS), a non-parametric technique capable of decomposing complex time-series data into trend, seasonal, and residual components. The STL procedure applies polynomial regression at each time step of the time-series to capture these components [38]. The procedure uses an eigenvalue and frequency response analysis on the analysed time-series. The STL approach involves an iterative process of detrending and updating the seasonal component from the resulting sub-series. Each iteration generates weights based on the estimated irregular component, which are then used to downweight outliers in subsequent calculations. This iterative process effectively captures both short-term fluctuations and long-term trends, making STL a robust method for handling time series with irregular or evolving patterns.

In our application, the STL decomposition was applied to current and voltage time-series data sampled at 15 min intervals. For defining the seasonal period, a value of 97 was chosen, representing the number of 15 min intervals within a 24-hour day.

3.5.3. Current degradation prediction

The current time-series data from the *FC1 Dataset* and *FC2 Dataset* were decomposed using STL into trend, seasonal, and residual components. Each component was then predicted using a pre-configured LSTM and an optimised ESN to compare their performance. The previous 125 hr of experimental data were used to generate predictions 125

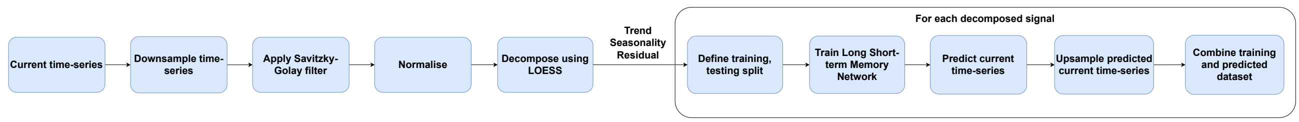

Figure 6: Process of preprocessing current time-series data and predicting with Long Short-term Memory Network.

steps ahead, with each step representing 1 hr. For each prediction phase of the *FC1 Dataset*, a new ESN was created and trained using the past 125 hours to predict the next 125 hours. The final ESN, trained on the complete *FC1 Dataset*, was re-used for investigating transfer learning on the *FC2 Dataset*. An overview of the preprocessing steps and the current prediction steps with an LSTM is provided in Figure 6.

3.5.4. Voltage degradation prediction

For the voltage time-series predictions, STL was again utilised to decompose the time-series into trend, seasonal, and residual components. The predicted current components were used to assist in forecasting the voltage components. Only the ESN was applied to predict the voltage components, allowing for further analysis of the ESN's performance for stable iterative predictions with two input parameters. Furthermore, transfer learning was *not* applied for the voltage predictions to isolate the use of an ESN for specific operating condition. For the *FC1 Dataset*, an ESN was trained with 500 hr of experimental current and voltage data and optimised with 153 hr of validation data. For the *FC2 Dataset*, an ESN was trained with 200 hr of experimental current and voltage data and optimised with 80 hr of validation data. The ESN then iteratively predicted the voltage using the predicted current data from the last time step and its previous voltage prediction. The iterative predictions continued until the end of the durability test without limiting the number of iterative predictions, with each time step representing 15 min.

3.6. Membrane degradation models

This subsection discusses the degradation models to assess the health of the membrane, the most critical PEM fuel cell component. In subsubsection 3.6.1 an empirical membrane model is introduced, based on oxygen crossover rate, to determine degradation in membrane thickness. A semi-empirical model, based on fluoride release rate, is presented in subsubsection 3.6.2 to model the degradation in membrane thickness.

3.6.1. Empirical membrane model

Karpenko-Jereb et al. [35] developed a new empirical model that incorporates physico-chemical properties polymer electrolyte membrane to assess the degradation rates of the membrane thickness and conductivity in relation to the oxygen crossover rate. This model is integrated with a validated Computational Fluid Dynamics (CFD) model to simulate three-dimensional cell performance. By coupling these models, the study analyses the temporal behaviour of the cell, revealing that membrane degradation is non-uniform across the plane. The simulations also demonstrate that cell current density decreases more rapidly with reduced relative humidity and increased temperature. Input parameters for the model, specifically the degradation rates of membrane thickness and conductivity, were acquired from Yuan et al. [87, 88].

Chemical degradation in perfluorinated sulfonated membranes, such as Nafion, is primarily driven by interactions between hydroxyl radicals and the polymer chains. These interactions lead to a reduction in membrane thickness and conductivity, and the formation of pinholes and cracks. Hydroxyl radicals are generated from hydrogen peroxide, a byproduct of reactions involving oxygen and hydrogen protons, with their concentration being proportional to the oxygen concentration in the fuel cell. Consequently, a decrease in membrane thickness can significantly increase hydrogen crossover current density.

Experimental data shows that the hydrogen crossover rate varies with parameters such as temperature, pressure, relative humidity, and membrane thickness. A mathematical expression is proposed to estimate the hydrogen crossover rate under different operating conditions. The study suggests that the ratio of oxygen to hydrogen crossover flux through the membrane remains relatively constant regardless of environmental conditions. This allows for simplification of calculations related to oxygen crossover.

Experimental data indicates that the hydrogen crossover rate is influenced by temperature, pressure, relative humidity, and membrane thickness. A mathematical expression is proposed to estimate the hydrogen crossover rate under varying operating conditions. It is suggested that the ratio of oxygen to hydrogen crossover flux through the membrane remains relatively constant across different environmental conditions, simplifying calculations related to oxygen crossover.

Simulation results provide insights into the relationship between oxygen crossover flux and cell voltage. A linear fitting equation is used to describe how the oxygen crossover flux changes with voltage. This relationship allows for the calculation of degradation rates for membrane thickness and conductivity, considering the impact of cell voltage on oxygen crossover flux. The application of the empirical model is presented in Figure 7. Detailed descriptions of the mathematical expression to estimate hydroegn crossover rate and oxygen crossover flux can be found in [35].

3.6.2. Semi-empirical membrane model

Chandesris et al. [36] developed a semi-empirical relationship for determining membrane thickness based on

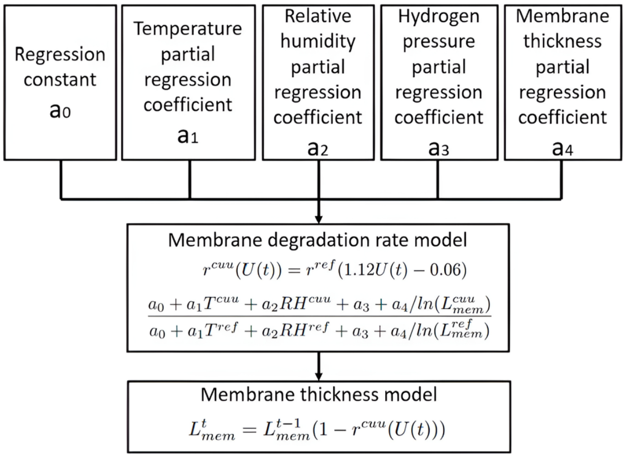

Figure 7: Membrane empirical degradation model [35].

fluoride release. The process involves three main steps to evaluate membrane thinning due to fluoride release.

First, the fluoride release rate is computed as a function of operating conditions, as shown in Equation 2. Second, the change in membrane thickness over time is calculated by assuming that the membrane thickness is proportional to the fluoride release rate times the volume of dry Nafion corresponding to 1 g of fluoride, as shown in Equation 3. This assumption holds because the fluoride release rate is normalised by the geometric active surface area of the membrane electrode assembly. Third, the updated membrane thickness is computed using Equation 4. This process is iterative.

Several assumptions are made when applying the model to the *FCLAB datasets*. Since cell temperature is not available in the *FCLAB datasets*, the highest available temperature measurements, which is the outlet coolant temperature, are used. It is expected that the actual cell temperature is higher than the outlet coolant temperature.

The saturated pressure of water is calculated using the Antoine equation, as shown in Equation 5. The parameters A, B, and C are obtained from the NIST Chemistry WebBook [89]. The parameters provided by Stull [90] are selected due to their applicable temperature range of -17 °C to 100°C.

$$\upsilon_{F^-} = A_1 \frac{\Delta P_{O_2}}{P_0} \frac{e_M^0}{e_M} \exp\left(\frac{\alpha_{eq} F}{RT} U\right) \exp\left(-\frac{E_a}{R}\left(\frac{1}{T} - \frac{1}{T_0}\right)\right) \tag{2}$$

$$\frac{de_M}{dt} = A_2 \upsilon_{F^-} V_{\text{Nafion}} \tag{3}$$

$$e_M = e_M^{t-1} \frac{de_M}{dt}\, dt \tag{4}$$

$$log_{10}(P_{sat}) = A - \frac{B}{C + T_{air}} \tag{5}$$

3.6.3. Membrane degradation prediction

The degradation in membrane thickness is modelled by using an empirical and semi-empirical model based on experimental data. For the *FC1 Dataset*, 653 hr of experimental data are utilised, while the *FC2 Dataset* uses 600 hr of experimental data. Linear regression is applied to predict membrane thickness after modelling the degradation trend, thus reducing the dependency on experimental data. The membrane thickness degradation is evaluated for all five-cells in the tested PEM fuel cell and averaged to understand the overall degradation trend. Both empirical and semi-empirical models are applied in this manner, and the average of both models is used to understand the overall membrane thickness degradation.

3.7. Remaining useful life prediction

For the *FC1 Dataset* and *FC2 Dataset*, two RUL forecast are created for each dataset: one based solely on predicted total stack voltage degradation and another incorporating both predicted total stack voltage degradation and predicted membrane thickness degradation. The RUL is dependent on system and component degradation, thus it is expected that both parameters are helpful in RUL predictions with the linear regression technique. Determining the RUL requires understanding of the EoL, which is based on a voltage threshold, similar to methods used in other studies [8, 19, 59]. A voltage degradation threshold of 3.5% is selected for determining the EoL of the PEM fuel cell, consistent with thresholds used in literature [19, 20, 21]. The accuracy of the RUL results is evaluated using the $\alpha-\lambda$ metric, with an initial allowed error of 35% that reduces as the RUL decreases. This ensures that the RUL forecast remains within an acceptable range of accuracy.

4. Results & Discussion

This section discusses the results of the proposed prognostic method. First, the predictions of the decomposed current time-series are presented in subsection 4.1. Second, the decomposed and reconstructed voltage time-series prediction are shown in subsection 4.2. In subsection 4.3 the membrane thickness modelling and prediction results are discussed. Lastly, the RUL forecast are presented in subsection 4.4.

4.1. Decomposed current time-series prediction

The *FC1 Dataset* trend predictions are shown in Figure 8 and Figure 9, the seasonal predictions in Figure 10 and Figure 11, and the residual predictions in Figure 12 and Figure 13.

By analysing these predictions, several conclusions can be drawn. For the current trend, the ESN captures the baseline more accurately than the LSTM. Both models face difficulties to predict the large deviation in the current trend at the end of the durability test. However, the ESN manages to predict the baseline of the deviation, whereas the LSTM fails to capture it. This demonstrates the ESN's ability to quickly adapt to the latest temporal data while maintaining the overall dynamics of the time-series. In contrast, the LSTM tends to return to the trend observed in its 1^{st}, 2^{nd}, and 3^{rd} prediction. Regarding current seasonal, the ESN fails to capture the repeating pattern in the time-series with its fluctuating amplitude, likely due to a failure in the hyperparameter optimisation process. Conversely, the LSTM is able to capture the current seasonality quite well. For the current residual, the LSTM also outperforms the ESN. However, both struggle to predict the anomalies in the time-series which is normal for predicting residual components [38]. These anomalies are partly caused by interruptions in the durability test due to scheduled characterisation tests to inspect the degradation of the PEM fuel cell. These characterisation tests cause a drop in current and lead to a recovery in voltage, as shown in Figure 14. The performance of both techniques on the *FC1 Dataset* are quantified in terms of RMSE, as presented in Table 4.

The LSTM and ESN models trained on the *FC1 Dataset* were directly applied to the *FC2 Dataset* to explore transfer learning. Despite the quasi-dynamic operating conditions of the *FC2 Dataset* compared to the static conditions of the *FC1 Dataset*, it is valuable to assess how these networks perform on different datasets without additional training. For the *FC2 Dataset*, trend predictions are shown in Figure 15 and Figure 16, the seasonal predictions in Figure 17 and Figure 18, and the residual predictions in Figure 19 and Figure 20.

Similar to the trend prediction for the *FC1 Dataset*, the ESN outperforms the LSTM in predicting the trend for the *FC2 Dataset*, with only one out of seven predictions failing to capture the trend. In contrast, the LSTM fails to capture the baseline of the trend entirely. For seasonal and residual predictions, the LSTM performs better than the ESN, especially in capturing seasonality, which the ESN misses altogether. Both networks struggle with predicting

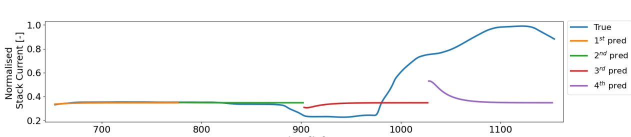

Figure 8: Trend of FC1 stack current forecast 125 hours ahead by Long Short-term Memory Network by applying previous 125 hour of experimental data.

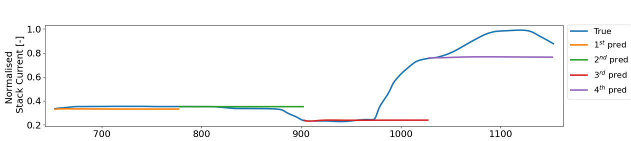

Figure 9: Trend of FC1 stack current forecast 125 hours ahead by Echo State Network by applying previous 125 hour of experimental data.

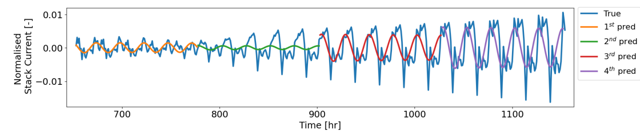

Figure 10: Seasonality of FC1 stack current forecast 125 hours ahead by Long Short-term Memory Network by applying previous 125 hour of experimental data.

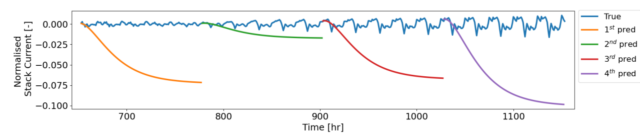

Figure 11: Seasonality of FC1 stack current forecast 125 hours ahead by Echo State Network by applying previous 125 hour of experimental data.

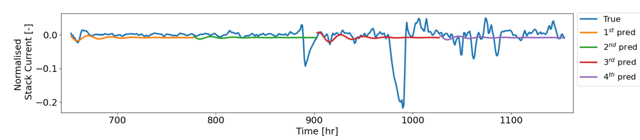

Figure 12: Residual of FC1 stack current forecast 125 hours ahead by Long Short-term Memory Network by applying previous 125 hour of experimental data.

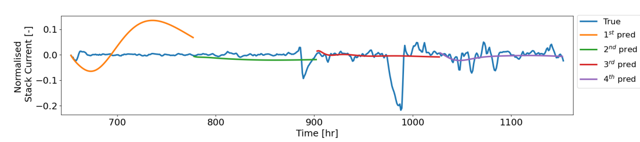

Figure 13: Residual of FC1 stack current forecast 125 hours ahead by Echo State Network by applying previous 125 hour of experimental data.

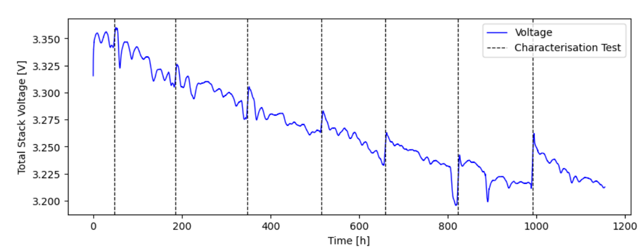

Figure 14: Impact of characterisation tests on voltage recovery for *FC1 Dataset*.

the residual anomalies in the *FC2 Dataset*, partly due to interruptions in the durability test caused by characterisation tests. These characterisation tests cause a drop in current and lead to a recovery in voltage as shown in Figure 21. The performance of both techniques on the *FC2 Dataset* is quantified in terms of RMSE, as presented in Table 4. In summary, the ESN achieves higher accuracy for trend predictions, while the LSTM achieves higher accuracy for the seasonal and residual predictions. Therefore, the ESN's current trend predictions will be used to assist in voltage trend predictions, while the LSTM's predictions for current

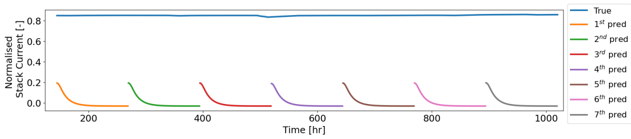

Figure 15: Trend of FC2 stack current forecast 125 hours ahead by Long Short-term Memory Network* by applying previous 125 hour of experimental data. *Trained LSTM on *FC1 Dataset* is applied on *FC2 Dataset* to investigate transfer learning.

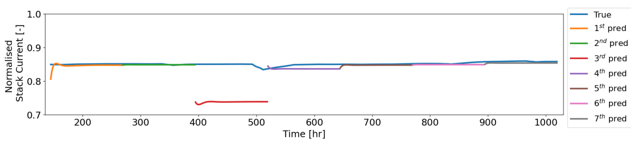

Figure 16: Trend of FC2 stack current forecast 125 hours ahead by Echo State Network* by applying previous 125 hour of experimental data. *Trained ESN on *FC1 Dataset* is applied on *FC2 Dataset* to investigate transfer learning.

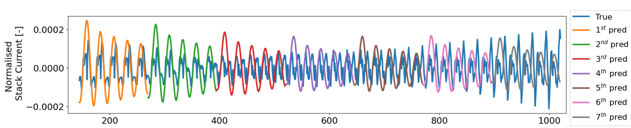

Figure 17: Seasonality of FC2 stack current forecast 125 hours ahead by Long Short-term Memory Network* by applying previous 125 hour of experimental data. *Trained LSTM on *FC1 Dataset* is applied on *FC2 Dataset* to investigate transfer learning.

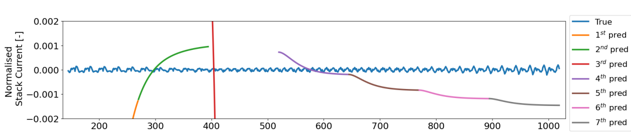

Figure 18: Seasonality of FC2 stack current forecast 125 hours ahead by Echo State Network* by applying previous 125 hour of experimental data. *Trained ESN on *FC1 Dataset* is applied on *FC2 Dataset* to investigate transfer learning.

seasonality and residual will be utilised to assist in voltage seasonality and residual predictions.

4.2. Decomposed and reconstructed voltage time-series prediction

For voltage time-series predictions, STL decomposed the data into trend, seasonal, and residual components. The ESN, assisted by predicted current components, handled all voltage predictions. The ESN iteratively predicted voltage using the previous time step's current data and its last voltage prediction, with each step representing 15 min, continuing until the test's end. This resulted in 2004 iterative voltage predictions for the *FC1 Dataset* and 2961 iterative voltage predictions for the *FC2 Dataset*. It is important to note that during the prediction phase, a time window of 125 hr of experimental current data was required to generate a prediction

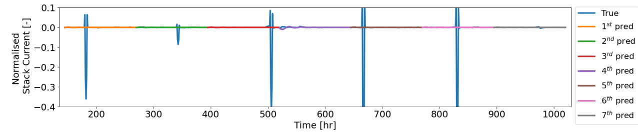

Figure 19: Residual of FC2 stack current forecast 125 hours ahead by Long Short-term Memory Network* by applying previous 125 hour of experimental data. *Trained LSTM on *FC1 Dataset* is applied on *FC2 Dataset* to investigate transfer learning.

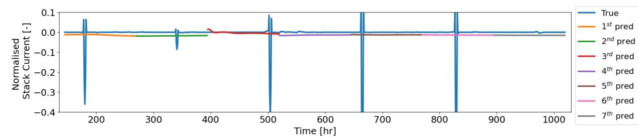

Figure 20: Residual of FC2 stack current forecast 125 hours ahead by Echo State Network* by applying previous 125 hour of experimental data. *Trained ESN on *FC1 Dataset* is applied on *FC2 Dataset* to investigate transfer learning.

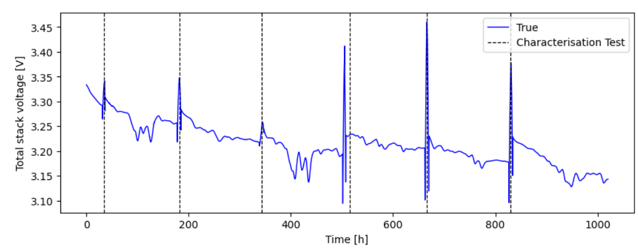

Figure 21: Impact of characterisation tests on voltage recovery for *FC2 Dataset*.

Table 4
Root-mean-square error of predicted current degradation data for decomposed signals of dataset FC1 and FC2 with Echo State Network versus Long Short-term Memory Network. *Trained ESN/LSTM on dataset FC1 is applied on dataset FC2 to investigate transfer learning.

RMSE	*FC1 Dataset*		*FC2 Dataset*	
Type of current signal	*ESN*	*LSTM*	*ESN**	*LSTM**
Trend	**0.14906**	0.28514	**0.23086**	0.50714
Seasonality	0.05261	**0.00326**	0.08976	**0.00010**
Residual	0.05521	**0.03211**	0.11313	**0.05814**

for the next 125 hr of current time-series data. Additionally, no experimental voltage data was used after validation was completed. This means that after using 653 hr and 280 hr of experimental voltage data of the *FC1 Dataset* and *FC2 Dataset*, respectively, no further experimental voltage data was required by the ESN to predict the next voltage value - only the previous voltage and current predictions were needed.

For the *FC1 Dataset*, the voltage trend prediction in Figure 22 demonstrates that the ESN effectively captures the overall trend of the voltage degradation. While there are some discrepancies between the true experimental data and

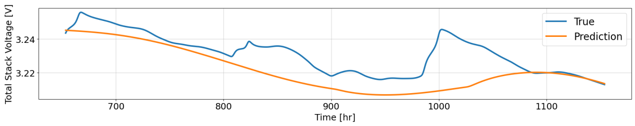

Figure 22: Trend stack voltage degradation of *FC1 Dataset* compared with predicted trend by optimised Echo State Network.

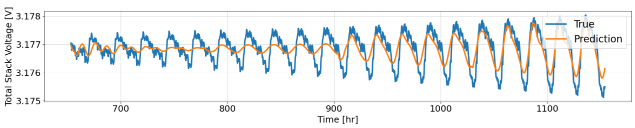

Figure 23: Seasonality stack voltage degradation of *FC1 Dataset* compared with predicted seasonality by optimised Echo State Network.

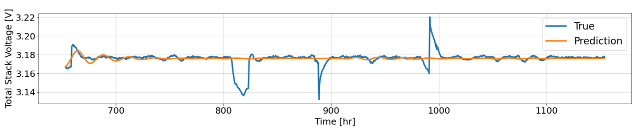

Figure 24: Residual stack voltage degradation of *FC1 Dataset* compared with predicted seasonality by optimised Echo State Network.

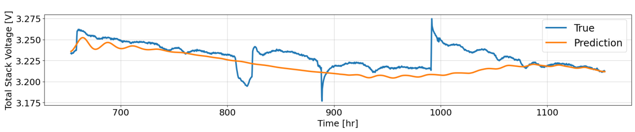

Figure 25: Total stack voltage degradation of *FC1 Dataset* compared with predicted total stack voltage based on decomposed voltage signal prediction of trend, seasonality, and residual.

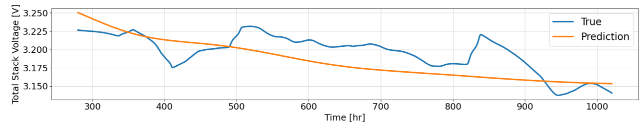

Figure 26: Trend stack voltage degradation of *FC2 Dataset* compared with predicted trend by optimised Echo State Network.

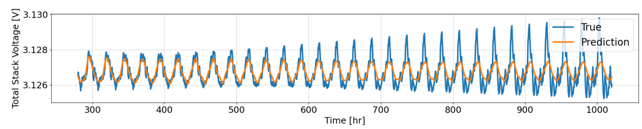

Figure 27: Seasonality stack voltage degradation of *FC2 Dataset* compared with predicted seasonality by optimised Echo State Network.

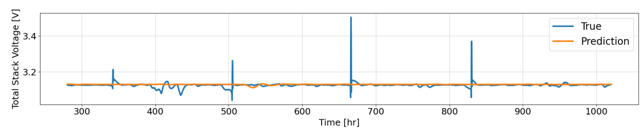

Figure 28: Residual stack voltage degradation of *FC2 Dataset* compared with predicted residual by optimised Echo State Network.

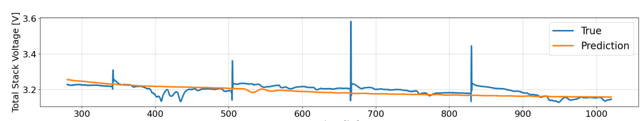

Figure 29: Total stack voltage degradation of *FC2 Dataset* compared with predicted total stack voltage based on decomposed voltage signal prediction of trend, seasonality, and residual.

the predicted data, particularly in predicting voltage recoveries, the ESN remains stable and closely follows the final trend of the experimental data even after performing 2004 iterative predictions. The seasonality of the *FC1 Dataset*, presented in Figure 23, is accurately predicted by the ESN, largely thanks to the LSTM's predicted current seasonality, as shown in Figure 10. Although the amplitude of the predicted seasonality does not always match the experimental data perfectly, the ESN achieves a RMSE of 0.00038. The final predicted voltage component, the residual of the *FC1 Dataset*, captures the baseline of the residual but not the spikes in the time-series, which is expected as the residual is the hardest component to be predicted. When all predicted components are combined to reconstruct the original total stack voltage time-series, as shown in Figure 25, the overall trend is well-captured by the ESN. However, it faces difficulties in predicting the voltage recoveries, partly due to the characterisation tests which impact is presented in Figure 14. Since voltage recoveries are infrequent, the ESN struggles to capture this dynamic within the time-series, resulting in a stable voltage trend prediction with few fluctuations. The seasonal component helps introduce more fluctuations into the predicted total stack voltage, but its impact is limited, as seen in Figure 25.

For the *FC2 Dataset*, the predicted voltage trend, shown in Figure 26, has similar characteristics as the predicted voltage trend of the *FC1 Dataset*. The ESN is able to capture the overall trend and ends at the same voltage level as the experimental data after generating 2961 iterative predictions. The seasonal component of the *FC2 Dataset*, depicted in Figure 27, is well predicted by the ESN with a RMSE of 0.00056. Although the amplitude of the repeating pattern is sometimes underpredicted, this is likely due to the stable ESN model developed. For the final voltage component of the *FC2 Dataset*, the residual, the ESN faces difficulties in predicting the spikes in the time-series. However, the overall time-series prediction remains a sufficient estimate. In Figure 29, the total stack voltage prediction is compared with the experimental time-series. This comparison shows that the ESN can accurately predict the trend over 2961 iterative predictions. However, it has its limitations in terms of predicting voltage recoveries. The RMSE of all individual voltage components and total stack voltage predictions can be reviewed in Table 5.

Table 5
Root-mean-square error of predicted voltage degradation data for decomposed and reconstructed signal of dataset FC1 and FC2 with Echo State Network.

RMSE	*Dataset FC1*	*Dataset FC2*
Type of voltage signal	*ESN*	*ESN*
Trend	0.01283	0.06576
Seasonality	0.00038	0.00056
Residual	0.00706	0.01597
Total	0.08063	0.06428

This approach has demonstrated that current and voltage degradation in PEM fuel cells can be accurately predicted 125 hr in advance without the need for additional parameter measurements such as incoming hydrogen pressure or coolant temperature. This simplifies the monitoring requirements for PEM fuel cells, as only the the current and total stack voltage need to be tracked by internal sensors during normal operations. By relying solely on current and voltage measurements, this method is broadly applicable to various PEM fuel cells.

4.3. *Membrane thickness modelling and prediction*

For the *FC1 Dataset*, the results of the empirical model, semi-empirical model, and their average are presented in Figure 30a, Figure 30b, and Figure 30c, respectively. The initial membrane thickness is $1.5 \times 10^{-5} m$, which degrades quadratically for the empirical model and linearly for the semi-empirical model, resulting in a somewhat quadratic trend for the average degradation. Similar results are obtained for the *FC2 Dataset*, with corresponding results of the empirical model, semi-empirical model, and their average presented in Figure 30d, Figure 30e, and Figure 30f, respectively.

The critical membrane thickness, defined as $1.5 \times 10^{-6} m$ (10% of the initial membrane thickness), is not reached in either dataset. The membrane thickness degradation of the *FC2 Dataset* within 1000 hr is comparable to that of the *FC1 Dataset* within 1154, indicating slightly faster degradation under quasi-dynamic operating conditions compared to static conditions. Linear regression successfully predicts the trend of membrane degradation, with small discrepancies noted in the empirical model predictions, as shown in Figure 30a and Figure 30d. However, the largest discrepancies between the modelled and predicted membrane degradation are observed in the semi-empirical model for the *FC2 Dataset*, as seen in Figure 30e, possibly due to the limitations of the linear regression technique.

4.4. *Forecast remaining useful life*

The RUL results based solely on predicted voltage degradation are presented in Figure 31a, which meet the $\alpha - \lambda$ accuracy up to 125 hr ahead. Although the RUL prediction crosses the $\alpha - \lambda$ accuracy line at the EoL, this indicates that a conservative estimation where the predicted RUL is shorter than the actual RUL. For these predictions, voltage

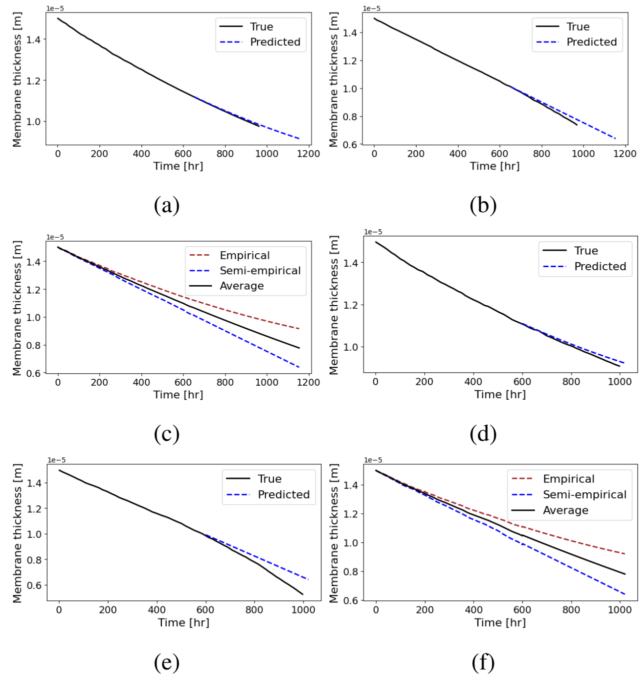

Figure 30: Membrane thickness degradation average of all five-cells, obtained by degradation model and linear regression. Degradation results obtained by: (a) Empirical model on *FC1 Dataset*, (b) Semi-empirical model on *FC1 Dataset*, (c) Average of both models on *FC1 Dataset*, (d) Empirical model on *FC2 Dataset*, (e) Semi-empirical model on *FC2 Dataset*, (f) Average of both models on *FC2 Dataset*.

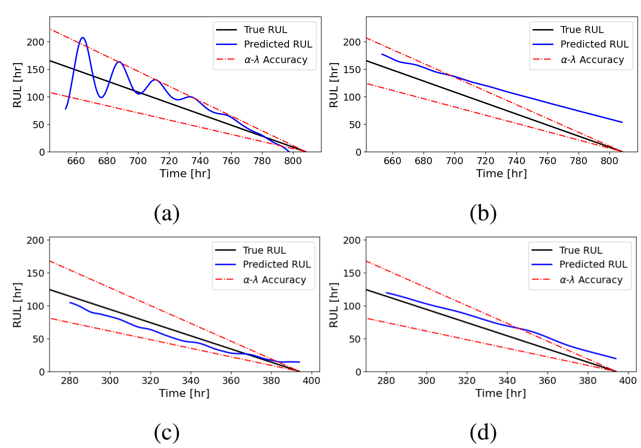

Figure 31: Remaining Useful Life (RUL) initial allowed error of 35% to define $\alpha - \lambda$ accuracy, and RUL prediction with linear regression of: (a) *FC1 Dataset* based on forecast of voltage degradation 125 hr ahead, (b) *FC1 Dataset* based on forecast of membrane thickness and voltage degradation 125 hr ahead, (c) *FC2 Dataset* based on forecast of voltage degradation 125 hr ahead, and (d) *FC2 Dataset* based on forecast of membrane thickness and voltage degradation 125 hr ahead.

degradation is forecast 125 hr in advance, providing a PH that is 25 hr longer than the most advanced method of Li et al. [19]. However, the RUL that incorporate additional membrane thickness degradation data do not achieve the same

PH of 125 hr, as seen in Figure 31b. Despite the membrane being the most critical component of the PEM fuel cell, these predictions overestimate the RUL. This discrepancy may be due to averaging the membrane thickness degradation across all five cells into a single value. Not all cells experience the same level of degradation; for example, Liu et al. [66] noted that cell 1's membrane thickness degradation is $2.0 \times 10^{-6} m$ greater than that of cell 5. Consequently, the impact of cell 1's degradation on the total stack voltage is not accurately reflected in the average membrane thickness value, leading to underestimation of the actual severity of degradation. For the *FC2 Dataset*, similar results are obtained, as shown in Figure 31c and Figure 31d. However, there is a notable discrepancy in Figure 31c, where the predicted RUL crosses the $\alpha - \lambda$ accuracy line close to the EoL with an error of 19.4 hr. This error is considered acceptable, but it raises questions about whether the PH of 125 hr can be confidently applied to the *FC2 Dataset*.

5. Conclusion

This study presents an approach for predicting the degradation of Proton-exchange Membrane (PEM) fuel cells by decomposing current time-series data from the *FC1* and *FC2* Datasets into trend, seasonal, and residual components using Seasonal and Trend decomposition via LOESS (STL). These components were predicted using pre-configured Long Short-term Memory (LSTM) Network and optimised Echo State Network (ESN) models, enabling accurate forecasts 125 hr ahead. Our results show the ESN outperforms in trend prediction, capturing the baseline and adapting quickly, even under quasi-dynamic conditions. Conversely, the LSTM is more effective for seasonal and residual predictions. Both models struggled with anomalies from interruptions in the durability tests due to characterisation tests.

For voltage predictions, the ESN was solely applied, leveraging the predicted current components to forecast voltage trends. The ESN effectively captured the overall voltage degradation trend over extended iterative predictions for both datasets, although it faced challenges in predicting voltage recoveries. This approach required no additional experimental voltage data after the initial training and validation phases, highlighting the ESN's capability for iterative prediction stability.

The study also explored membrane thickness degradation using empirical and semi-empirical models based on experimental data. Linear regression was applied to predict membrane thickness trends, which were averaged across all five cells in the PEM fuel cell. The degradation trends showed that the critical membrane thickness was not reached within the test durations, and the quasi-dynamic conditions of the *FC2 Dataset* led to slightly faster degradation compared to static conditions.

Remaining Useful Life (RUL) forecasts were created based on predicted total stack voltage degradation and combined voltage and membrane thickness degradation. The predictions based solely on voltage degradation met the $\alpha - \lambda$ accuracy up to 125 hr ahead, offering a practical Prognostic Horizon (PH) of 125 hr. However, incorporating membrane thickness data led to overestimations, indicating the complexity of modelling individual cell degradation dynamics.

In summary, this research demonstrates that current and voltage degradation in PEM fuel cells can be accurately predicted up to 125 hr in advance using STL decomposition and a LSTM coupled with an ESN, without additional parameter measurements. This simplifies monitoring requirements and provides a broadly applicable method for various PEM fuel cells. Future work should focus on refining models to better capture individual cell degradation dynamics and extending the approach to other fuel cell types and operating conditions, thereby enhancing the reliability and efficiency of fuel cell systems.

6. Future Work

This study explored the use of Echo State Networks (ESNs) for generating iterative predictions based on time-series data from Proton-exchange Membrane (PEM) fuel cells. The current predictions are constrained by the availability of only two datasets from the FCLAB Research Federation (FR CNRS 3539). To extend this work to degradation predictions for PEM fuel cells used in regional aircraft, it is crucial to conduct durability or accelerated stress tests under relevant operating conditions.

Future research should focus on several key advancements beyond conducting these tests. First, developing a Generative Adversarial Network (GAN) to augment data across static, quasi-dynamic, and dynamic operating conditions is crucial. This GAN could be tailored to specific mission profiles, enabling the generation of datasets that align with current profiles. Additionally, a GAN could be developed to create polarisation curves, building on the approach of Morizet et al. [91], which would streamline the fuel cell stack delivery process and reduce time-to-market.

Beyond data augmentation, the proposed methodology should be expanded to provide actionable maintenance recommendations, including strategies for fuel cell recovery through characterisation tests. On the ESN front, it is important to apply multiple ESNs with varying hyperparameters to assess prediction uncertainty and optimise hyperparameter settings. By averaging predictions from different ESN configurations, we can provide more accurate forecasts with confidence intervals.

Regarding membrane degradation, while current models offer useful insights, they are limited by their assumptions. For PEM fuel cells utilised in different applications, such as regional aircraft, developing tailored empirical and semi-empirical models to better capture membrane thickness degradation is advisable. If such specific applications are not relevant, the impact of these efforts may be minimal.

Acknowledgements

I would like to thank Hendrie Derking from Cryoworld for connecting me with ZAL Center of Applied Aeronautical Research GmbH. Additionally, I am grateful to my daily supervisor, Márcia Baptista from Delft University of Technology, for her guidance and encouragement. I am also deeply thankful to Holger Kuhn, Sebastian Altmann, Leonid Lichtenstein, and Roland Gerhards for the opportunity and support to conduct this research at ZAL. Furthermore, I would like to thank my colleagues, Tuan Nguyen, Louis-Marie Audoin, Sai Vijay Siva Prasad, Fynn Schroeder, Tobias Riedel, and Soeren Huss, for their valuable discussions and assistance with various experiments related to my research.

I would also like to express my gratitude to my parents for their support during my educational journey. They have shown me how to push myself to work hard and the importance of perseverance. Their encouragement has given me the opportunity to become the first person in our family to attend university. Lastly, I want to thank my girlfriend, Lyana Usa, for her unconditional love and support. I will never forget her ability to lift my moods and stand by me during my toughest moments.

CRediT authorship contribution statement

Matthew Georgio Dekkers: Conceptualisation of this study, Methodology, Software, Investigation, Validation, Writing - review & editing.

References

[1] Clean Aviation. Strategic Research and Innovation Agenda, 12 2021. URL https://clean-aviation.eu/sites/default/files/2022-01/CAJU-GB-2021-12-16-SRIA_en.pdf.

[2] McKinsey. Hydrogen powered aviation: A fact-based study of hydrogen technology, economics, and climate impact by 2050. 2020. doi: 10.2843/766989.

[3] C Hartmann, J K Noland, R Nilssen, and R Mellerud. Dual Use of Liquid Hydrogen in a Next-Generation PEMFC-Powered Regional Aircraft with Superconducting Propulsion. *IEEE Transactions on Transportation Electrification*, 8(4):4760–4778, 2022. ISSN 23327782 (ISSN). doi: 10.1109/TTE.2022.3170827.

[4] M Schröder, F Becker, and C Gentner. Optimal design of proton exchange membrane fuel cell systems for regional aircraft. *Energy Conversion and Management*, 308, 2024. ISSN 01968904 (ISSN). doi: 10.1016/j.enconman.2024.118338.

[5] Georgi Atanasov. EXACT Mid Term Review: 70 PAX Fuel Cell Aircraft D70-FCLH2-2040, 3 2022. URL https://elib.dlr.de/193115/1/EXACT_MTR_D70FCLH2.pdf.

[6] Yifu Zhang, Zunyan Hu, Liangfei Xu, Huize Liu, Kang Ye, Jianqiu Li, and Minggao Ouyang. Fuel cell system for aviation applications: Modeling, parameter sensitivity, and control. *Energy Conversion and Management*, 312:118555, 7 2024. ISSN 0196-8904. doi: 10.1016/J.ENCONMAN.2024.118555.

[7] T L Kösters, A G von Schweinitz, M Heere, J Friedrichs, and X Gao. Experimental study and simulations of hydrogen cooling effectiveness for aviation PEM fuel cells. *Scientific Reports*, 13(1), 2023. ISSN 20452322 (ISSN). doi: 10.1038/s41598-023-49309-5.

[8] Z Hua, Z Zheng, E Pahon, M.-C. Péra, and F Gao. Remaining useful life prediction of PEMFC systems under dynamic operating conditions. *Energy Conversion and Management*, 231, 2021. ISSN 01968904 (ISSN). doi: 10.1016/j.enconman.2021.113825.

[9] S Kazula, S de Graaf, and L Enghardt. Review of fuel cell technologies and evaluation of their potential and challenges for electrified propulsion systems in commercial aviation. *Journal of the Global Power and Propulsion Society*, 7:43–57, 2023. ISSN 25153080 (ISSN). doi: 10.33737/jgpps/158036.

[10] PowerCell Group. PowerCellution P Stack, 2023. URL https://powercellgroup.com/wp-content/uploads/2023/10/p-stack-v-222.pdf.

[11] Rolls-Royce. AE 3007 Engine Embraer ERJ Lifetime, 10 2017. URL https://www.rolls-royce.com/~/media/Files/R/Rolls-Royce/documents/civil-aerospace-downloads/AE-3007-infographic-24-10-17.pdf.

[12] J. Z. Sikorska, M. Hodkiewicz, and L. Ma. Prognostic modelling options for remaining useful life estimation by industry. *Mechanical Systems and Signal Processing*, 25(5):1803–1836, 7 2011. ISSN 0888-3270. doi: 10.1016/J.YMSSP.2010.11.018.

[13] Y Alomari, M Andó, and M L Baptista. Advancing aircraft engine RUL predictions: an interpretable integrated approach of feature engineering and aggregated feature importance. *Scientific Reports*, 13(1), 2023. ISSN 20452322 (ISSN). doi: 10.1038/s41598-023-40315-1. URL https://www.scopus.com/inward/record.uri?eid=2-s2.0-85168393847&doi=10.1038%2fs41598-023-40315-1&partnerID=40&md5=e94a51e8ce52eb60f8feccce70892d2c.

[14] Marine Jouin, Rafael Gouriveau, Daniel Hissel, Marie Cécile Péra, and Noureddine Zerhouni. Degradations analysis and aging modeling for health assessment and prognostics of PEMFC. *Reliability Engineering & System Safety*, 148:78–95, 4 2016. ISSN 0951-8320. doi: 10.1016/J.RESS.2015.12.003.

[15] Zhiguang Hua, Zhixue Zheng, Elodie Pahon, Marie Cécile Péra, and Fei Gao. A review on lifetime prediction of proton exchange membrane fuel cells system, 5 2022. ISSN 03787753.

[16] R Gouriveau, M Hilairet, D Hissel, S Jemei, M Jouin, E Lechartier, S Morando, E Pahon, M C Pera, and N Zerhouni. IEEE PHM 2014 data challenge: Outline, experiments, scoring of results, winners. In *Proc. IEEE Conf. Prognostics Health Management*, pages 1–6, 2014. URL https://search-data.ubfc.fr/fclab/FR-18008901306731-2021-07-19_IEEE-PHM-Data-Challenge-2014.html#gen.

[17] Hao Liu, Jian Chen, Daniel Hissel, Jianguo Lu, Ming Hou, and Zhigang Shao. Prognostics methods and degradation indexes of proton exchange membrane fuel cells: A review. *Renewable and Sustainable Energy Reviews*, 123:109721, 5 2020. ISSN 1364-0321. doi: 10.1016/J.RSER.2020.109721.

[18] M Jouin, R Gouriveau, D Hissel, M.-C. Péra, and N Zerhouni. Prognostics of PEM fuel cell in a particle filtering framework. *International Journal of Hydrogen Energy*, 39(1):481–494, 2014. ISSN 03603199 (ISSN). doi: 10.1016/j.ijhydene.2013.10.054. URL https://www.scopus.com/inward/record.uri?eid=2-s2.0-84890393879&doi=10.1016%2fj.ijhydene.2013.10.054&partnerID=40&md5=96faa485c64de6833fbd2d004b1cc94c.

[19] Songyang Li, Weiling Luan, Chang Wang, Ying Chen, and Zixian Zhuang. Degradation prediction of proton exchange membrane fuel cell based on Bi-LSTM-GRU and ESN fusion prognostic framework. *International Journal of Hydrogen Energy*, 47(78):33466–33478, 9 2022. ISSN 0360-3199. doi: 10.1016/J.IJHYDENE.2022.07.230.

[20] Khaled Benaggoune, Meiling Yue, Samir Jemei, and Noureddine Zerhouni. A data-driven method for multi-step-ahead prediction and long-term prognostics of proton exchange membrane fuel cell. *Applied Energy*, 313, 5 2022. ISSN 03062619. doi: 10.1016/j.apenergy.2022.118835.

[21] K Sahajpal, K P S Rana, and V Kumar. Accurate long-term prognostics of proton exchange membrane fuel cells using recurrent and convolutional neural networks. *International Journal of Hydrogen Energy*, 48(78):30532–30555, 2023. ISSN 03603199 (ISSN). doi: 10.1016/j.ijhydene.2023.04.143. URL https://www.scopus.com/inward/record.uri?eid=2-s2.0-85158106768&doi=10.1016%2fj.ijhydene.2023.04.143&partnerID=40&md5=50fb5c3fd7af2f694aee8a0953afde0f.

[22] A Saxena, J Celaya, B Saha, S Saha, and K Goebe. On applying the prognostic performance metrics. In *Annual Conference of the Prognostics and Health Management Society, PHM 2009*. Prognostics and Health Management Society, 2009. ISBN 978-193626300-4 (ISBN). URL https://www.scopus.com/inward/record.uri?eid=2-s2.0-84920568894&partnerID=40&md5=5dff11933797f7a1b7c748eea0f223e9.

[23] A Saxena, J Celaya, B Saha, S Saha, and K Goebel. Evaluating prognostics performance for algorithms incorporating uncertainty estimates. In *IEEE Aerospace Conference Proceedings*, 2010. ISBN 1095323X (ISSN); 978-142443888-4 (ISBN). doi: 10.1109/AERO.2010.5446828. URL https://www.scopus.com/inward/record.uri?eid=2-s2.0-77952832979&doi=10.1109%2fAERO.2010.5446828&partnerID=40&md5=c5e5cad030cca6b821149f382a3032a2.

[24] R Zhang, T Chen, F Xiao, and J Luo. Bi-directional gated recurrent unit recurrent neural networks for failure prognosis of proton exchange membrane fuel cells. *International Journal of Hydrogen Energy*, 47(77):33027–33038, 2022. ISSN 03603199 (ISSN). doi: 10.1016/j.ijhydene.2022.07.188. URL https://www.scopus.com/inward/record.uri?eid=2-s2.0-85136093004&doi=10.1016%2fj.ijhydene.2022.07.188&partnerID=40&md5=0f63b7ab144f973f27eadd60490e263c.

[25] Z Xia, Y Wang, L Ma, Y Zhu, Y Li, J Tao, and G Tian. A Hybrid Prognostic Method for Proton-Exchange-Membrane Fuel Cell with Decomposition Forecasting Framework Based on AEKF and LSTM. *Sensors*, 23(1), 2023. ISSN 14248220 (ISSN). doi: 10.3390/s23010166. URL https://www.scopus.com/inward/record.uri?eid=2-s2.0-85145968628&doi=10.3390%2fs23010166&partnerID=40&md5=46cb623035fbf14844141f0d025a6972.

[26] Herbert Jaeger. The “echo state” approach to analysing and training recurrent neural networks-with an erratum note. *Bonn, Germany: German National Research Center for Information Technology GMD Technical Report*, 148(34):13, 2001.

[27] S Ghosh, K Nakajima, T Krisnanda, K Fujii, and T C H Liew. Quantum Neuromorphic Computing with Reservoir Computing Networks. *Advanced Quantum Technologies*, 4(9), 2021. ISSN 25119044 (ISSN). doi: 10.1002/qute.202100053. URL https://www.scopus.com/inward/record.uri?eid=2-s2.0-85109383683&doi=10.1002%2fqute.202100053&partnerID=40&md5=e7d4a6a4f19501e2681da230966b1ab5.

[28] K Bai, L Liu, and Y Yi. Spatial-Temporal Hybrid Neural Network with Computing-in-Memory Architecture. *IEEE Transactions on Circuits and Systems I: Regular Papers*, 68(7):2850–2862, 2021. ISSN 15498328 (ISSN). doi: 10.1109/TCSI.2021.3071956. URL https://www.scopus.com/inward/record.uri?eid=2-s2.0-85104686417&doi=10.1109%2fTCSI.2021.3071956&partnerID=40&md5=b930875a65200a7adae72b2890a3daa1.

[29] Graham E Rowlands, Minh-Hai Nguyen, Guilhem J Ribeill, Andrew P Wagner, Luke C G Govia, Wendson A S Barbosa, Daniel J Gauthier, and Thomas A Ohki. Reservoir Computing with Superconducting Electronics, 2021. URL https://arxiv.org/abs/2103.02522.

[30] K Mustaqeem, A El Saddik, F S Alotaibi, and N T Pham. AAD-Net: Advanced end-to-end signal processing system for human emotion detection & recognition using attention-based deep echo state network. *Knowledge-Based Systems*, 270, 2023. ISSN 09507051 (ISSN). doi: 10.1016/j.knosys.2023.110525. URL https://www.scopus.com/inward/record.uri?eid=2-s2.0-85152592535&doi=10.1016%2fj.knosys.2023.110525&partnerID=40&md5=369c9b76daf5a6856790d1bfcb8350f9.

[31] R Soltani, E Benmohamed, and H Ltifi. Newman-Watts-Strogatz topology in deep echo state networks for speech emotion recognition. *Engineering Applications of Artificial Intelligence*, 133, 2024. ISSN 09521976 (ISSN). doi: 10.1016/j.engappai.2024.108293. URL https://www.scopus.com/inward/record.uri?eid=2-s2.0-85188726397&doi=10.1016%2fj.engappai.2024.108293&partnerID=40&md5=a5f6f88ab033858131d131ba68018087.

[32] Zhiguang Hua. *Lifespan Prediction of Proton Exchange Membrane Fuel Cell System*. PhD thesis, Université Bourgogne Franche-Comté, 12 2021. URL https://theses.hal.science/tel-03793342.

[33] Z Deng, Q Chen, L Zhang, K Zhou, Y Zong, H Liu, J Li, and L Ma. Degradation Prediction of PEMFCs Using Stacked Echo State Network Based on Genetic Algorithm Optimization. *IEEE Transactions on Transportation Electrification*, 8(1):1454–1466, 2022. ISSN 23327782 (ISSN). doi: 10.1109/TTE.2021.3111906. URL https://www.scopus.com/inward/record.uri?eid=2-s2.0-85115191402&doi=10.1109%2fTTE.2021.3111906&partnerID=40&md5=043f2598937f3c22d1fbc11b5889d7d1.

[34] J Jin, Y Chen, C Xie, and F Wu. Degradation prediction of PEMFC based on data-driven method with adaptive fuzzy sampling. *IEEE Transactions on Transportation Electrification*, page 1, 2023. ISSN 23327782 (ISSN). doi: 10.1109/TTE.2023.3296719. URL https://www.scopus.com/inward/record.uri?eid=2-s2.0-85165239853&doi=10.1109%2fTTE.2023.3296719&partnerID=40&md5=63a3040adb0ab0bed8211e2cf241c9c6.

[35] L Karpenko-Jereb, C Sternig, C Fink, and R Tatschl. Membrane degradation model for 3D CFD analysis of fuel cell performance as a function of time. *International Journal of Hydrogen Energy*, 41(31):13644–13656, 2016. ISSN 03603199 (ISSN). doi: 10.1016/j.ijhydene.2016.05.229. URL https://www.scopus.com/inward/record.uri?eid=2-s2.0-84991813348&doi=10.1016%2fj.ijhydene.2016.05.229&partnerID=40&md5=700eb133a59003e0b5b3895cf6e07400.

[36] M. Chandesris, R. Vincent, L. Guetaz, J. S. Roch, D. Thoby, and M. Quinaud. Membrane degradation in PEM fuel cells: From experimental results to semi-empirical degradation laws. *International Journal of Hydrogen Energy*, 42(12):8139–8149, 3 2017. ISSN 0360-3199. doi: 10.1016/J.IJHYDENE.2017.02.116.

[37] R. Cleveland, W. Cleveland, J. McRae, and I. Terpennin. STL: A seasonal-trend decomposition procedure based on loess. *J Off Stat*, 6: 3–73, 1990.

[38] M Theodosiou. Disaggregation & aggregation of time series components: A hybrid forecasting approach using generalized regression neural networks and the theta method. *Neurocomputing*, 74(6):896–905, 2011. ISSN 09252312 (ISSN). doi: 10.1016/j.neucom.2010.10.013. URL https://www.scopus.com/inward/record.uri?eid=2-s2.0-79751533755&doi=10.1016%2fj.neucom.2010.10.013&partnerID=40&md5=05437844c028d7d2279a56d4deacf5f9.

[39] Z Xu, L Mo, J Zhou, W Fang, and H Qin. Stepwise decomposition-integration-prediction framework for runoff forecasting considering boundary correction. *Science of the Total Environment*, 851, 2022. ISSN 00489697 (ISSN). doi: 10.1016/j.scitotenv.2022.158342. URL https://www.scopus.com/inward/record.uri?eid=2-s2.0-85137059487&doi=10.1016%2fj.scitotenv.2022.158342&partnerID=40&md5=338000828f85dad3e8d3331092565dcb.

[40] W Li and X Jiang. Prediction of air pollutant concentrations based on TCN-BiLSTM-DMAttention with STL decomposition. *Scientific Reports*, 13(1), 2023. ISSN 20452322 (ISSN). doi: 10.1038/s41598-023-31569-w. URL https://www.scopus.com/inward/record.uri?eid=2-s2.0-85150818915&doi=10.1038%2fs41598-023-31569-w&partnerID=40&md5=1bfdc26ff51e6558ce854ecedfd0e393.

[41] Jakob Aungiers and Christian Clauss. Time series prediction using lstm deep neural networks, 2018. URL https://github.com/jaungiers/LSTM-Neural-Network-for-Time-Series-Prediction.

[42] Takuya Akiba, Shotaro Sano, Toshihiko Yanase, Takeru Ohta, and Masanori Koyama. Optuna: A Next-generation Hyperparameter Optimization Framework. In *Proceedings of the 25th ACM SIGKDD International Conference on Knowledge Discovery and Data Mining*, 2019.

[43] Jian Zuo, Hong Lv, Daming Zhou, Qiong Xue, Liming Jin, Wei Zhou, Daijun Yang, and Cunman Zhang. Deep learning based prognostic framework towards proton exchange membrane fuel cell for automotive application. *Applied Energy*, 281:115937, 1 2021. ISSN 0306-2619. doi: 10.1016/J.APENERGY.2020.115937.

[44] B Long, K Wu, P Li, and M Li. A Novel Remaining Useful Life Prediction Method for Hydrogen Fuel Cells Based on the Gated Recurrent Unit Neural Network. *Applied Sciences (Switzerland)*, 12(1), 2022. ISSN 20763417 (ISSN). doi: 10.3390/app12010432. URL https://www.scopus.com/inward/record.uri?eid=2-s2.0-85122160366&doi=10.3390%2fapp12010432&partnerID=40&md5=ef7b25dc5898513ee71824c7c8029367.

[45] J Liu, Q Li, W Chen, Y Yan, Y Qiu, and T Cao. Remaining useful life prediction of PEMFC based on long short-term memory recurrent neural networks. *International Journal*

of Hydrogen Energy, pages 5470–5480, 2019. ISSN 03603199 (ISSN). doi: 10.1016/j.ijhydene.2018.10.042. URL https://www.scopus.com/inward/record.uri?eid=2-s2.0-85055506236&doi=10.1016%2fj.ijhydene.2018.10.042&partnerID=40&md5=46ac787508c1d2834d7539d4fbefa313.

[46] C Wang, M Dou, Z Li, R Outbib, D Zhao, and B Liang. A fusion prognostics strategy for fuel cells operating under dynamic conditions. *eTransportation*, 12, 2022. ISSN 25901168 (ISSN). doi: 10.1016/j.etran.2022.100166. URL https://www.scopus.com/inward/record.uri?eid=2-s2.0-85129556150&doi=10.1016%2fj.etran.2022.100166&partnerID=40&md5=10da4f18bf64b5578ae63b2aeceee15c.

[47] Chang Liu, Jiabin Shen, Zhen Dong, Qiaohui He, and Xiaowei Zhao. Accuracy improvement of fuel cell prognostics based on voltage prediction. *International Journal of Hydrogen Energy*, 58:839–851, 3 2024. ISSN 0360-3199. doi: 10.1016/J.IJHYDENE.2024.01.238.

[48] Y Peng, T Chen, F Xiao, and S Zhang. Remaining useful lifetime prediction methods of proton exchange membrane fuel cell based on convolutional neural network-long short-term memory and convolutional neural network-bidirectional long short-term memory. *Fuel Cells*, 23(1):75–87, 2023. ISSN 16156846 (ISSN). doi: 10.1002/fuce.202200106. URL https://www.scopus.com/inward/record.uri?eid=2-s2.0-85143508979&doi=10.1002%2ffuce.202200106&partnerID=40&md5=11b7ef904acaea702b294e8c96eec35d.

[49] J Lv, Z Yu, H Zhang, G Sun, P Muhl, and J Liu. Transformer Based Long-Term Prognostics for Dynamic Operating PEM Fuel Cells. *IEEE Transactions on Transportation Electrification*, page 1, 2023. ISSN 23327782 (ISSN). doi: 10.1109/TTE.2023.3266803. URL https://www.scopus.com/inward/record.uri?eid=2-s2.0-85153343859&doi=10.1109%2fTTE.2023.3266803&partnerID=40&md5=1ef460c73f6042cb7a2622925274db0d.

[50] X Tang, X Qin, K Wei, and S Xu. A novel online degradation model for proton exchange membrane fuel cell based on online transfer learning. *International Journal of Hydrogen Energy*, 48(36):13617–13632, 2023. ISSN 03603199 (ISSN). doi: 10.1016/j.ijhydene.2022.12.260. URL https://www.scopus.com/inward/record.uri?eid=2-s2.0-85146307477&doi=10.1016%2fj.ijhydene.2022.12.260&partnerID=40&md5=6795abba4cc90fcf8e88a16a7d0009a2.

[51] Shengxiang Fu, Dongfang Zhang, Yao Xiao, and Chunhua Zheng. A non-stationary transformer-based remaining useful life prediction method for proton exchange membrane fuel cells. *International Journal of Hydrogen Energy*, 60:1121–1133, 3 2024. ISSN 0360-3199. doi: 10.1016/J.IJHYDENE.2024.02.150.

[52] S Morando, S Jemei, D Hissel, R Gouriveau, and N Zerhouni. Proton exchange membrane fuel cell ageing forecasting algorithm based on Echo State Network. *International Journal of Hydrogen Energy*, 42(2):1472–1480, 2017. ISSN 03603199 (ISSN). doi: 10.1016/j.ijhydene.2016.05.286. URL https://www.scopus.com/inward/record.uri?eid=2-s2.0-85001955801&doi=10.1016%2fj.ijhydene.2016.05.286&partnerID=40&md5=0f2b5c9f30d0e0bdc2cc5fe92bfd867f.

[53] L Vichard, F Harel, A Ravey, P Venet, and D Hissel. Degradation prediction of PEM fuel cell based on artificial intelligence. *International Journal of Hydrogen Energy*, 45(29):14953–14963, 2020. ISSN 03603199 (ISSN). doi: 10.1016/j.ijhydene.2020.03.209. URL https://www.scopus.com/inward/record.uri?eid=2-s2.0-85083317235&doi=10.1016%2fj.ijhydene.2020.03.209&partnerID=40&md5=10924ae3170b264cce2e9960a3d47168.

[54] C Wang, Z Li, R Outbib, M Dou, and D Zhao. A novel long short-term memory networks-based data-driven prognostic strategy for proton exchange membrane fuel cells. *International Journal of Hydrogen Energy*, 47(18):10395–10408, 2022. ISSN 03603199 (ISSN). doi: 10.1016/j.ijhydene.2022.01.121. URL https://www.scopus.com/inward/record.uri?eid=2-s2.0-85124176684&doi=10.1016%2fj.ijhydene.2022.01.121&partnerID=40&md5=5f52e4b1e249ac852f80c1faf8d36fdb.

[55] Min Yan, Can Huang, Peter Bienstman, Peter Tino, Wei Lin, and Jie Sun. Emerging opportunities and challenges for the future of reservoir computing. *Nature Communications*, 15(1):2056, 2024. ISSN 2041-1723. doi: 10.1038/s41467-024-45187-1. URL https://doi.org/10.1038/s41467-024-45187-1.

[56] R Mezzi, N Yousfi-Steiner, M C Péra, D Hissel, and L Larger. An Echo State Network for fuel cell lifetime prediction under a dynamic micro-cogeneration load profile. *Applied Energy*, 283, 2021. ISSN 03062619 (ISSN). doi: 10.1016/j.apenergy.2020.116297. URL https://www.scopus.com/inward/record.uri?eid=2-s2.0-85097452614&doi=10.1016%2fj.apenergy.2020.116297&partnerID=40&md5=d9b1b8c0f9c18736511e2d14ab66ce98.

[57] M Lukoševičius. A practical guide to applying echo state networks. *Lecture Notes in Computer Science (including subseries Lecture Notes in Artificial Intelligence and Lecture Notes in Bioinformatics)*, 7700 LECTURE NO:659–686, 2012. ISSN 03029743 (ISSN); 978-364235288-1 (ISBN). doi: 10.1007/978-3-642-35289-8{_}36. URL https://www.scopus.com/inward/record.uri?eid=2-s2.0-84872502995&doi=10.1007%2f978-3-642-35289-8_36&partnerID=40&md5=b6f6f3dc73bb8b31af7adca4d96b81b7.

[58] Cesar H. Valencia, Marley M.B.R. Vellasco, and Karla Figueiredo. Echo State Networks: Novel reservoir selection and hyperparameter optimization model for time series forecasting. *Neurocomputing*, 545: 126317, 8 2023. ISSN 0925-2312. doi: 10.1016/J.NEUCOM.2023.126317.

[59] R Mezzi, S Morando, N Y Steiner, M C Péra, D Hissel, and L Larger. Multi-reservoir echo state network for proton exchange membrane fuel cell remaining useful life prediction. In *Proceedings: IECON 2018 - 44th Annual Conference of the IEEE Industrial Electronics Society*, pages 1872–1877. Institute of Electrical and Electronics Engineers Inc., 2018. ISBN 978-150906684-1 (ISBN). doi: 10.1109/IECON.2018.8591345. URL https://www.scopus.com/inward/record.uri?eid=2-s2.0-85061533100&doi=10.1109%2fIECON.2018.8591345&partnerID=40&md5=04a02c86c1071ae3b9c8316e82140507.

[60] Shisheng Zhong, Xiaolong Xie, Lin Lin, and Fang Wang. Genetic algorithm optimized double-reservoir echo state network for multi-regime time series prediction. *Neurocomputing*, 238:191–204, 5 2017. ISSN 0925-2312. doi: 10.1016/J.NEUCOM.2017.01.053.

[61] Z Hua, Z Zheng, E Pahon, M.-C. Pera, and F Gao. Multi-Timescale Lifespan Prediction for PEMFC Systems under Dynamic Operating Conditions. *IEEE Transactions on Transportation Electrification*, 8(1):345–355, 2022. ISSN 23327782 (ISSN). doi: 10.1109/TTE.2021.3103921. URL https://www.scopus.com/inward/record.uri?eid=2-s2.0-85127531957&doi=10.1109%2fTTE.2021.3103921&partnerID=40&md5=1ed04a914d0de7b8d104d1d4fdd798d0.

[62] Z Hua, Z Zheng, E Pahon, M.-C. Pera, and F Gao. Lifespan Prediction for Proton Exchange Membrane Fuel Cells Based on Wavelet Transform and Echo State Network. *IEEE Transactions on Transportation Electrification*, 8(1):420–431, 2022. ISSN 23327782 (ISSN). doi: 10.1109/TTE.2021.3121179. URL https://www.scopus.com/inward/record.uri?eid=2-s2.0-85118254862&doi=10.1109%2fTTE.2021.3121179&partnerID=40&md5=9dc32b667b1606562a073b8217487661.

[63] A M González-Zapata, E Tlelo-Cuautle, B Ovilla-Martinez, I Cruz-Vega, and L G De la Fraga. Optimizing Echo State Networks for Enhancing Large Prediction Horizons of Chaotic Time Series. *Mathematics*, 10(20), 2022. ISSN 22277390 (ISSN). doi: 10.3390/math10203886. URL https://www.scopus.com/inward/record.uri?eid=2-s2.0-85140641105&doi=10.3390%2fmath10203886&partnerID=40&md5=9bf4623aad125871ce60beec1ca3ab6d.

[64] Hiroyasu Ando and Hanten Chang. Road traffic reservoir computing. Technical report, 2019.

[65] Craig S. Gittleman, Frank D. Coms, and Yeh Hung Lai. Membrane Durability: Physical and Chemical Degradation. *Polymer Electrolyte Fuel Cell Degradation*, pages 15–88, 1 2012. doi: 10.1016/B978-0-12-386936-4.10002-8.

[66] Hao Liu, Jian Chen, Daniel Hissel, Ming Hou, and Zhigang Shao. A multi-scale hybrid degradation index for proton exchange membrane fuel cells. *Journal of Power Sources*, 437:226916, 10 2019. ISSN 0378-7753. doi: 10.1016/J.JPOWSOUR.2019.226916.

[67] K H Wong and E Kjeang. Mitigation of chemical membrane degradation in fuel cells: Understanding the effect of cell voltage and iron ion redox cycle. *ChemSusChem*, 8(6):1072–1082, 2015. ISSN 18645631 (ISSN). doi: 10.1002/cssc.201402957. URL https://www.scopus.com/inward/record.uri?eid=2-s2.0-84924942469&doi=10.1002%2fcssc.201402957&partnerID=40&md5=fdf7b78f0bc5a0f628f4f378d96e31c6.

[68] R Borup, J Meyers, B Pivovar, Y S Kim, R Mukundan, N Garland, D Myers, M Wilson, F Garzon, D Wood, P Zelenay, K More, K Stroh, T Zawodzinski, J Boncella, J E McGrath, M Inaba, K Miyatake, M Hori, K Ota, Z Ogumi, S Miyata, A Nishikata, Z Siroma, Y Uchimoto, K Yasuda, K.-I. Kimijima, and N Iwashita. Scientific aspects of polymer electrolyte fuel cell durability and degradation. *Chemical Reviews*, 107(10):3904–3951, 2007. ISSN 00092665 (ISSN). doi: 10.1021/cr050182l. URL https://www.scopus.com/inward/record.uri?eid=2-s2.0-35748941340&doi=10.1021%2fcr050182l&partnerID=40&md5=4202e567c207a403b580d04823a60073.

[69] J Wu, X Z Yuan, J J Martin, H Wang, J Zhang, J Shen, S Wu, and W Merida. A review of PEM fuel cell durability: Degradation mechanisms and mitigation strategies. *Journal of Power Sources*, 184(1):104–119, 2008. ISSN 03787753 (ISSN). doi: 10.1016/j.jpowsour.2008.06.006. URL https://www.scopus.com/inward/record.uri?eid=2-s2.0-48149094359&doi=10.1016%2fj.jpowsour.2008.06.006&partnerID=40&md5=a590360375f0603136f163cebd1ab3d9.

[70] Adam Z Weber. Gas-Crossover and Membrane-Pinhole Effects in Polymer-Electrolyte Fuel Cells. *Journal of The Electrochemical Society*, 155(6):B521, 2008. ISSN 1945-7111. doi: 10.1149/1.2898130. URL https://dx.doi.org/10.1149/1.2898130.

[71] Yinqi Shen. *Mechanical Degradation of Membrane Electrode Assemblies in Proton Exchange Membrane Fuel Cells*. PhD thesis, 2017. URL http://hdl.handle.net/10012/11990.

[72] D Qiu, L Peng, X Lai, M Ni, and W Lehnert. Mechanical failure and mitigation strategies for the membrane in a proton exchange membrane fuel cell. *Renewable and Sustainable Energy Reviews*, 113, 2019. ISSN 13640321 (ISSN). doi: 10.1016/j.rser.2019.109289. URL https://www.scopus.com/inward/record.uri?eid=2-s2.0-85069628672&doi=10.1016%2fj.rser.2019.109289&partnerID=40&md5=c6985aa07d37fabb252b5ea7b4a2902a.

[73] Soowhan Kim, Byung Ki Ahn, and M. M. Mench. Physical degradation of membrane electrode assemblies undergoing freeze/thaw cycling: Diffusion media effects. *Journal of Power Sources*, 179(1):140–146, 4 2008. ISSN 0378-7753. doi: 10.1016/J.JPOWSOUR.2007.12.114.

[74] C Lee, X Wang, J.-K. Peng, A Katzenberg, R K Ahluwalia, A Kusoglu, S Komini Babu, J S Spendelow, R Mukundan, and R L Borup. Toward a Comprehensive Understanding of Cation Effects in Proton Exchange Membrane Fuel Cells. *ACS Applied Materials and Interfaces*, 14(31):35555–35568, 2022. ISSN 19448244 (ISSN). doi: 10.1021/acsami.2c07085. URL https://www.scopus.com/inward/record.uri?eid=2-s2.0-85135768059&doi=10.1021%2facsami.2c07085&partnerID=40&md5=24f90181c3c0a216e498932979cd312a.

[75] R Singh, P C Sui, K H Wong, E Kjeang, S Knights, and N Djilali. Modeling the effect of chemical membrane degradation on PEMFC performance. *Journal of the Electrochemical Society*, 165(6):F3328–F3336, 2018. ISSN 00134651 (ISSN). doi: 10.1149/2.0351806jes. URL https://www.scopus.com/inward/record.uri?eid=2-s2.0-85046859894&doi=10.1149%2f2.0351806jes&partnerID=40&md5=787447f385eb5a5b4f997ffb75afef41.

[76] Natalia Macauley, Mark Watson, Michael Lauritzen, Shanna Knights, G. Gary Wang, and Erik Kjeang. Empirical membrane lifetime model for heavy duty fuel cell systems. *Journal of Power Sources*, 336:240–250, 12 2016. ISSN 0378-7753. doi: 10.1016/J.JPOWSOUR.2016.10.068.

[77] P Frühwirt, A Kregar, J T Törring, T Katrašnik, and G Gescheidt. Holistic approach to chemical degradation of Nafion membranes in fuel cells: Modelling and predictions. *Physical Chemistry Chemical Physics*, 22(10):5647–5666, 2020. ISSN 14639076 (ISSN). doi: 10.1039/c9cp04986j. URL https://www.scopus.com/inward/record.uri?eid=2-s2.0-85081720658&doi=10.1039%2fc9cp04986j&partnerID=40&md5=7e32f7b9f5d737132bbf1216e04abd05.

[78] M Hinaje, S Raël, P Noiying, D A Nguyen, and B Davat. An equivalent electrical circuit model of proton exchange membrane fuel cells based on mathematical modelling. *Energies*, 5(8):2724–2744, 2012. ISSN 19961073 (ISSN). doi: 10.3390/en5082724. URL https://www.scopus.com/inward/record.uri?eid=2-s2.0-84865783705&doi=10.3390%2fen5082724&partnerID=40&md5=85a260bcbde11a0ac4f6082810815840.

[79] D. Verstraeten, B. Schrauwen, M. D'Haene, and D. Stroobandt. An experimental unification of reservoir computing methods. *Neural Networks*, 20(3):391–403, 4 2007. ISSN 0893-6080. doi: 10.1016/J.NEUNET.2007.04.003.

[80] W Maass, T Natschläger, and H Markram. Real-time computing without stable states: A new framework for neural computation based on perturbations. *Neural Computation*, 14(11):2531–2560, 2002. ISSN 08997667 (ISSN). doi: 10.1162/089976602760407955. URL https://www.scopus.com/inward/record.uri?eid=2-s2.0-0036834701&doi=10.1162%2f089976602760407955&partnerID=40&md5=bd266474cc562ac276ce5de6032dadce.

[81] U D Schiller and J J Steil. Analyzing the weight dynamics of recurrent learning algorithms. *Neurocomputing*, 63(SPEC. ISS.):5–23, 2005. ISSN 09252312 (ISSN). doi: 10.1016/j.neucom.2004.04.006. URL https://www.scopus.com/inward/record.uri?eid=2-s2.0-12144261601&doi=10.1016%2fj.neucom.2004.04.006&partnerID=40&md5=e4b01268f6bf37362f2a5f666694d9d3.

[82] N Trouvain, L Pedrelli, T T Dinh, and X Hinaut. ReservoirPy: An Efficient and User-Friendly Library to Design Echo State Networks. In I Farkaš, P Masulli, and S Wermter, editors, *Lecture Notes in Computer Science (including subseries Lecture Notes in Artificial Intelligence and Lecture Notes in Bioinformatics)*, volume 12397 LNCS, pages 494–505. Springer Science and Business Media Deutschland GmbH, 2020. ISBN 03029743 (ISSN); 978-303061615-1 (ISBN). doi: 10.1007/978-3-030-61616-8{_}40. URL https://www.scopus.com/inward/record.uri?eid=2-s2.0-85094107174&doi=10.1007%2f978-3-030-61616-8_40&partnerID=40&md5=27e97ad53982aaa2a3dce5a529f15fe5.

[83] Herbert Jaeger, Mantas Lukoševičius, Dan Popovici, and Udo Siewert. Optimization and applications of echo state networks with leaky-integrator neurons. *Neural Networks*, 20(3):335–352, 4 2007. ISSN 0893-6080. doi: 10.1016/J.NEUNET.2007.04.016.

[84] Z Zheng, S Morando, M.-C. Pera, D Hissel, L Larger, R Martinenghi, and A Baylon Fuentes. Brain-inspired computational paradigm dedicated to fault diagnosis of PEM fuel cell stack. *International Journal of Hydrogen Energy*, 42(8):5410–5425, 2017. ISSN 03603199 (ISSN). doi: 10.1016/j.ijhydene.2016.11.043. URL https://www.scopus.com/inward/record.uri?eid=2-s2.0-85007496713&doi=10.1016%2fj.ijhydene.2016.11.043&partnerID=40&md5=c77aa63d4a9ebef178f8604c24526cfa.

[85] Shuhei Watanabe. Tree-Structured Parzen Estimator: Understanding Its Algorithm Components and Their Roles for Better Empirical Performance, 2023. URL https://arxiv.org/abs/2304.11127.

[86] R Chandra, S Goyal, and R Gupta. Evaluation of Deep Learning Models for Multi-Step Ahead Time Series Prediction. *IEEE Access*, 9:83105–83123, 2021. ISSN 21693536 (ISSN). doi: 10.1109/ACCESS.2021.3085085. URL https://www.scopus.com/inward/record.uri?eid=2-s2.0-85107341900&doi=10.1109%2fACCESS.2021.3085085&partnerID=40&md5=8f337b31471c63ddd318629ca3aeaed5.

[87] Xiao Zi Yuan, Shengsheng Zhang, Shuai Ban, Cheng Huang, Haijiang Wang, Vengatesan Singara, Michael Fowler, Mathias Schulze, Andrea Haug, K. Andreas Friedrich, and Renate Hiesgen. Degradation of a PEM fuel cell stack with Nafion® membranes of different thicknesses. Part II: Ex situ diagnosis. *Journal of Power Sources*, 205:324–334, 5 2012. ISSN 0378-7753. doi: 10.1016/J.JPOWSOUR.2012.01.074.

[88] Xiao Zi Yuan, Shengsheng Zhang, Haijiang Wang, Jinfeng Wu, Jian Colin Sun, Renate Hiesgen, K. Andreas Friedrich, Mathias Schulze, and Andrea Haug. Degradation of a polymer exchange

membrane fuel cell stack with Nafion® membranes of different thicknesses: Part I. In situ diagnosis. *Journal of Power Sources*, 195(22): 7594–7599, 11 2010. ISSN 0378-7753. doi: 10.1016/J.JPOWSOUR.2010.06.023.

[89] The National Institute of Standards and Technology (NIST). Antoine Equation Parameters; Data from NIST Standard Reference Database 69: NIST Chemistry WebBook, 2023. URL https://webbook.nist.gov/cgi/cbook.cgi?ID=C7732185&Mask=4&Type=ANTOINE&Plot=on#ANTOINE.

[90] Daniel R Stull. Vapor Pressure of Pure Substances. Organic and Inorganic Compounds. *Industrial & Engineering Chemistry*, 39(4): 517–550, 4 1947. ISSN 0019-7866. doi: 10.1021/ie50448a022. URL https://doi.org/10.1021/ie50448a022.

[91] Nicolas Morizet, Perceval Desforges, Christophe Geissler, Elodie Pahon, Samir Jemei, and Daniel Hissel. Time to market reduction for hydrogen fuel cell stacks using Generative Adversarial Networks. *Journal of Power Sources*, 579:233286, 9 2023. ISSN 0378-7753. doi: 10.1016/J.JPOWSOUR.2023.233286.

Part II

Literature Study

1
Summary

This report discusses how long-term prediction on the remaining useful life of proton-exchange membrane (PEM) fuel cells can be further improved. Two main points of improvements are identified: 1) extended prediction horizon of remaining useful life with a multi-step ahead prediction technique based on an echo state network; 2) system and component health indicators that have a relationship to the remaining useful life. Validated degradation models for the most critical components, the membrane and electrode, are explained. Membrane thickness and electrochemical catalyst surface area are identified as health indicators for membrane and electrode, respectively. Available durability datasets from ZAL and FCLAB are discussed. From ZAL, a dataset of 8000 hr with static conditions on a single cell is available. From FCLAB, two datasets are available of 1155 hr and 1021 hr with static and quasi-dynamic conditions, respectively.

2
Introduction

In the aviation industry, hydrogen is regarded as one of the fuels that can be used to meet net-zero emissions [1]. Hydrogen-electric powertrains are considered to be one of the solutions to meet climate goals related to transportation vehicles [2]. One of the largest aircraft manufacturers, Airbus, has the ambition to bring hydrogen-powered aircraft to the market by 2035[1]. Next to Airbus, there are other companies such as ZeroAvia, Universal Hydrogen, H3Dynamics, ZAL[2], which focus on applying hydrogen as an alternative fuel in aircraft and drones. Hydrogen combustion and hydrogen fuel cells are regarded as the two propulsion systems for the various concepts.

These propulsion systems are not only new to manufacturers but also to airlines and drone operators. When these systems are operational, it is essential that the operators understand how to perform maintenance and when to perform it. Preventive and predictive maintenance are current techniques applied by airlines to understand when maintenance needs to be performed on aero-engines, among other components, according to *Stanton et al.* [3]. Predictive maintenance can assist in prognosing the remaining useful life (RUL) of a system or even a specific failure. Thereby, reducing safety risks and costs by preventing failures and use-beyond-repair.

A proton-exchange membrane (PEM) fuel cell is considered most suitable and advanced for aviation compared to other type of fuel cells according to the study from *McKinsey & Company* [**?**]. However, a PEM fuel cell has limited durability due to degradation of the components, impurities in fuel and oxidants, and operating conditions [4]. For instance in hydrogen-electric cars, a maximum lifetime of 4000-5000 hr was achieved while a 8000 hr lifetime is the ultimate goal [5]. Predictive maintenance can play a critical role in enhancing the reliability of PEM fuel cells by predicting the health of components and degradation trends of the overall system [6]. Moreover, the integration of predictive maintenance strategies into PEM fuel cell systems holds the promise of extending their lifespan, maximising energy efficiency, and ensuring optimal performance throughout their operational lifecycle [7].

Current research is investigating three approaches to predict the remaining useful life of PEM fuel cells: 1) physical models; 2) data-driven techniques; 3) hybrid - combination of physical models and data-driven techniques [8]. Physical models are based on fundamental principles of physics and electrochemistry governing the operation of PEM fuel cells [9, 10]. These models describe the degradation behaviour of various components such as membrane, electrodes, gas diffusion layers, and distribution plates [11, 12]. In some cases, the models are validated by various experimental datasets [13]. These models enable the investigation of specific degradation mechanisms of components. Uncertainties associated with parameter estimation, boundary conditions, and simplifications in physical models can affect the accuracy of prognostic predictions [14]. Data-driven techniques leverage historical operational data, sensor measurements, and performance metrics to identify patterns, correlations, and trends which can indicate degradation in PEM fuel cells [15]. These techniques can be used to build predictive models that forecast future performance degradation based on observed data patterns. Data-driven techniques require sufficient historical data for training robust

[1] `https://www.airbus.com/en/innovation/low-carbon-aviation/hydrogen/zeroe` (accessed 03-01-2024)
[2] `https://zal.aero/en/innovation-rt/rt/` (accessed 10-01-2024)

predictive models, which may not always be available, especially for novel or custom fuel cell systems [16]. Hybrid prognostic approaches combine the strength of both physical models and data-driven techniques to enhance the accuracy and reliability of prognostic predictions for PEM fuel cells. Combining physics-based models with data-driven techniques may increase the computational time, particularly for real-time prognostics [17].

Experimental data for PEM fuel cell prognostics can be obtained through laboratory-based durability tests which offer controlled environments. Therefore, specific degradation mechanisms can be isolated and studied in detail. Accelerated stress tests, constant load cycling, and accelerated aging protocols are commonly applied in a laboratory to simulate long-term operation and assess the durability of PEM fuel cells [18]. In 2014, IEEE and FCLAB released a durability dataset of two PEM fuel cells to accelerate research in prognostics and health management for PEM fuel cells [19]. The PEM fuel cells operated under static and quasi-dynamic current conditions. In static operating conditions, a PEM fuel cell maintains a constant load, ideal for scenarios with consistent power demand like the cruise phase of drones or aircraft. This stability ensures efficient and predictable performance without frequent adjustments. However, static conditions may not suit applications with fluctuating power needs. Quasi-dynamic conditions involve gradual load variations over longer periods, adaptable to scenarios like an aircraft's landing phase. Dynamic conditions, with rapid load changes, demand quick response from the fuel cell system, critical for optimal performance in scenarios like vehicle propulsion systems during rapid acceleration or deceleration.

The relationship between degradation indicators and remaining useful life of PEM fuel cells is often nonlinear and complex. Degradation may occur gradually over time, exhibiting nonlinear trends that are not easily captured by simple correlations or a single health indicator. Moreover, the rate of degradation may vary depending on operating conditions, environmental factors, and maintenance practices. However, current advancements in remaining useful life predictions of PEM fuel cells are related to a single performance health indicator [20][21]. In terms of predictive maintenance, this indicator does not provide useful information on component degradation and the state of the components within the PEM fuel cell.

In recent years, significant advancements have been made in the development of prognostic techniques for PEM fuel cells, enabling researchers and engineers to forecast the RUL with increasing accuracy and reliability [22] [23]. However, the prediction horizon of RUL, which represents the time frame over which prognostic models can reliably forecast the remaining useful life of PEM fuel cells, remains a limiting factor. Understanding and extending the prediction horizon is essential for real-world applicability of prognostic solutions for PEM fuel cells.

Based on the addressed lack of research, the following research question is proposed:

Research Question

How to quantify, assess, and forecast the long-term health of proton-exchange membrane fuel cells and their critical components tested in a laboratory under static and quasi-dynamic operating conditions?

The sub-questions that support the main research question are:

Sub-research Questions

1. *Which health indicator(s) is/are most suitable for expressing the degradation of PEM fuel cells tested under static and quasi-dynamic conditions?*
2. *How to model long-term degradation of the membrane and electrode within PEM fuel cells?*
3. *How to enhance the prediction horizon of long-term predictions on the remaining useful life of PEM fuel cells tested under static and quasi-dynamic conditions?*
4. *How can system and component degradation indicators be linked to the remaining useful life of PEM fuel cells?*

The main objective of this thesis is described by the following statement:

Research Objective

This research aims to combine various degradation models and generate a multi-step ahead prediction tool to enhance the prediction horizon of the RUL of PEM fuel cells and the interpretability of stack degradation through component health indicators.

Report structure

The report is structured as follows. First, in chapter 3 background information is provided on hydrogen-electric transportation, predictive maintenance and ZAL Centre of Applied Aeronautical Research. Then, chapter 4 introduces the working principle of a PEM fuel cell, performance analysis techniques and categories of operating conditions. In chapter 5, the degradation modes and health indicators are explained and the remaining useful life is introduced. As a basis for predictions, chapter 8 discusses data available from experiments and simulations. Component degradation models, which can be applied with the available data, are explained in chapter 6. Then, in chapter 9 the prediction horizon of various prediction techniques is presented. An overview of data-driven techniques with detailed information is provided in chapter 7. In chapter 10 the research gap, research questions and research objective is discussed and the approach is explained in chapter 11. The report is concluded in chapter 12. This work will provide a contribution to long-term predictions on the remaining useful life of PEM fuel cells by applying a multi-step ahead prediction technique.

3
Background

This chapter discusses the rise of hydrogen-electric transportation as a sustainable mobility solution. From aircraft to maritime vessels, hydrogen-electric powertrains offer clean and efficient propulsion. Furthermore, background information is provided on ZAL Centre of Applied Aeronautical Research.

3.1. Hydrogen-electric Transportation

Sustainable transportation solutions has driven the exploration and development of alternative energy sources, with hydrogen-electric transportation emerging as a promising solution. Significant advancements have been made in deploying hydrogen-electric powertrains across various modes of transportation, including aircraft, drones, cars, buses, trains, and even maritime vessels. The increasing pressure to reduce the environmental footprint in the aviation industry caused aircraft manufacturers and research institutions to initiate projects towards a hydrogen-electric aerial vehicle. Even student team AeroDelft, located in Delft, started in 2017 with proving and promoting liquid hydrogen as an alternative fuel in aviation. AeroDelft managed to create a drone and manned aircraft with a hydrogen-electric powertrain which is yet in its testing phase. The efforts by the student team serves as a statement to industry that if students are capable of building a hydrogen-electric aircraft then so can industry. In Figure 3.1 the manned aircraft of AeroDelft is presented[1].

Figure 3.1: AeroDelft's Project Phoenix Full-scale: A two passenger kit aircraft from Sling Aircraft serving as a testbed for AeroDelft's hydrogen-electric powertrain.

[1]https://aerodelft.nl/project-phoenix/ (accessed 26-02-2024)

A hydrogen-electric powertrain consists mainly of a hydrogen tank, a fuel cell and an electric motor. Compressed or liquid hydrogen is safely stored in the tank until needed, then fed into the fuel cell where hydrogen reacts with oxygen to generate electricity through electrolysis. This electricity powers the vehicle's electric motor, providing efficient and clean propulsion. The only byproduct of this process is water vapour, making hydrogen-electric powertrains an environmentally friendly alternative to traditional fossil fuel engines.

3.2. ZAL Centre of Applied Aeronautical Research

ZAL Centre of Applied Aeronautical Research, located in Hamburg, Germany, represents an innovative tech centre within the aerospace industry. From cutting-edge laboratories to advanced simulation environments, ZAL provides a dynamic ecosystem for the conceptualisation, prototyping, and validation of groundbreaking aerospace solutions. ZAL's mission is to be a leading technological research and development platform for civil aviation. The projects are related to the integration and industrialisation of innovative aviation technologies. There are three technical domains present within ZAL: 1) Advanced Materials; 2) Automation; 3) Data & Power Networks. The third domain, "Data & Power Networks", works on developments related to fuel cell and electrical power systems, among other things. A team of fuel cell engineers test and integrate fuel cell systems into hydrogen-electric powertrains to be deployed in a drone. The level of expertise in fuel cell systems within the team provides a supporting environment to conduct this thesis in combination with Delft University of Technology.

4 PEM Fuel Cell

The various functions of each component within a proton-exchange membrane fuel cell are described. This information forms a basis for understanding the impact of different degradation modes discussed in section 5.1. Furthermore, the topics of polarisation curves, electrochemical impedance spectroscopy, and operating conditions of PEM fuel cells are explained.

4.1. Working Principle of PEM Fuel Cells

A polymer electrolyte membrane (PEM) fuel cell produces electricity from an electrochemical process with hydrogen and oxygen from air. The fuel cell consists of a solid membrane and two electrodes which are called the anode and cathode. Each electrode consists of one catalyst layer. At the anode side, hydrogen enters the fuel cell through a flow channel, diffuses through a gas diffusion layer and reacts with the anode's catalyst layer as can be seen on the left in Figure 4.1. The reaction of hydrogen with a catalyst causes the hydrogen molecules to split into protons and electrons. Only the protons, which are positively charged particles called cations, can pass through the membrane and reach the cathode [24]. The electrons cannot pass through the membrane because of the membrane's high electric resistance [25]. Instead, the electrons are transported by an electric circuit to the cathode. The flow of electrons creates an electric current which can be linked to a load, such as a motor. At the cathode side, oxygen enters the fuel cell through a flow channel and diffuses through a gas diffusion layer. The oxygen reacts with the transported protons, electrons and the cathode's catalyst layer to form water and heat.

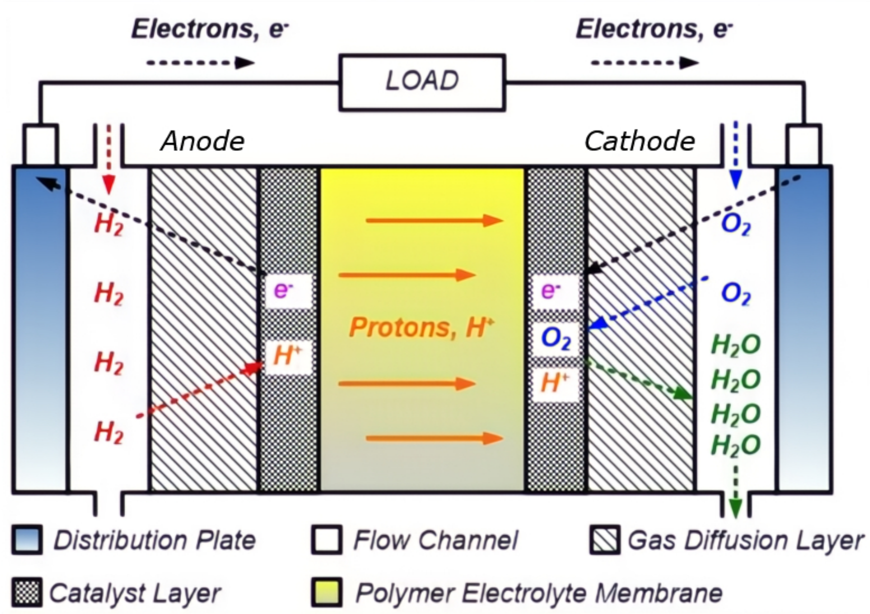

Figure 4.1: Architecture and working principle of a proton-exchange membrane fuel cell [25].

The performance of a PEM fuel cell is expressed in terms of voltage and current or voltage and current density. For a reversible system there are no losses present and this describes the open circuit voltage, which is also called electromotive force [24]. In this case, the electrical work equals the Gibbs free energy. However, during normal operations there are several losses present. The losses can be categorised into four types which are activation losses, fuel crossover and internal current losses, ohmic losses, and mass transport or concentration losses.

The activation loss appears due to internal reactions that do not take place instantaneously. A portion of the output voltage is required to start the chemical reactions and is therefore lost. This amount of voltage is called overvoltage. The overvoltage can be described by the natural logarithm form of Tafel equation. This formulation leads to an indication of the reaction speed. The overvoltage depends on exchange current density, current density and Tafel slope. The Tafel slope is dependent on the charge transfer coefficient which represents the amount of electrical energy required to change the rate of the electrochemical reaction. A reduction in overvoltage can be obtained by changing the exchange current density which has the largest impact on overvoltage. The chemical reactions and its inverse are continuously taking place within a PEM fuel cell. Thus, at zero current density the electrodes are active. This activity is represented by the exchange current density.

4.1.1. Membrane

The membrane requires to conduct protons from anode to cathode side, insulate electrons, separate hydrogen and oxygen reactants, and be mechanically and chemically strong [18]. The thickness of the membrane influences the membrane's ability to conduct protons and be mechanically strong. A thicker membrane improves electric insulation, and the chemical and mechanical bond, however, the protonic resistance is higher which is not beneficial in terms of conductance and vice versa [26].

4.1.2. Electrode

The electrode consists of a catalyst layer and a carbon support. The catalyst is made of platinum (Pt) or platinum metal compounds. The carbon support provides an electrical conductive porous structure and distributes the catalyst nanoparticles. The functions of the catalyst are to transport the electrons and protons [27], provide reaction sites, and to provide a flow path for reactants supply and products removal [28]. The catalyst consists often of platinum and is supported by high-surface-area carbon particles.

4.1.3. Gas diffusion layers

The gas diffusion layers not only diffuse the incoming hydrogen or oxygen gas. It also carries the reaction product water away from the cathode, acts as a protective layer for the very thin layers of catalyst, and it forms an electrical connection between the carbon-supported catalyst and distribution plates [24]. The functions of the gas diffusion layers are to protect the catalyst layers as physical supports [25], transport the reactants [29], remove the produced water [30], and to conduct the electrons [31][32]. Degradation impacts the ability of the gas diffusion layers to fulfill its functions.

4.1.4. Distribution plates

The functions of distribution plates, also called bipolar plates, are to insulate reactants and coolant between different cells, collect electrons and to distribute reactants homogeneously [24]. The material that is used to perform these functions can be graphite, graphite composites or metals such as stainless steel, aluminium or titanium. There are durability issues for graphite and graphite composites distribution plates when exposed to a shock or an environment with vibrations. Although the material is a recommended candidate due to its light weight, high corrosion resistance, and high electrical and thermal conductivity, it faces issues with gaseous hydrogen permeability [33].

4.2. Polarisation Curve

The polarisation curve of a single proton-exchange membrane fuel cell is presented in Figure 4.2. The output voltage is depending on the current density, which is the current normalised by the area of the fuel cells. There are three sections within the polarisation curve due to the influence of activation losses, ohmic losses and concentration losses.

Activation loss is present due to resistance of electrochemical reactions. To start the reaction of transferring electrons and protons a certain level of electrons and protons is required. A portion of the voltage is used to obtain this level and start the reaction. This part of the voltage is lost and is called activation loss. The reaction slowness is mainly caused by the reactions in the catalyst layers and can be influenced by concentration, electrode properties, pressure and temperature [34].

Ohmic loss is caused by transportation of electrons and ions through the fuel cell's components. Reduction in resistance can be achieved by improving electronic and ionic conductivity of the cell [34].

Concentration loss is an irreversible loss and influences the voltage due to concentration changes, flow rate fluctuations of reactants in the catalyst layers, cell temperature and the structure of the catalyst layers and gas diffusion layers [34].

Another irreversible loss is fuel crossover and internal current. The membrane acts as a barrier but small amounts of electrons and reactants still pass through the membrane. This leads to a reduction in open circuit voltage. This loss becomes negligible when sufficient amount of current is drawn from the fuel cell.

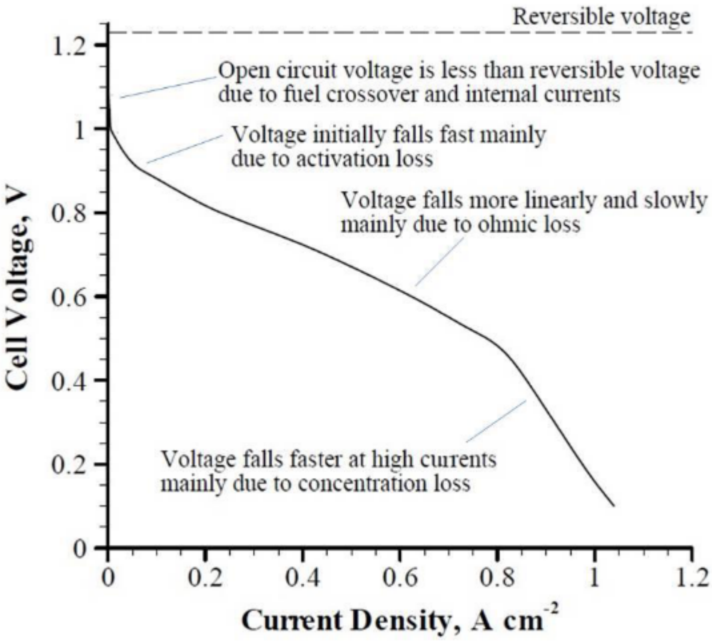

Figure 4.2: Typical polarisation curve of a single proton-exchange membrane fuel cell with clarification of cell voltage drop as current density increases [34].

4.3. Electrochemical Impedance Spectroscopy

Electrochemical impedance spectroscopy (EIS) is a technique used to analyse the electrical behaviour of proton exchange membrane fuel cells. In PEM fuel cells, hydrogen and oxygen are electrochemically converted into water, releasing electrical energy in the process. EIS helps to understand and optimise this energy conversion process. Through frequency sweeps, EIS systematically explores the impedance characteristics of the fuel cell system across a spectrum of frequencies. This variation in frequency allows for the characterisation of different electrochemical processes occurring within the fuel cell at various rates.

An electrochemical system is not only resistive. Impedance incorporates the different processes of the electrode, such as diffusion, and the dependency on time and/or frequency. For an electrochemical system, impedance is the alternating current response of the system when exposed to an alternating current signal. Measuring the alternating current impedance of an electrochemical system is called electrochemical impedance spectroscopy [35]. The impedance is related to the voltage to current fraction which is a function of time. Another way to describe the impedance is by rewriting it into Cartesian coordinates which results into a real and an imaginary part. These components can be plotted into a so-called Nyquist plot. An example of a Nyquist plot for a PEM fuel cell is provided in ??. The width of the semi-circle represents the charge transfer resistance (R_{ct}) and the high-frequency part represents the membrane resistance.

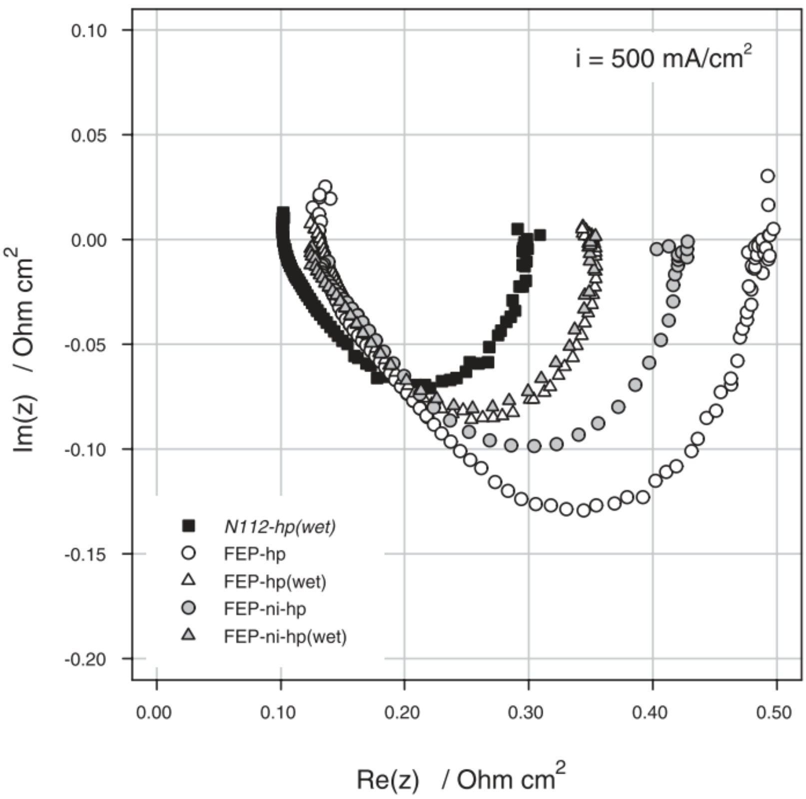

Figure 4.3: Electrochemical impedance spectra, Nyquist plot, of a single cell PEM fuel cell with a current density of 500 cm^2 [36].

4.4. Operating Conditions

A PEM fuel cell operates under different conditions which depend on factors such as load demand, temperature, and reactant flow rates. Depending on load demand, the operating conditions can be categorised into static, quasi-dynamic, and dynamic operating conditions.

In static operating conditions, a PEM fuel cell operates at a constant load. This mode is ideal for scenarios where power demand remains consistent over time, such as during the cruise phase of a drone or aircraft. The stability provided by static conditions allows for efficient and predictable performance, enabling the fuel cell system to maintain steady power output without the need for frequent adjustments. However, while static conditions offer stability, they may not be well-suited for applications with fluctuating power demands.

Quasi-dynamic operating conditions involve gradual variations in load occurring over relatively longer periods compared to dynamic conditions. In those scenarios, the PEM fuel cell system can adapt to these changes. Quasi-dynamic conditions are commonly encountered in applications where power demand fluctuates gradually over time, such as in an aircraft that starts its landing phase.

Dynamic operating conditions present rapid and significant changes in load, requiring the PEM fuel cell system to respond quickly to maintain efficient and stable operation. These conditions are common in applications where power demand varies rapidly, such as during rapid acceleration or deceleration in vehicle propulsion systems. Effective control strategies and rapid response times are crucial for ensuring optimal performance and preventing degradation under dynamic operating conditions.

5

Degradation and Health Indicators

This chapter discusses how degradation of each component in a proton-exchange membrane fuel cell can be identified. Each component degrades in a different manner, and due to various causes. Therefore, the various degradation modes are explained for the membrane, electrode, gas diffusion layers, and distribution plates. Health indicators are introduced based on stack performance and component degradation. For stack performance, three indicators are discussed: voltage, power, and relative power-loss rate. For component degradation, two indicators are discussed: parametric model-based indicator and multi-scale hybrid degradation index. In depth degradation models are applied for the multi-scale hybrid degradation index which are further discussed in chapter 6.

5.1. Degradation Modes

Degradation modes can be classified into two main categories which are *early stage degradation* and *late stage degradation*. Early stage degradation represents degradation due to incorrect assembly of the fuel cell or other imperfections during the production phase that can influence the performance of the fuel cell at an early stage. Late stage degradation represents degradation due to long-term operations of the fuel cell and is influenced by e.g. cyclic loading or start-stop cycles [34]. This section discusses only late stage degradation of the membrane, electrode, gas diffusion layers and distribution plates.

Component hierarchy from *Jouin et al.* [11] in Figure 5.1 presents the importance of membrane and electrode degradation within the PEM fuel cell. Therefore, degradation of membrane and electrode are discussed in more detail than the gas diffusion layers and distribution plates.

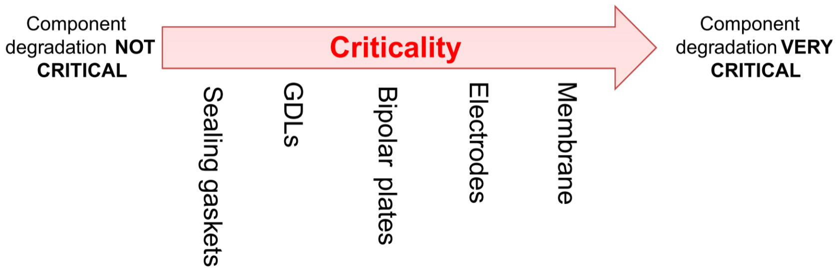

Figure 5.1: An overview of components and its importance on degradation of a proton-exchange membrane fuel cell [11].

5.1.1. Membrane

Membrane degradation can be divided into five main groups: 1) chemical degradation; 2) mechanical degradation; 3) thermal degradation; 4) membrane shorting; 5) membrane contamination [11]. Thermal degradation is not a primary cause of membrane failure because of the presence of a thermal control system within a PEM fuel cell stack. According to *Liu et al.* [13] thermal control systems always maintain the inner temperature of the stack between 60 and 80 °C. Membrane shorting is a form of mechanical degradation and is caused by electrons directly moving from the anode to cathode instead of through the load [11]. It can lead to micro-holes and melting of the membrane, according to *Gittleman et al.* [37]. It is caused by penetration of external objects and membrane compression. It is hard to dinstinguish membrane shorting from mechanical degradation and to model membrane shorting. Therefore, membrane shorting can be considered as a form of mechanical degradation. Membrane contamination can occur due to the presence of foreign species due to catalyst degradation or because of impurities from incoming gases or the humidifier tank [11]. The largest impact is caused by catalyst degradation which can lead to foreign cations, such as cobalt cations, that replace hydrogen cations and thereby reduce conductivity [38]. Membrane contamination can be considered to be part of chemical degradation.

Chemical degradation is considered the primary cause for limited lifetime of a membrane according to *Gittleman et al.* [37]. Chemical reactions and membrane contamination cause membrane decomposition. Chemical degradation can be analysed by monitoring gas crossover rate and quantifying fluoride release rate. Chemical degradation is characterised by membrane thickness degradation, and the release of HF, CO_2, H_2SO_4 [11] [13]. To summarise, oxygen crossover rate and fluoride release rate are analysed to estimate chemical degradation rate [11].

Mechanical degradation includes assembly stress, local stress, membrane contraction, swelling under changing operating conditions, differences in expansion between reaction and non-reactive zones, and chemical degradation resulting in fluoride and membrane thickness losses [39]. Such degradation can lead to the formation of micro-holes, tears, perforations, blisters, and membrane deformations [11]. Thereby, inreasing gas crossover. These mechanical deteriorations can be present due to manufacturing defects and cause for instance pinholes, cracks, and delamination [30]. Pinholes and cracks may develop due to reactant crossover, while stress cycling can lead to membrane electrode assembly delamination [40]. Reactant crossover can also disrupt thermal and water management systems. Furthermore, improper humidity conditions during fuel cell operation may cause membrane shrinkage or swelling, resulting in in-plane tension or compression, respectively. The effects of mechanical degradation generally become apparent only after thousands of hours of normal operation [13]. Permanent membrane deformation can occur under high relative humidity, causing membrane expansion but potentially improving cell performance. However, a low swelling expansion coefficient could enhance the cell's durability [34].

Gas crossover, as discussed by *Jouin et al.* [11], involves the movement of hydrogen and oxygen across the membrane to the opposite electrode. While oxygen crossover is less frequently addressed in literature, hydrogen crossover is known for causing significant failures, often resulting in stack shutdown. Large quantities of hydrogen crossover can even cause a hazardous failure due to the presence of oxygen. *De Bruijn et al.* [41] proposed an end-of-life threshold for the membrane subjected to hydrogen crossover, corresponding to a crossover current of 10 mA/cm^2.

Membrane thickness serves as an indicator due to its correlation with gas crossover and fluoride release rate. The impact of gas crossover, particularly significant in cases of hydrogen crossover, can lead to combustion and direct stack failure.

Karpenko-Jereb et al. [10] established a correlation between oxygen crossover rate and membrane thickness reduction, especially evident in perfluorinated sulfonated membranes like Nafion, commonly used in fuel cells. Membrane thickness degradation can arise from chemical reactions with hydroxyl radicals, formed as byproducts from the reaction of hydrogen protons and oxygen at the anode and cathode [42].

5.1.2. Electrode

The health of an electrode can be indicated by the electrochemical catalyst surface area (ECSA) and reduces due to catalyst and carbon support degradation [11]. A visualisation of the electrochemical catalyst surface area of platinum particles is provided in Figure 5.2. Specifically, a reduction in ECSA can be caused by catalyst isolation due to carbon support corrosion, catalyst isolation due to catalyst/ionomer interface loss, loss of catalyst loading due to platinum detachment or dissolution, and coarsening of catalyst nanoparticles due to mechanisms such as Ostwald ripening. According to *Sharma et al.* [43] degradation of ECSA is for 45% caused by carbon support corrosion, 19% by catalyst/ionomer interface loss, 6% by platinum dissolution, and 30% by platinum particle growth through Ostwald ripening. Degradation in electrochemical surface area can be measured through cyclic voltammetry. The electrochemical behaviour of a catalyst is analysed during cyclic voltammetry by measuring its current response to a range of voltages. The resulting current-voltage curve is known as a voltammogram. The area under certain peaks in the resulting voltammograms corresponds to the ECSA.

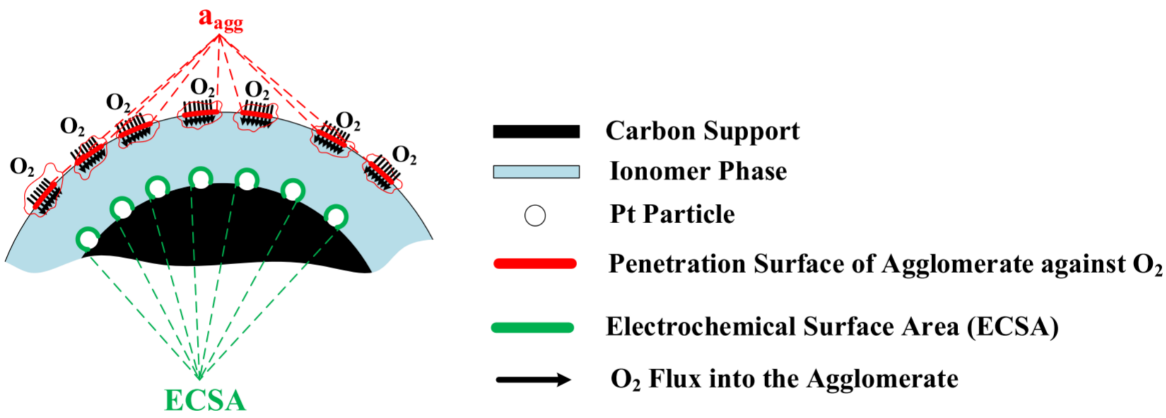

Figure 5.2: Oxygen flux into membrane, i.e. ionomer phase, to reach electrochemical surface area of platinum particles [44].

Carbon support corrosion can be caused by oxidisation with water and oxygen at the cathode leading to disintegration of the catalyst layer [11]. This effect can lead to a loss in electron connectivity [43]. Thereby, influencing the electrochemical surface area of the electrode.

Catalyst/ionomer interface loss can only be determined by obtaining the total ECSA degradation and the impact of carbon support corrosion, platinum dissolution, and Ostwald ripening. *Sharma et al.* [43] created two experimental test set-ups to perform tests, such as cyclic voltammetry, to determine total ECSA degradation and the impact of the four mechanisms on ECSA degradation. According to *Gubler et al.* [36] part of the interface deterioration can be analysed by the diameter of the impedance half-circle in a Nyquist diagram. This diameter relates to the charge transfer resistance which can be an indication of a reduced platinum surface and an increase in platinum catalyst particles at the cathode.

Platinum dissolution is a process in which platinum particles are oxidised by both water and oxygen at the cathode [45]. Platinum oxidation causes formation of platinum ions from a single platinum particle, which can diffuse in the membrane, i.e. ionomer media, or also leave the cell with the produced water [9]. Thus, platinum dissolution causes a reduction in platinum particle size as presented in Figure 5.3(a), under the assumption that the overall particle number is unaffected. Thereby, leading to a reduction in electrochemical catalyst surface area. According to *Gubler et al.* [36] formation of platinum oxide can be caused by continuous operation at a constant current density. The platinum oxide at the cathode can be reduced by lowering cathode potential.

Ostwald ripening is a process in which small dissolved platinum nanoparticles attach to a large platinum nanoparticle. Thereby, inducing a reduction in particle number and an increase in single particle diameter as presented in Figure 5.3(b) and Figure 5.4 which decreases the electrochemical catalyst surface area. Coalescence, a similar process to Ostwald ripening, relates to merging smaller platinum nanoparticles into a large platinum nanoparticle. Defining a distinct difference between Ostwald ripening and coalescence is difficult. Therefore, existing catalyst degradation models define Ostwald ripening and coalescence as a single process and define this process as Ostwald ripening [44][9][14].

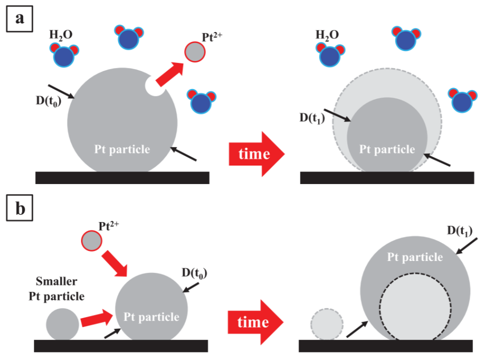

Figure 5.3: Degradation mechanisms of catalyst layer in a PEM fuel cell: (a) platinum dissolution and (b) Ostwald ripening [44].

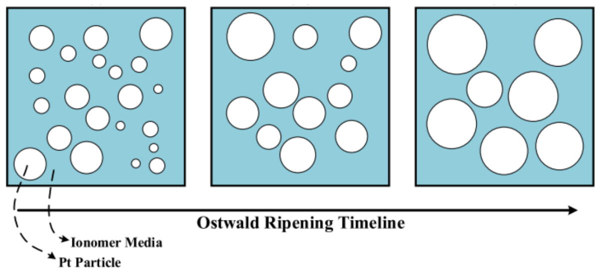

Figure 5.4: Ostwald ripening process over time of platinum particles in ionomer [44].

5.1.3. Gas diffusion layers

The gas diffusion layers serve a crucial role in facilitating reactions in fuel cells by allowing reactants to diffuse to active sites, managing water within the cell, and ensuring electron transfer. Degradation of gas diffusion layers can be noticed by three main changes [11]. First, changes in water behaviour due to degrdadation of the carbon surface and its loss of hydrophobicity which affect water management within the membrane and catalyst layer [40]. Radical species attack to the hydrophobic coating. This is only happening when the gas diffusion layers have a hydrophobic binder. There are also gas diffusion layers without this type of binder. This type of gas diffusion layers are called raw gas diffusion layers [34]. The reason for using a hydrophobic binder is to improve water management capabilities [46][47]. Second, structural changes due to carbon corrosion which leads to a reduction in the pore structure of the gas diffusion layer, its hydrophobicity, conductivity, and thereby the overall performance [48][30]. Third, electrical and thermal resistance degradation which affects the overall conductivity and the efficiency of electron transfer [34].

5.1.4. Distribution plates

The degradation of distribution plates involves three main mechanisms according to *Nguyen et al.*[49]: corrosion, formation of a resistive surface layer, and deformations or fractures. Corrosion can lead to dissolution of plate materials and is caused by the chemical environment in a PEM fuel cell. It can result in the production of multivalent cations, such as cobalt, which can adversely affect the durability of the membrane and catalyst layers by for instance membrane poisoning [38]. Formation of a resistive layer on the distribution plate can result in a high ohmic resistance. This resistive layer is created over time and may form due to exposure to reactive species or chemical reactions within the fuel cell environment. Deformations and possible factures can be caused mechanical stresses due to operational factors such as thermal cycles, uneven temperature distribution, or non-uniform currents [30].

5.2. Health Indicator

The purpose of a health indicator is to express the level of degradation in a quantitative or qualitative manner. Various health indicators have been created to describe the state of health of a fuel cell stack. Either a top-level or a bottom-up strategy is applied to indicate degradation. Top-level indicators are related to the reduction in performance to the stack or a component, e.g. reduction in power over time, and are not related to specific degradation modes. Thus, there is no understanding of the root cause that leads to the reduction in performance. On the other hand, an indicator with a bottom-up strategy is linked to a specific degradation mode of a component to express reduction in component performance, e.g. oxygen crossover rate through the membrane. This section provides an overview of the various health indicators that have been created for PEM fuel cells.

5.2.1. Voltage and Power

Degradation in voltage and power is considered as one of the most traditional health indicators with prognosing the RUL of PEM fuel cells, especially for static and quasi-dynamic operating conditions [50]. Under these operating conditions there is a clear degradation trend present within the obtained data. Phenomena that cause voltage recovery, such as rehumidification of the stack or polarisation tests, are well understood and can therefore be taken into account during RUL prognosis. In Figure 5.5 the impact of voltage recovery by characterisation tests is presented by applying power as a health indicator.

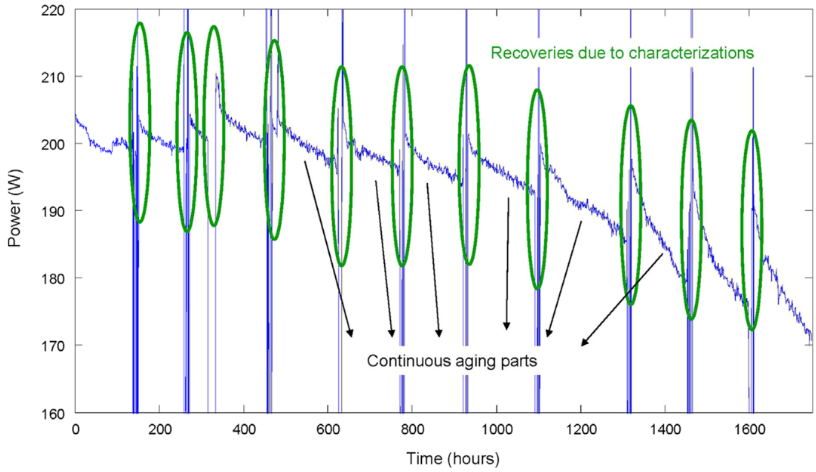

Figure 5.5: Power degradation of PEM fuel cell stack with 5 cells and an active area of 100 cm^2 over 1750 hr under a constant current of 60A and planned polarisation tests [11].

5.2.2. Relative power-loss rate

A traditional health indicator, e.g. voltage, cannot be applied for expressing degradation of a fuel cell that is operated under dynamic conditions. Fluctuations in voltage due to dynamic operating conditions make it difficult to capture a monotone decreasing trend. Therefore, a different indicator is proposed by *Hua et al.* [22] called the relative power-loss rate (RPLR), which can handle dynamic changes in load, and can be computed by use of a polarisation curve and the measured electrical signal [21].

The RPLR indicator defines the reduction in power delivered by the stack with respect to the beginning of life power at various current settings. The delivered power is not a single value but a curve that represent power (W) versus current (A). The power output can be computed from stack voltage and stack current from a polarisation curve. A beginning of life power curve is created by using experimental power data and the Thrust-region optimisation method to fit a curve through the experimental data as presented in Figure 5.6. The RPLR health indicator is linked to the RUL by a defined failure threshold as shown in Figure 5.7.

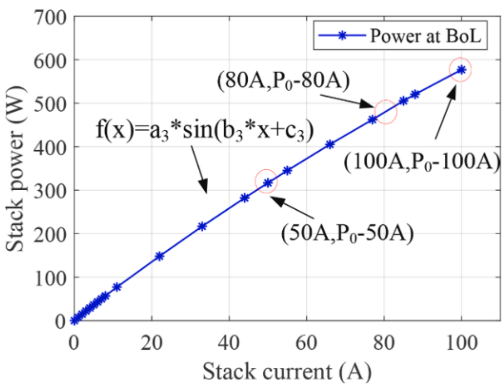

Figure 5.6: Beginning of life power curve for a PEM fuel cell tested within project PROPICE [51].

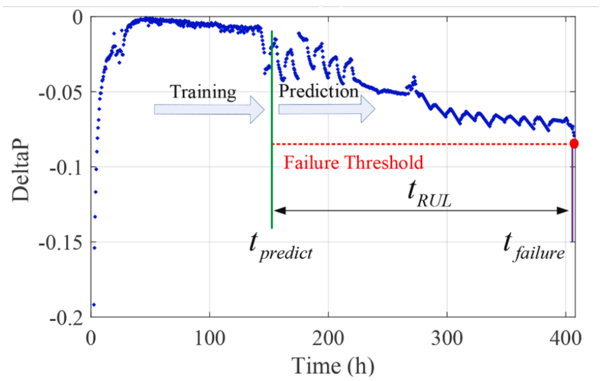

Figure 5.7: Relative power-loss rate over time with defined failure threshold to indicate remaining useful life [22].

5.2.3. Parametric model-based indicator

Yue et al. [6] created a health indicator α that indicates catalyst degradation and membrane degradation based on a parametric model of the fuel cell stack and cell voltage [52][11]. The parametric model considers irreversible losses and for each type of loss a parameter is selected that can indicate component degradation. The irreversible losses are activation, crossover, ohmic, and concentration losses as shown in Equation 5.1 [52][11]. Exchange current (i_0) is selected for activation and crossover losses, and is a function of electrode catalyst loading and catalyst specific surface area [6]. A decrease in exchange current is linked to a loss in active area of the catalyst, thereby, causing catalyst degradation. Equivalent ohmic resistance (R_{eq}) is selected for ohmic loss. An increase in equivalent ohmic resistance includes an increase in electronic, contact, and ionic resistance which is related to membrane degradation [11]. Limiting current at the cathode (i_L) is selected for concentration loss. A variation in limiting current at the cathode is related to gas diffusion layer degradation. However, the thickness of gas diffusion layer cannot vary more than a few µm [11][53]. The selected parameters are determined over time by fitting the parametric model with polarisation curves of experiments. The fitted parameters and the resemblance of polarisation curves between experiments and parametric model are presented in Figure 5.8 and Figure 5.9 respectively. Only exchange current (i_0) and equivalent ohmic resistance (R_{eq}) vary over time with rather the same value. Therefore, a linear correlation is assumed and a single health indicator α is introduced which describes the change in R_{eq} and i_0 as shown in Equation 5.2.

$$
\begin{aligned}
V_{fc} &= nV_{cell} = n\left(V_0 - V_{\text{act + cross}} - V_{\text{ohmic}} - V_{\text{conc}}\right) \\
V_{cell}(i) &= V_0 - \frac{RT}{2aF}\ln\left(\frac{i_{\text{loss}}+i}{i_0}\right) - iR_{eq} - B_c\ln\left(1-\frac{i}{i_L}\right)
\end{aligned}
\tag{5.1}
$$

$$
\begin{aligned}
R_{eq} &= R_{eq,\text{ init}}\cdot(1+\alpha(t)) \\
i_0 &= i_{0,\text{ init}}\cdot(1-\alpha(t))
\end{aligned}
\tag{5.2}
$$

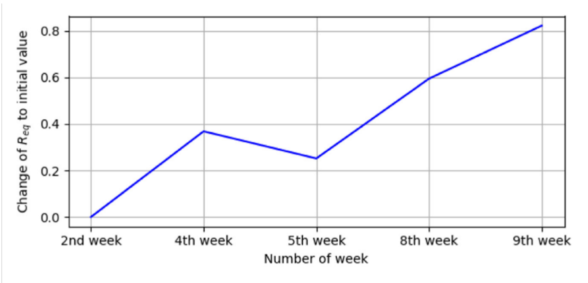

(a) Change of R_{eq} to its initial value

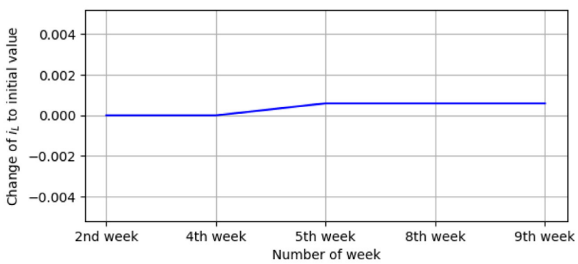

(c) Change of i_L to its initial value

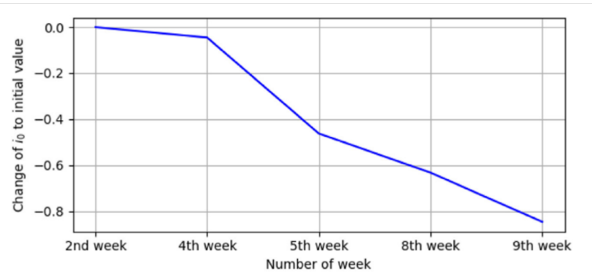

(b) Change of i_0 to its initial value

Figure 5.8: Fitted component degradation parameters R_{eq}, i_0, i_L over time by use of parametric model and experimental data.

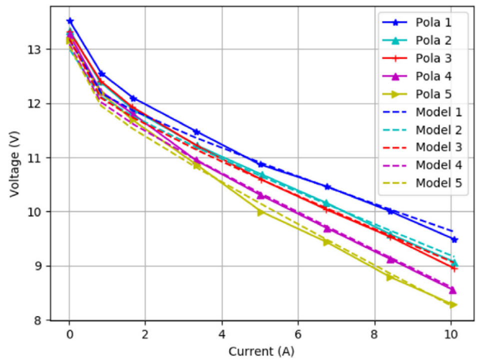

Figure 5.9: Polarisation curves of a proton-exchange membrane fuel cell from experiments and parametric model.

5.2.4. Multi-scale hybrid degradation index

A hybrid multi-scale degradation indicator is generated by *Liu et al.* [13] which combines various degradation models of a membrane and electrode into a single health indicator. In total there are three indexes which are computed from degradation models by the use of operational data from a PEM fuel cell. The operational data is discussed in section 8.2. Membrane health is indicated by membrane thickness degradation which is obtained by averaging an emperical and semi-emperical degradation model which analyses oxygen crossover rate and fluoride release rate, respectively. Electrode health is indicated by an ECSA degradation index and a reduction in radius of catalyst particles index. The index for ECSA degradation is obtained by averaging an ECSA emperical and mechanism degradation model. Then, all three indexes are normalised and fused together into a single health indicator by use of weighted coefficients. The weighted coefficients are determined by assuming a linear degradation curve and applying information on component degradation dependency on stack degradation. According to *Liu et al.* [13][54], 43% of degradation in the operational dataset is caused by membrane and electrode of which 60% of degradation is due to electrode degradation and 40% of degradation is due to membrane degradation. The coefficients of electrode health indexes are obtained by applying the assumption on linear degradation. The process of applying various degradation models on nano-scale and micro-scale, and obtaining a hybrid degradation index by fusing different indexes is summarised in Figure 5.10 and Figure 5.11.

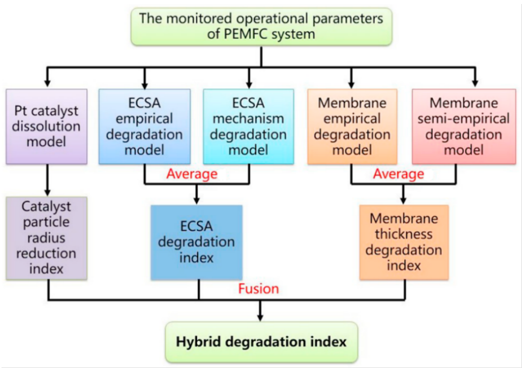

Figure 5.10: Constructing of multi-scale hybrid health indicator from catalyst particle radius reduction index, ECSA degradation index, and membrane thickness degradation index [13].

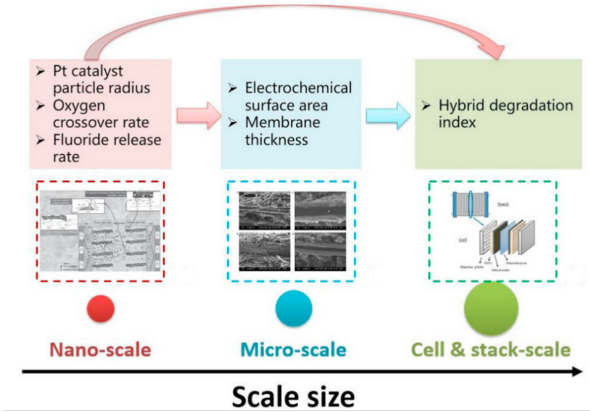

Figure 5.11: Multi-scale information of hybrid health indicator [13]. Images are from *Franco* [55], *Yuan et al.* [56], and *Jouin et al.* [11].

5.3. Remaining Useful Life

The remaining useful life (RUL) is the remaining time that a fuel cell stack can perform according to the requirements of the government or user [5]. This requirement can be defined in multiple ways. One example is that an airline requires the stack to deliver at least 80% of its maximum power output during its operational lifetime due to take-off requirements. When the power output is below this threshold then the fuel cell does not meet the operational requirement of the client and replacement or maintenance is required. Different definitions on remaining useful life are mentioned in literature. The remaining useful life can for instance be defined as the end-of-test or end-of-life. To ensure that the results can be compared among different studies, the voltage degradation rate, in $\mu V \cdot h^{-1}$, at a reference current density is often mentioned within a fuel cell study [18]. The key events that influence the degradation, and therefore the remaining useful life, are start-stop cycles, high-power loading, load-changing cycles, and idle conditions [57].

6

Degradation Models

This chapter discusses validated degradation models which can be applied to understand degradation of the membrane and electrode. These two components have been identified as critical components and the degradation can be indicated by membrane thickness and electrochemical catalyst surface area for the membrane and electrode, respectively. Three validated degradation models are discussed for the electrode and two for the membrane. At the end of this chapter an overview is provided on the various degradation models and their mathematical equations.

6.1. Platinum dissolution model

Robin et al. [58] developed a platinum dissolution model to simulate the reduction in the average radius of platinum particles as they age within the electrode. The modelling approach is based on a three-step process of platinum dissolution at an atomic level. This involves removal of platinum from the crystal through platinum sintering, platinum oxidation through electrochemical reactions, and desorption of oxidated platinum. These processes are associated with the variation of free Gibbs energy ΔG. The modelling approach is summarised in Figure 6.4(a) which is validated against two 2000 hr experimental aging tests. The novel method is introduced to estimate the loss of equivalent active surface area during aging tests. While the computed electrochemical catalyst surface area profile fits reasonably well with experimental measures from cyclic voltammetry, it underestimates the PEM fuel cell's performance loss. To accurately predict performance degradation observed in polarisation curves during aging tests, an equivalent active surface area is derived through model inversion. This methodology successfully recovers the experimental cell voltage decay over time.

While the cathode catalyst material from *Robin et al.* [58] is Pt_3Co, the final estimation results remain unaffected. The findings demonstrate that even if the catalyst material comprises of platinum metal compounds, the model's accuracy is not affected. Given that state-of-the-art PEMFC electrodes typically consist of a blend of polycrystalline platinum metal compound nanoparticles supported on carbon and proton-conducting membrane in a ratio of 70:30 (w:w) [43], this platinum dissolution model is applicable across various PEM fuel cell configurations.

6.2. ECSA empirical degradation model

Moein-Jahromi et al. [44] developed a degradation model that determines ECSA degradation based on carbon corrosion and coarsening of particles in the catalyst by Ostwald ripening. Carbon corrosion is analysed by an analogy with fatigue of carbon steel. Even though there might be other aspects of fatigue which are not considered in this ECSA degradation model, the model provides ECSA degradation approximations within an acceptable bound from experimental ECSA values from 26 studies involving various PEM fuel cells as presented in Figure 6.1. The empirical degradation model for ECSA accounts for temperature, relative humidity, and current load effects. An outline of the model is provided in Figure 6.4(b). An observation from experimental results presented that ECSA stabilises at a constant minimum value during degradation. Therefore, parameter S_{min} was introduced to assist degradation of ECSA towards this minimum value. The results indicate that the empirical degradation model ensures high precision across diverse PEM fuel cell applications.

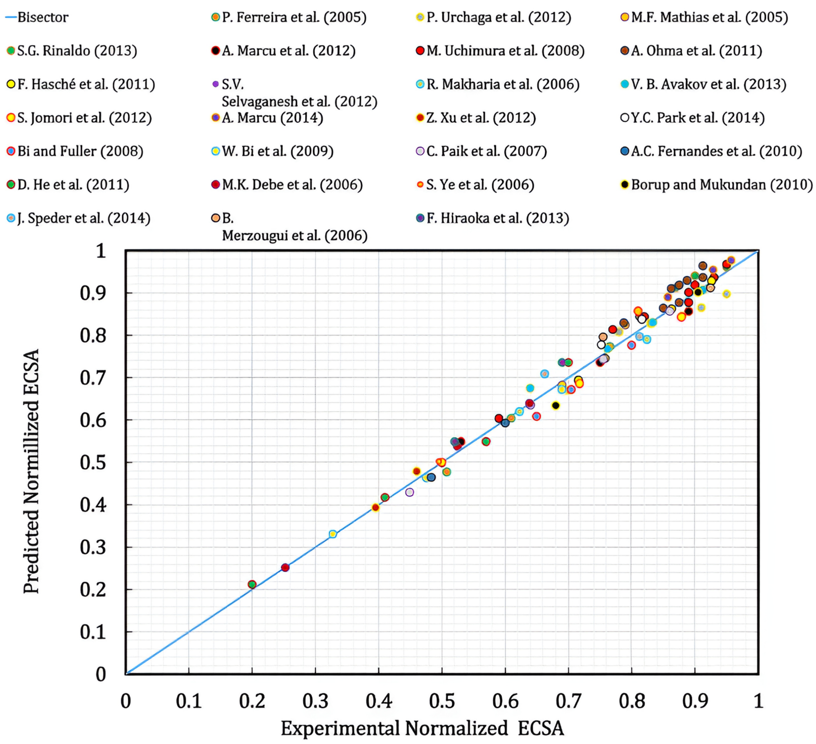

Figure 6.1: Validation of normalised electrochemical catalyst surface area with 26 different experimental studies which contain various PEM fuel cell configurations [13].

6.3. ECSA mechanism degradation model

Polverine and Pianese [9] developed a degradation model based on platinum dissolution and coarsening of platinum particles through Ostwald ripening. A relation is created between the two degradation modes to the output voltage of the stack and the remaining useful life of the system. The model enables estimation of the electrochemical catalyst surface area and voltage degradation under constant and cyclic current loads. This degradation model can be applied to various PEM fuel cell systems. The model was validated with 168 hr of experimental data from *Wang et al.* [59] . The approach from *Moein-Jahromi et al.* [44] to have a minimum ECSA value is incorporated in this model due to initial model outputs that converged to zero which is contradicting with real-world ECSA degradation. An overview of the ECSA degradation model is provided in Figure 6.4-c.

6.4. Oxygen crossover rate based membrane empirical degradation model

Karpenko-Jereb et al. [10] developed a new semi-empirical model which takes physico-chemical properties into account of a polymer electrolyte membrane to understand degradation rates of the membrane thickness and conductivity depending on oxygen crossover rate. Furthermore, a validated CFD model is created to compute 3D cell performance. The semi-empirical model and CFD model are coupled to analyse cell behaviour as a function of time. The simulation presents that in-plane degradation of the membrane is non-uniform and that cell current density decreases faster by lowering relative humidity and increasing temperature. The semi-empirical model requires degradation rates of membrane thickness and conductivity as inputs which were acquired from *Yuan et al.* [56][60].

The chemical degradation of perfluorinated sulfonated membranes, such as Nafion, primarily occurs due to the interaction of hydroxyl radicals with the polymer chains of the membrane. These reactions result in a decrease in membrane thickness and membrane conductivity, leading to the formation of pinholes and cracks. Hydroxyl radicals are formed from hydrogen peroxide which is one of the products from the reaction with oxygen and hydrogen protons. The concentration of hydroxyl radicals correlates with oxygen concentration in the fuel cell. A reduction in membrane thickness can cause a significant increase in hydrogen crossover current density, as presented in Figure 6.2 and Figure 6.3.

Experimental data shows that the hydrogen crossover rate varies with parameters such as temperature, pressure, relative humidity, and membrane thickness. A mathematical expression is proposed to estimate the hydrogen crossover rate under different operating conditions. The study suggests that the ratio of oxygen to hydrogen crossover flux through the membrane remains relatively constant regardless of environmental conditions. This allows for simplification of calculations related to oxygen crossover.

Using simulation results, the relationship between oxygen crossover flux and cell voltage is analysed. A linear fitting equation describes the relative change in oxygen crossover flux as a function of voltage. The degradation rate of membrane thickness and conductivity can be calculated considering the influence of cell voltage on oxygen crossover flux.

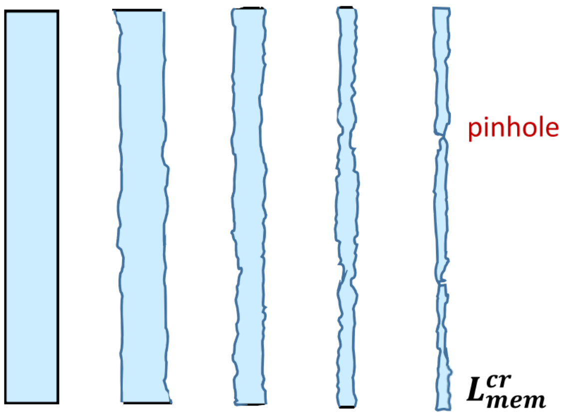

Figure 6.2: Reduction in membrane thickness and formation of pinholes [10].

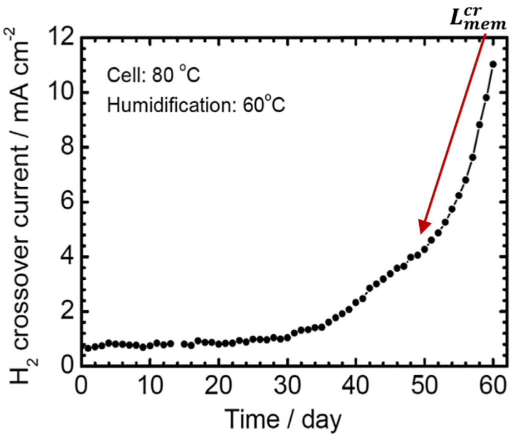

Figure 6.3: Experimental data on time changes of hydrogen crossover current density [10].

6.5. Fluoride release rate based membrane semi-empirical degradation model

Chandesris et al. [42] proposes a semi-empirical degradation model that relates membrane thickness degradation to the release of fluoride from the membrane due to hydroxyl radicals reacting with the membrane. The release of fluoride is an indication that the membrane is thinning due to e.g. reactions with hydroxyl radicals. Hydroxyl radicals form from peroxide species in the presence of metal impurities. When oxygen crosses the membrane and reaches the anode, oxygen can react with hydrogen to form these peroxide species. Also the cell voltage influences the formation of peroxide and the concentration of iron ions according to *Wong and Kjeang* [61].

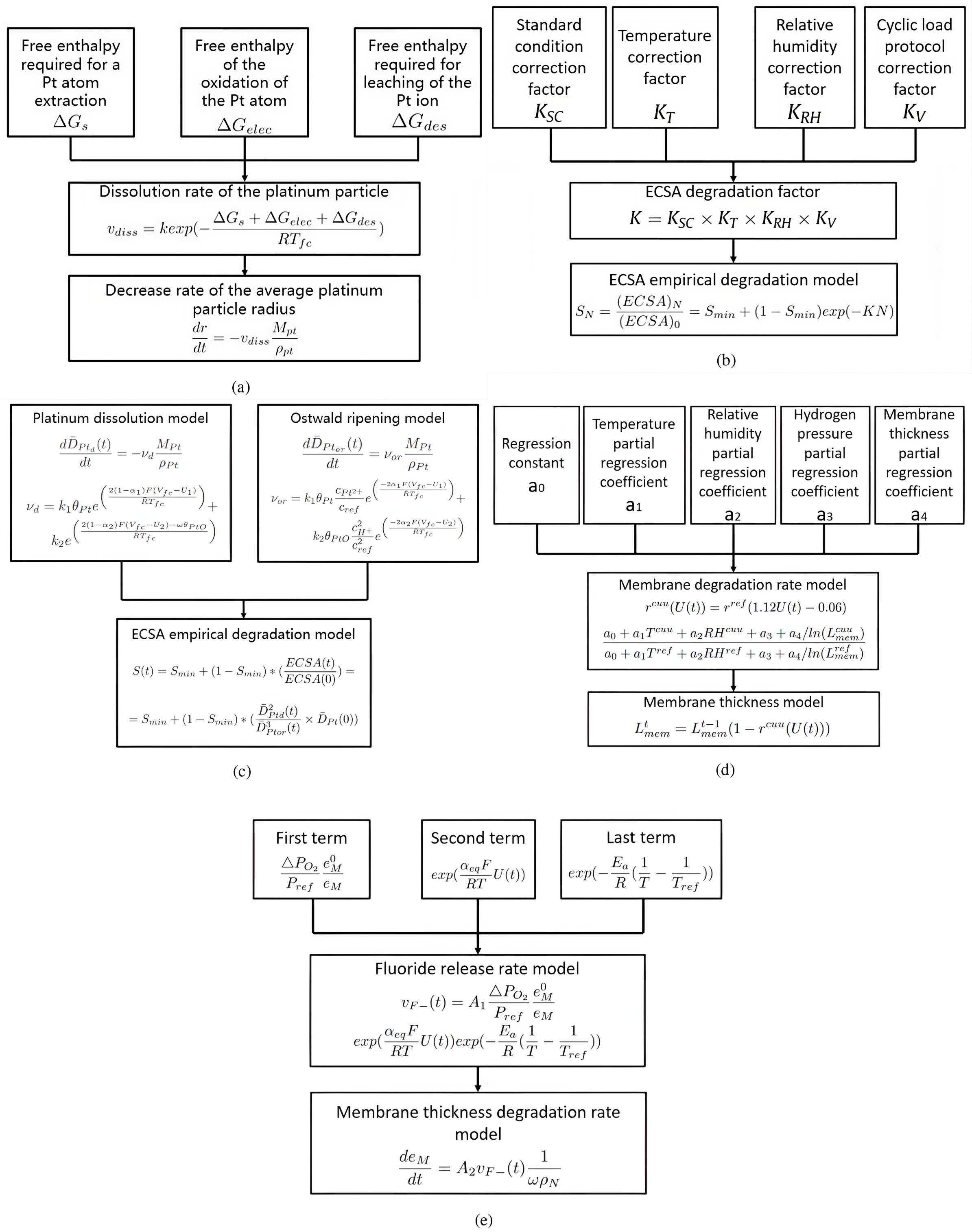

Figure 6.4: Modelling approach of (a) platinum dissolution model [58], (b) ECSA empirical degradation model [44], (c) ECSA mechanism degradation model [9], (d) membrane empirical degradation model [10], and (e) membrane semi-empirical degradation model [42]. Overview of degradation models obtained from *Liu et al.* [13]

7

Prognostic Techniques

This chapter discusses various recurrent neural networks, especially Echo State Networks that were compared in section 8.3. Different multi-step ahead prediction techniques are introduced and a general overview is provided on long short-term memory networks and gated recurrent units.

7.1. Recurrent Neural Network

Recurrent neural networks do not work with traditional backpropagation. Instead, it uses backpropagation through time (BPTT) which differs from traditional backpropagation by summing the error at each time step. This takes place to support reinforcement learning by modifying the weights of parameters that are shared across each layer. Complications of recurrent neural networks with exploding gradients or vanishing gradients can be solved by reducing the number of hidden layers within the network. Thereby, reducing the complexity of the neural network which diminishes issues of having an unstable neural network or a network that no longer learns [1].

Theoretically a simple recurrent neural network is able to preserve all information from a long time-series input, however, due to the vanishing gradient problem the network has difficulties with learning such long-term dependencies [62].

7.1.1. Long Short-term Memory Network

The long short-term memory (LSTM) network is a type of recurrent neural network which is designed to overcome the vanishing gradient problem in traditional RNNs [63]. A LSTM consists of memory blocks with each memory block containing one or more cells with an input gate i_t, forget gate f_t, and output gate o_t. The input gate determines to what extend new information is allowed within the memory of a cell. The forget gate controls how old information is preserved or discarded from the memory cell. The output gate controls how the current memory of the cell should be applied in order to compute the output. A visual representation of a memory cell within a LSTM is presented in Figure 7.1.

[1] `https://www.ibm.com/topics/recurrent-neural-networks` (accessed 29-11-2023)

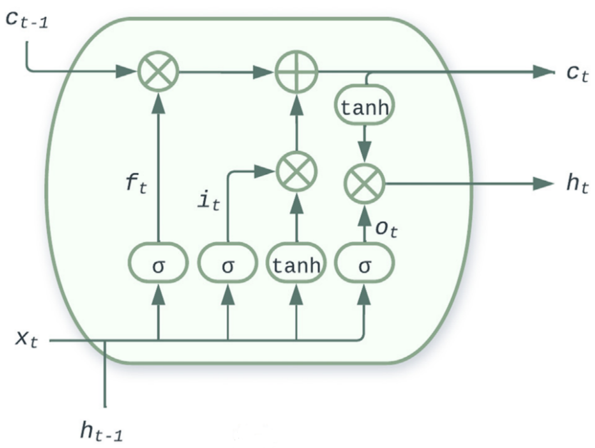

Figure 7.1: Architecture of a single memory cell within a long short-term memory network [63].

According to the results of Sahajpal et al. a long short-term memory network presents the best overall performance when it is deployed in transfer learning [63]. However, the transfer learning performance of a model is dependent on the similarity between different datasets. Not only the stack characteristics and the loading conditions play a role in transfer learning performance but also the set-up of the balance of plant around the stack.

7.2. Gated Recurrent Unit

The gated recurrent unit (GRU) is another recurrent neural network which differs slighly from a LSTM in respect to the memory cell. The configuration of the cell consists of an update gate z_t, reset gate r_t, and output gate. The update gate represents the input gate and forget gate from a LSTM. The reset gate determines to what extend past information needs to be forgotten or ignored. Therefore, the reset gate filters irrelevant information from the past within the model. The memory content h in a GRU represents the information from the previous time step and is updated by the update gate based on the input from the current time step. The architecture of a GRU is presented in Figure 7.2.

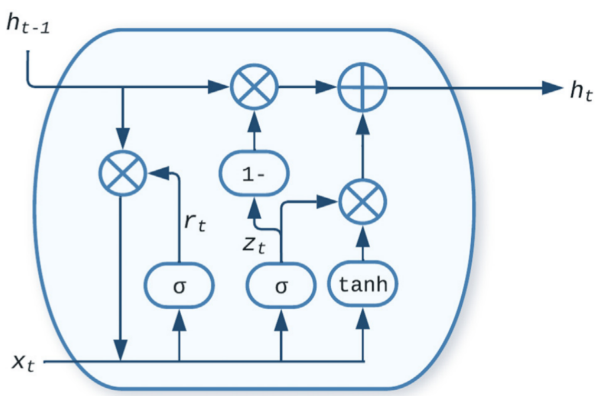

Figure 7.2: Architecture of a single memory cell within a gated recurrent unit [63].

The presented LSTM and GRU architectures in Figure 7.1 and Figure 7.2 process the input only in a forward direction. However, the input sequence can also be processed in a forward and backward direction by separation the neurons in the hidden layer into two sets which results in a bidirectional recurrent neural network. The information from the two sets can be linked to the output layer to improve prediction performance [64][65].

Gated recurrent units and long short-term memory networks can remember sequences of only 100 seconds, and is not able to remember sequences in the order of 1,000 seconds, 10,000 seconds or even longer sequences [62].

7.3. Echo State Network

The Echo State Network (ESN) is a type of Recurrent Neural Network (RNN). An Echo State Network consists of an input layer, a reservoir and an output layer. Generally a recurrent neural network consists of a hidden layer, however, in an Echo State Network the hidden layer is replaced by a reservoir. This reservoir is randomly generated and contains sparse connected neurons. The architecture of an ESN can be reviewed in Figure 7.3. The input, internal and feedback weight matrices are randomly generated. Only the output weights are trainable. *Schiller et al.* [66] presented that during training of recurrent neural networks dominant weight changes occur for the output weights. An Echo State Network takes advantage of this phenomenon by keeping the input and internal weights fixed. This reduces the number of parameters that need to be trained. The output weight matrix is trained by applying linear regression. The parameters that need to be defined are the number of neurons N_n in the dynamic reservoir, spectral radius ρ which represents the maximum eigenvalue of internal weight matrix W, leaking rate α which represents dynamic performance of the reservoir, regularisation parameter β, and coefficients of input and internal weight matrices W_{in} and W. According to *Xu* [62], the activation function is one of the key hyperparameters when constructing the reservoir. The activation function describes the behaviour of the reservoir units.

The dynamics of the neurons inside the reservoir needs to be optimised to obtain a balance between the stability of the network and the computational complexity of the output weights [22]. Furthermore, an optimised reservoir should preserve fading memory and result in neurons with a considerable level of dynamics. The level of dynamics of the reservoir is expressed by the Echo State Property (ESP), and needs to be considered carefully to obtain the aforementioned balance in an Echo State Network. *Jaeger* [67] states that a leaky integrator ESN has the Echo State Property if the initial conditions are washed out at a rate that is independent from the input. In practice, ESP is obtained when the effective spectral radius $|\lambda|_{max}(\hat{W})$ is smaller than 1 for zero inputs and larger or equal to 1 for non-zero inputs [68].

The parameters of an Echo State Network can be divided into three categories: assigned parameters, adjustable parameters, and a calculated parameter [22]. The assigned parameters are input, internal and feedback weight matrices (W_{in}, W, W_{fb}), and the dimension of the input and output signal (K, L). The adjustable parameters are number of neurons N_n, spectral radius ρ, leaking rate α, and regularisation parameter β. The calculated parameter is output matrix W_{out}. *Lukoševičius* [69] provide a detailed guide on manual parameter settings of an Echo State Network.

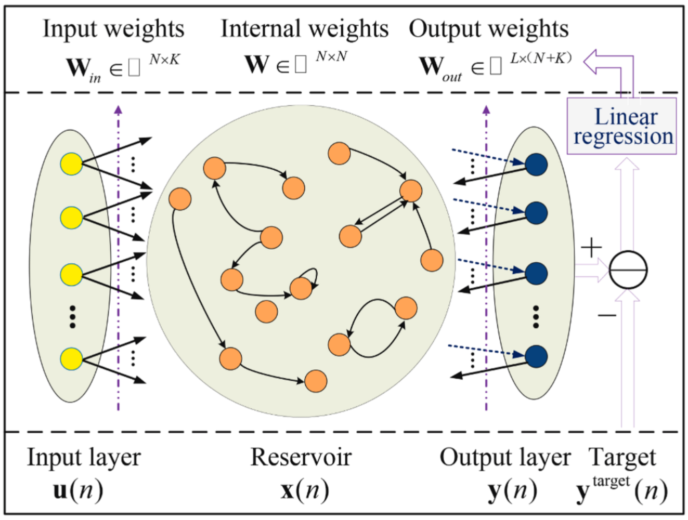

Figure 7.3: Architecture of Echo State Network [22].

7.3.1. SI-ESN and DI-ESN

Both single- and double-input Echo State Networks apply an iterative prediction procedure to generate multi-step ahead predictions [22]. The only input for the single-input ESN is the health indicator RPLR and for the double-input ESN the stack current is added as a second input parameter. A double-input ESN is only useful for PEM fuel cells which are used with a scheduled current profile such as the μ-CHP applications for which the load is related to seasonal changes.

A sensibility analysis is performed on the leaking rate α, spectral radius ρ, and regularisation parameter β, to understand the influence of the parameters on the prediction performance and the interactions between the parameters. An analysis of variance (ANOVA) is applied for this anaylsis which is a collection of statistical models and procedures to compare the effects of different variables [70]. A low, medium and high range of values were applied for each parameter; leaking rate α (0.3 for low level, 0.6 for middle level, and 0.9 for high level), spectral radius ρ (0.5 for low level, 1.0 for middle level, and 1.5 for high level), and regularisation parameter β (8×10^3 for low level, 8×10^2 for middle level, and 8×10^1 for high level). In total there were 27 test scenarios for which the root mean square error (RMSE) was analysed. The lowest RMSE was obtained by applying a high leaking rate of 0.9, a medium spectral radius of 0.7, and a medium regularisation parameter of 8×10^2.

7.3.2. DWT-EESN

Hua et al. [21] separated the relative power-loss rate signals into several layers by applying discrete wavelet transform (DWT). This results into a decomposition of the health indicator into multiple signals as presented in Figure 7.4. At each layer there is an approximation component cA_i and a detail component cD_i, which are of low-frequency and high-frequency, respectively. The approximation components can be utilised for long-time intervals of the original signal and detail components for short-time intervals. The number of decomposition layers were determined empirically, applying more layers for tests with a higher level of complexity. Each decomposed signal, or sub-waveform, is normalised and then predicted by several independent Echo State Networks with different dynamic parameters. The predicted results of each sub-waveform are denormalised and ensembled into a final result. The remaining useful life is computed based on the new relative power-loss rate. New measurements are not needed during the prediction phase because the relative power-loss rate of the last step is used to predict the new relative power-loss rate by the ensemble Echo State Network.

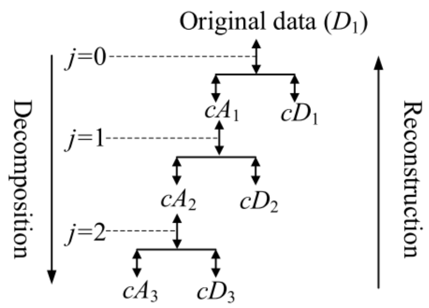

Figure 7.4: Wavelet transform for signal decomposition. This results into several layers containing an approximation component coefficient cA_i and a detail component coefficient cD_i. These components can be combined to reconstruct the original signal [20].

7.3.3. DWT-ESN-GA

A genetic algorithm is added to an Echo State Network with a discrete wavelet transform element [20]. The genetic algorithm optimises three key parameters of the Echo State Network. Namely, the leaking rate α, the spectral radius ρ and the regression coefficient γ which is a different name for the regularisation parameter β. Only a single Echo State Network is applied to predict the approximation component coefficient of one layer. A quantitative analysis, called relative wavelet energy, is performed to understand if important information is lost by only incorporating this single approximation component coefficient for predicting the health indicator. The energy of the approximation component coefficient is compared to the total energy. This analysis showed that the detail component coefficients only contain $1 \times 10^{-2} - 1 \times 10^{-7}$ of the total signal energy. Thus, the approximation component coefficient can be utilised as a decent representation of the original signal.

7.4. Forecasting Approach

Multi-step ahead predictions can be divided into two categories: single output approaches and multiple output approaches [71]. The iterative, direct, and DirRec approaches are single output approaches, and parallel and multiple-input several multiple-outputs (MISMO) approaches are multiple output approaches. An overview is provided in Figure 7.5.

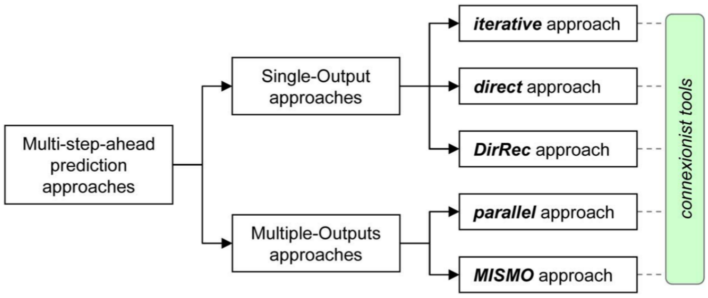

Figure 7.5: Overview of multi-step ahead prediction techniques [72].

The general approach which is known for multi-step predictions is the iterative approach. A single model is fine-tuned for one-step ahead predictions and the model used the predicted value for the next prediction step until the prediction horizon is reached. The method is prone to propagation error due to the iterative nature of the technique. Therefore, special care must be given to extended prediction horizons in order to reach accurate results [72].

The direct approach consists of multiple models with each model generating a prediction at a specific prediction horizon [72]. Furthermore, the same input data is used to generate a different single prediction. Therefore, this approach is not beneficial when limited training data is required to generate long-term predictions.

DirRec approach, introduced by *Sorjamaa and Lendasse* [73], is a combination of a direct and recursive technique [74]. The difference between the DirRec approach and the iterative approach is the use of a model which is updated based on the information that is predicted. The difficulties with error propagation is also present within the DirRec approach because of the iterative nature [72].

The parallel approach is based on a single model which creates a prediction of multiple parameters simultaneoulsy. This approach requires less computing time compared to the direct approach because there is only one model to be tuned.

The MISMO approach consists of multiple models each with a set of outputs determined by the input parameters. The number of models can be defined and when only a single model is applied then the approach is similar to the direct approach.

8

Experimental and Simulation Data

This chapter discusses available experimental datasets and a simulation tool from ZAL for prediction on the remaining useful life of PEM fuel cells. There are three available datasets, one from ZAL and two from FCLAB, which are based on durability tests and are applicable to the research. The operating conditions and monitored data are discussed.

8.1. ZAL Experimental Data

Within ZAL there are two datasets available which contain 82.5 hr and 8000 hr of test data. The first dataset contains test data of a 20kW Hydrogenics stack from 2005 which was used within a ground airport vehicle and arrived at ZAL in 2018. No data is available before the arrival of the stack at ZAL. Furthermore, no detailed documentation is present on the type of current profiles that were tested. Lastly, the total duration of the test data does not aid in reaching the thesis objective of long-term predictions in the order of weeks because 82.5 hr of test data represents half a week of continuous operating time. The second dataset contains durability test data of a 9.75W single cell with a wet bonded FEP membrane (FEP-hp(wet)) and an active area of 30 cm^2 tested at a constant current density of 500 mA/cm^2 by *Gubler et al.* [36]. Access to the dataset was provided by ZAL's thesis supervisor and co-author *Kuhn*. Performance characteristics of the single cell were monitored over time. Polarization curves were recorded at different intervals during the experiment. Electrochemical impedance spectra were recorded initially and at different run times to analyse cell performance. Furthermore, cyclic voltammetry was performed at the end of the test to inspect the cathode electrode and the membrane was inspected on potential cracks, discolouration, and other types of degradation.

An initial test plan was drafted to perform a durability test for 500 hr on a H3Dynamics Aerostack A1500 LV with a dynamic current profile that represents a drone. However, due to an early malfunction within the fuel cell stack the stack had to be returned to the manufacturer and the durability test was deemed impractical within the timespan of this thesis.

8.2. IEEE PHM 2014 Data Challenge Datasets

The IEEE PHM 2014 Data Challenge Datasets [19] contains durability test data of two identical PEM fuel cells which was publicly released to accelerate research in predicting remaining useful life of PEM fuel cells. The PEM fuel cell is a 1.0kW five-cell stack, from manufacturer UBZM, with each cell having an active area of 100 cm^2 and a nominal current density of 0.70 A/cm^2. Two experiments are conducted to two identical fuel cells with a duration of 1155 hr and 1021 hr. One with a constant 70A load current and the other with added high-frequency triangular ripples of 7A current. These experimental datasets are denoted as *FCLAB-1* and *FCLAB-2* for the static and quasi-dynamic dataset, respectively. The current profiles applied during experimental testing and the test bench are presented in Figure 8.1 and Figure 8.2, respectively. The dataset with current ripples is an important test scenario because it represents the connection between a PEM fuel cell and a power converter according to *Sahajpal et al.* [63] which is an essential component in a hydrogen-electric powertrain.

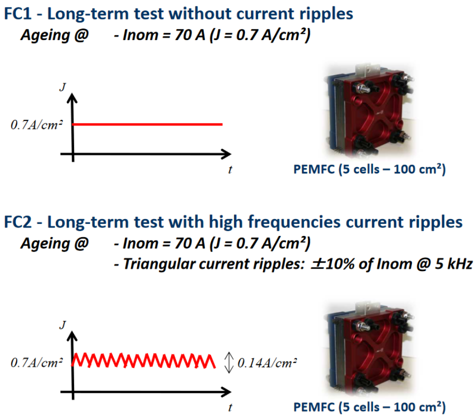

Figure 8.1: Static and quasi-dynamic current profiles applied to two identical UBZM five-cell PEM fuel cell stack within IEEE PHM 2014 Data Challenge [19].

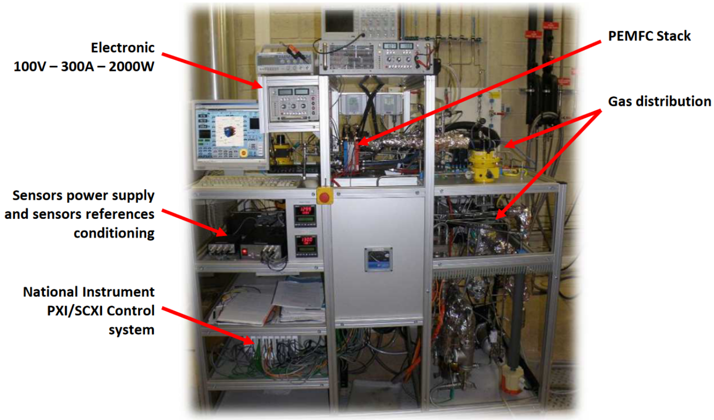

Figure 8.2: Test bench of PEM fuel cell durability test from IEEE PHM 2014 Data Challenge [19].

The data monitored during each durability test includes the aging time, the five cell voltages, the stack voltage, the load current, the load current density, the inlet and outlet temperatures, the flow rates of hydrogen, air, and cooling water, the inlet and outlet pressures of hydrogen and air, and the estimated relative humidity of hydrogen and air were obtained during the experiments. An overview of the monitored data is provided in Table 8.1. Weekly characterisation tests and electrochemical impedance spectroscopy were performed to further analyse degradation within the PEM fuel cell. *Liu et al.* identified that degradation in cell 3 for *FC 1* and in cell 5 for *FC 2* is most serious, with a degradation rate of 31 μV/h and 30 μV/h, respectively. In both datasets, degradation of cell 1 is the smallest. Cell 1 in the PEM fuel cell represents the cell closest to the gas inlet, and cell 5 represents the cell farthest from the gas inlet.

Table 8.1: Data montitored during IEEE PHM 2014 Data Challenge [19].

Index in Dataset	Physical Meaning
Time	Aging time (h)
U_1 to U_5	Single cell voltages (V)
U_{tot}	Stack voltage (V)
I	Current (A)
J	Current Density $\left(\mathrm{A/cm^2}\right)$
TinH2 & ToutH2	Inlet and outlet temperatures of H_2 (°C)
TinAIR & ToutAIR	Inlet and outlet temperatures of air (°C)
TinWAT & ToutWAT	Inlet and outlet temperatures of cooling water (°C)
PinH2 & PoutH2	Inlet and outlet pressure of H_2 (mbar)
DinH2 & DoutH2	Inlet and outlet flow rate of H_2 (l/mn)
DinAIR & DoutAIR	Inlet and outlet flow rate of air (l/mn)
DWAT	Flow rate of cooling water (l/mn)
HrAIRFC	Estimated air inlet hygrometry (%)

8.3. FCLAB μ-CHP Datasets

Another durability dataset is introduced due to the research conducted by *Hua et al.* [20–22] for long-term prediction of PEM fuel cells used in combined heat and power of buildings. Three dynamic tests are performed for the PROPICE project, “Prognostic and Health Management of PEM Fuel Cell Systems", for which eight 1.0 kW fuel cell stacks are tested. The duration of the tests are 383 hr, 1000 hr and 405 hr [22]. Each test is divided into different stages. During each stage a different load current density is applied. The load current density is either alternating between two or several values within a stage or is defined at a fixed value. Data-driven techniques are applied for predicting the RUL and the performance of the different techniques are compared in section 9.2.

8.4. ZAL Simulation Model

A simulation model of an air cooled PEM fuel cell is created in Dymola Behaviour Modeling, which is a package within 3DExperience. The components of a PEM fuel cell are placed in the model as building blocks that interact with each other. The physical interactions are described by mathematical equations. The model consists of a membrane, cathode channel, anode channel, cooling channel, and incoming and outcoming ports at each building block. The electrochemical reactions within the membrane are described by a detailed model. The gas properties are handled by a heat transfer model at the cathode and anode. No degradation is considered within the simulation model of ZAL. Furthermore, selection of parameters is conducted iteratively based on experimental data. Therefore, there are limitations to how this simulation model can be applied.

9 Prediction Horizon

This chapter discusses the prediction horizon of various data-driven techniques for the available IEEE PHM 2014 Data Challenge Datasets and the non-available FCLAB μ-CHP Datasets.

9.1. IEEE PHM 2014 Data Challenge Datasets

Various techniques have been created to predict voltage degradation, component degradation, and/or remaining useful life based on IEEE PHM 2014 Data Challenge Datasets, as mentioned in ??. A voltage threshold is defined to indicate the RUL. Besides voltage threshold dependency, is RUL also dependent on the split in training-validation-testing datasets. Different techniques are discussed and compared to understand current prediction capabilities.

Sahajpal et al. [63] tested six deep learning techniques to predict voltage degradation. The methods were long short-term memory (LSTM) networks, gated recurrent units (GRUs), and a combination of LSTMs and GRUs with a 1-D convolutional neural network (CNN) and a bidirectional element. Fuel cell stack measurements from the IEEE PHM 2014 Data Challenge Datasets were used as a data source. The fuel cell stack data was lagged by one timestep of 1 hr. Cell voltage data was removed, however, measurements on stack voltage were preserved in training, validation, and testing datasets. The data from a lagged timestep was used to predict the stack voltage of 1 hr later. The predicted stack voltage was not used as an input for the next prediction step. Therefore, the prediction horizon for voltage degradation as health indicator is just 1 hr. A threshold of 96% of initial stack voltage was applied to determine the remaining useful life. This threshold corresponds with previously defined voltage threshold on this dataset by Bennagoune et al. [75], Xia et al. [17], and Li et al. [23].

Li et al. [23] created a fusion model that consisted of a bidirectional-LSTM-GRU in combination with an ESN for voltage predictions. Features were extracted with a particle swarm optimisation (PSO) algorithm which were then processed into the ESN. A prediction horizon of 100 hr was obtained by integrating a sliding-window approach which led to a RUL prediction error up to 3% for 200 hr of training which is 20% of the complete dataset.

Table 9.1: RUL prediction of fusion technique with bi-directional-LSTM-GRU and ESN on dataset FC1 and FC2 [23].

Dataset	Voltage threshold (V)	Training phase (hr)	Actual RUL (hr)	Prediction RUL (hr)	E_r (%)
FC1	3.203	200	609	616.43	1.22%
		300	509	518.46	1.86%
		400	409	417.01	1.96%
		500	309	317.01	2.59%
FC2	3.182	200	195	189.19	2.98%

Bennagoune et al. [75] proposed a dilated and conditional convolutional neural network (CNN) with a multi-step ahead prediction method. For a prediction horizon of 24 hr, which consisted of 24 steps, a RMSE and

MAPE of 0.0092, 0.1625 and 0.0132, 0.2661 were achieved on voltage degradation with a dilated CNN for FC1 and FC2, respectively. A stacked dilated CNN is used in a conditional CNN for which the RUL predictions are presented in Table 9.2.

Table 9.2: RUL comparison of conditional CNN (ConCNN), dilated CNN (DilCNN), ESN, and LSTM [75].

PEMFC1	Prognostics starting at (hr)					
	591	691	791	891	991	
True RUL	437	337	237	137	37	
ConCNN	**364**	**288**	**191**	**167**	10	
DilCNN	90	115	77	221	54	
ESN	371	-	292	485	211	
LSTM	141	209	89	61	37	
PEMFC2	Prognostics starting at (hr)					
	681	731	781	831	881	931
True RUL	277	227	177	127	77	27
ConCNN	**227**	**179**	**157**	**108**	**58**	**16**
DilCNN	196	286	112	188	48	41
ESN	330	167	222	177	127	-
LSTM	190	-	14	91	26	14

Xia et al. [17] decomposed the voltage signal into a calendar aging component and a reversible aging component with a locally weighted regression method (LOESS). The calendar and reversible aging components are predicted by an adaptive extended Kalman filter and a LSTM neural network, respectively. A genetic algorithm is applied to optimise hyperparameters of the LSTM during the training process. The final voltage degradation is obtained by combining the two components. A voltage threshold of 4% and 5% is applied to predict the RUL.

Table 9.3: RUL comparison of 1D-CNN-Bi-GRU, conditional CNN (ConCNN), dilated CNN (DilCNN), Bi-LSTM-GRU-ESN, and T-AEKF-LSTM, on FC-2 dataset.

	1D-CNN-Bi-GRU	ConCNN	DilCNN	Bi-LSTM-GRU-ESN	T-AEKF-LSTM
Train-val-test Split	510-102-408	681-0-339	681-0-339	200-0-820	561-0-459
True RUL (hr)	277	277	277	195	359
Predicted RUL (hr)	274	227	196	189.2	348
Prediction Horizon (hr)	1	24	24	100	20
Health Indicator	Voltage	Voltage	Voltage	Voltage	Voltage
Year	2023	2022	2022	2022	2023
Reference	[63]	[75]	[75]	[23]	[17]

9.2. FCLAB μ-CHP Datasets

Four different data-driven techniques have been created by *Hua et al.* to predict long-term the remaining useful life of PEM fuel cells subjected to combined heating and power of a building. In Table 9.4 performance details are provided of a single-input and double-input echo state network based on the 1000 hr test from the PROPICE project. These two techniques are compared to two other echo state networks in Table 9.5 which contain a discrete wavelet transform component and a genetic algorithm. The discrete wavelet transform is further discussed in subsection 7.3.2.

Table 9.4: Prediction results of RUL and evaluation criteria on RPLR for single-input ESN (SI-ESN) and double-input ESN (DI-ESN) [22].

ESN type	Training length (%)	Actual RUL (h)	Prediction RUL (h)	%Er_(FT)(%)	RMSE	MAPE
SI-ESN	40	600	468	22.0	0.01331	0.12065
	50	500	497	0.6	0.00879	0.09849
	60	400	174	56.5	0.02819	0.19113
	70	300	110	63.3	0.02422	0.18926
	80	200	122	39.0	0.01244	0.10711
	90	100	90	10.0	0.00885	0.05098
DI-ESN	40	600	390	35.0	0.02065	0.14497
	50	500	438	12.4	0.00788	0.07125
	60	400	342	14.5	0.00810	0.06666
	70	300	215	28.3	0.01197	0.10634
	80	200	138	9.0	0.00631	0.03575
	90	100	40	0.0	0.00440	0.02720

Table 9.5: Comparison of prediction performance of single-input ESN (SI-ESN), double-input ESN (DI-ESN), discrete wavelet transform and ensemble ESN (DWT-EESN), genetic algorithm with DWT-ESN (DWT-ESN-GA).

	SI-ESN	DI-ESN	DWT-EESN	DWT-ESN-GA
Dataset	μ-CHP	μ-CHP	μ-CHP	μ-CHP
Test	1000 hr	1000 hr	1000 hr	1000 hr
Train-val-test Split	600-0-400	600-0-400	600-0-400	672-0-328
True RUL (hr)	400	400	-	160
Predicted RUL (hr)	174	342	-	168
Prediction Horizon (hr)	150	250	-	168
Health Indicator	RPLR	RPLR	RPLR	RPLR
RMSE of HI	0.02819	0.00810	0.00555	0.0036
MAPE of HI	0.19113	0.06666	0.07027	0.0438
Year	2021	2021	2022	2022
Reference	[22]	[22]	[21]	[20]

10
Research Framework

This chapter discusses the research gap within the field of prognostics and health management of PEM fuel cells. The main research question and sub-research questions are stated and the objective of this thesis is explained.

10.1. Research Gap

There is a limited prediction horizon of long-term multi-step ahead predictions on the remaining useful life of PEM fuel cells. A maximum prediction horizon of 100 hr and 250 hr is achieved by prediction techniques that applied IEEE PHM 2014 Data Challenge Datasets and FCLAB μ-CHP Datasets, respectively. From a client perspective an extended prediction horizon is beneficial because it provides an opportunity to take actions and prevent use-beyond-repair. The largest prediction horizon of 250 hr, which is 10.4 days if the system is continuously used, is a tight window for a client to schedule and execute a heavy maintenance check. Furthermore, health indicators that provide a long-term prediction horizon of the RUL are focused on fuel cell performance and do not provide any health information on component-level. This research will provide an extended prediction horizon of the RUL, a health indicator on fuel cell performance, and a health indicator on the membrane and electrode condition which are considered as the most crucial components.

10.2. Research Questions

The main research question of this project is as follows:

How to quantify, assess, and forecast the long-term health of proton-exchange membrane fuel cells and their critical components tested in a laboratory under static and quasi-dynamic operating conditions?

The sub-questions that support the main research question are:

1. *Which health indicator(s) is/are most suitable for expressing the degradation of PEM fuel cells tested under static and quasi-dynamic conditions?*
2. *How to model long-term degradation of the membrane and electrode within PEM fuel cells?*
3. *How to enhance the prognostic horizon of long-term predictions on the remaining useful life of PEM fuel cells tested under static and quasi-dynamic conditions?*
4. *How can system and component degradation indicators be linked to the remaining useful life of PEM fuel cells?*

10.3. Research Objective

The main objective of this thesis is described by the following statement:

This research aims to combine various degradation models and generate an iterative prediction tool to enhance *the prediction horizon of the RUL of PEM fuel cells and the interpretability of stack degradation through component health indicators.*

11
Approach

This chapter discusses the approach on how the health of a PEM fuel cell can be quantified, assessed, and forecasted. Information is provided on health indicators related to stack performance and on characteristics of critical components which can be extracted from the available datasets. The relationship options between remaining useful life and health indicators are proposed. Furthermore, an explanation is provided on how degradation models can be applied to compose health indicators for critical components within PEM fuel cells. A prognostic technique is proposed based on current prediction horizon and performance of various data-driven techniques. Lastly, a brief overview is discussed on how the activities and deadlines are planned throughout this thesis.

11.1. Quantify Health of PEM Fuel Cells

This section discusses the available datasets and the health indicator options to indicate the health of PEM fuel cells. An explanation is provided on how the health indicators can be associated with the remaining useful life and what the limitations are of the relation between health indicators and remaining useful life.

Stack and Component Health Indicator

To predict the health of a PEM fuel cell stack and the RUL it is essential to select health indicators which can be determined with the available datasets. There are three datasets available within this thesis. The first dataset is from ZAL which consists of 8000 hr of experimental data from a single cell with a static current profile. A second, and third dataset, are from the IEEE PHM 2014 Data Challenge, which contain 1155 hr with a static current profile and 1021 hr with a quasi-dynamic current profile of a five-cell stack, respectively.

As discussed in subsection 5.2.4, *Liu et al.* [13] presented that a multi-scale hybrid health indicator can be generated based on component degradation with the use of IEEE PHM 2014 Data Challenge Datasets and validated degradation models for membrane and electrode. The degradation models, which were discussed in chapter 6, can be applied to different PEM fuel cells when the catalyst material consists of a platinum metal compound, which is the case for all three datasets. However, utilisation of the membrane degradation models presents a challenge due to the absence of specific degradation models that are tailored to the GORE-SELECT membrane material of IEEE PHM 2014 Data Challenge Datasets. Instead, the commonly available membrane degradation models are designed for Nafion membranes. Nafion and GORE-SELECT membranes share similar primary materials, with both being composed of perfluorosulfonic acid (PFSA) membrane. Both types of membranes undergo similar destruction mechanisms during PEM fuel cell operation. Thereby, aligning their chemical degradation processes. Experimental evidence suggests comparable relative stability between Nafion and GORE-SELECT membranes under certain stress levels, further supporting the similarity of their chemical degradation processes [76**?** , 77]. By assuming an equivalence in chemical degradation rates under identical operating conditions, chemical degradation models established for Nafion can be considered applicable to GORE SELECT membranes.

The thesis proposes a modification to the approach outlined by *Liu et al.* [13]. Rather than generating a single health indicator for PEM fuel cells, multiple indicators are suggested to better express their health. This modified approach focuses on deploying degradation models for both the membrane and electrode, resulting in the generation of two distinct health indicators. One designated health indicator for the membrane and another for the electrode. The emphasis on the membrane and electrode health aligns with the findings of *Jouin et al.* [11], who highlighted these components as critical regarding degradation. By generating these component-specific indicators, the aim is to gain deeper insights into the reasons behind the degradation of overall stack performance over time.

Furthermore, as noted by *Hua et al.* [20], overall stack performance can be evaluated through degradation in voltage, power, or relative power-loss rate. Throughout the thesis, the impact of each performance indicator will be thoroughly evaluated. The objective of using both stack performance and component condition indicators is to provide details on the health status of the membrane and electrode when performance degradation occurs. This approach aims to provide a comprehensive understanding of PEM fuel cell health dynamics.

Relationship Health Indicators and Remaining Useful Life

There are two approaches for correlating the predicted health indicators with the remaining useful life. The first approach involves directly linking a stack performance health indicator to the RUL. The second approach entails merging multiple health indicators into a unified health indicator. In both cases, a common technique for RUL determination involves defining a failure threshold. These possibilities will be thoroughly explored throughout the thesis.

11.2. Assess Health of PEM Fuel Cell

The health of the membrane and electrode in PEM fuel cells, which are the most critical components, can be assessed by applying validated degradation models as discussed in chapter 6.

The determination of membrane thickness and electrochemical catalyst surface area (ECSA) serves as vital health indicators for the membrane and electrode in PEM fuel cells. *Karpenko-Jereb et al.* [10] proposed a semi-empirical model to assess membrane thickness, providing insights into membrane health. By integrating physico-chemical properties, this model facilitates the analysis of membrane degradation based on the oxygen crossover rate, crucial for evaluating membrane integrity over time. Moreover, *Chandesris et al.* [42] introduced a model linking membrane thickness degradation to fluoride release, offering further insights into membrane thickness. Understanding membrane thickness dynamics aids in assessing the health of membranes in PEM fuel cells. Thereby, providing essential information for maintenance.

Similarly, ECSA degradation, assessed through models like those proposed by *Moein-Jahromi et al.* [44] and *Polverine and Pianese* [9], offers valuable insights into electrode health. These models, accounting for catalyst degradation mechanisms such as platinum dissolution and particle coarsening, provide a means to evaluate electrode health indicators. By estimating ECSA and voltage degradation under various operating conditions, these models enable assessment of electrode performance and degradation trends. Additionally, *Robin et al.'s* [58] platinum dissolution model further assists in understanding ECSA dynamics within the electrode, enhancing the capability to assess electrode health indicators comprehensively. Utilising ECSA degradation models aids in monitoring electrode health, facilitating timely interventions to maintain PEMFC performance and prolong electrode lifespan. Together, membrane thickness and ECSA degradation models serve as tools for evaluating the health and life of PEM fuel cell membranes and electrodes, essential for ensuring optimal performance and durability of fuel cell systems.

Required information to apply aforementioned degradation models on the tested PEM fuel from IEEE PHM 2014 Data Challenge is provided by the manufacturer UBZM, documented by *Hinaje et al.* [78], and presented in Table 11.1. Further internal discussions with ZAL is required on the single cell specifications for applying the degradation models on the 8000 hr dataset from ZAL.

Table 11.1: Characteristics and experimental operating parameters of PEM fuel cell from IEEE PHM 2014 Data Challenge [13][19][78].

Parameter	Value
GDL thicknesses	400 μm
Membrane thickness	15 μm
Cell active area	100 cm^2
Membrane Electrode Assemblies type	GORE PRIMEA 5761
Membrane type	GORE-SELECT®
Open circuit voltage	1 V
Nominal voltage	0.6 V
Rated power	30 W
Cell number	5
Manufacturer	UBZM, Germany
Relative humidity of anode and cathode	50%
Temperature	60 °C
Absolute pressure of anode and cathode	1.5 bar
Stochiometry ratio of anode and cathode	1.5-2
Inlet Pressure of anode and cathode	1.3 bar

Other type of degradation which are considered as rapid phenomena, such as membrane drying and flooding, are not considered within the approach because of the limited data present. To monitor membrane drying and flooding it is essential to have access to data from the purge valve, among other things [79].

11.3. Forecast Health of PEM Fuel Cell

This section discusses the selection process of a prediction technique, which will be applied to improve current long-term predictions on the selected health indicators with a multi-step ahead approach.

Prediction Technique

From chapter 9, two prediction techniques are highlighted due to their high achieved prediction horizons. The first technique, proposed by *Hua et al.* [22], applies a single input echo state network to forecast the relative power-loss rate, and determine the remaining useful life. The multi-step ahead technique has a prediction horizon of 150 hr. However, the RUL errors are quite significant and further research can be performed on how to improve this technique. The second technique, introduced by *Li et al.* [23], combines three recurrent neural networks. Utilising a long short-term memory network and a gated recurrent unit, complemented by a bi-directional element for feature extraction. Additionally, an echo state network with a sliding window is used to predict stack voltage, which serves as the selected health indicator and is linked to the RUL. This method achieves a single prediction with a horizon of 100 hr. However, the sliding window technique requires continuously experimental data and does not re-use predicted values for a next prediction. Both techniques are based on echo state networks and showcase the robustness in health indicator predictions by leveraging the simplicity, efficiency, and effectiveness of echo state networks in predicting temporal data. However, it is crucial to acknowledge that the performance of echo state networks heavily depends on appropriate reservoir initialisation and parameter tuning [69].

To provide a baseline for hyperparameter tuning and reservoir initialisation, the work of Hua et al. [8, 20–22, 80] offers valuable insights, detailing tuned hyperparameters and reservoir initialisation procedures.

In the broader literature, various hyperparameter tuning techniques have been explored, including Optuna [63], particle swarm optimization [23], ANOVA [22], and genetic algorithms [20]. These diverse methodologies contribute to the refinement and optimisation of predictive models. These techniques will be investigated during the thesis.

Throughout this thesis, additional focus will be directed towards exploring different preprocessing techniques, parameter optimisation strategies, and the potential of transfer learning methods, aiming to enhance the predictive capabilities of the proposed models.

11.4. Thesis Planning

This section discusses the activities that take place during the thesis and its duration. The information is presented by use of a Gantt chart in Figure 11.1. This chart also shows the milestones and deadlines of the thesis project.

Figure 11.1: Gantt chart to provide overview of planned activities during the literature study and thesis, the milestones and holidays.

12

Conclusion

This thesis has demonstrated advancements in predicting the degradation and Remaining Useful Life (RUL) of Proton-exchange Membrane (PEM) fuel cells through the application of data-driven and empirical methodologies. By leveraging extensive datasets from the FCLAB Research Federation, including the *FC1 Dataset* and *FC2 Dataset*, this research has addressed the complex challenges associated with fuel cell prognostics.

The use of Seasonal and Trend decomposition via LOESS (STL) to break down current and voltage time-series data into trend, seasonal, and residual components has proven effective in isolating the underlying patterns and variations. Comparing the forecasting capabilities of Long Short-Term Memory (LSTM) networks and Echo State Networks (ESNs) has highlighted the strengths and limitations of these approaches. Notably, the optimised ESN demonstrated an ability to iteratively predict voltage components, achieving a Prognostic Horizon (PH) of 125 hr, which is a substantial improvement in medium-term predictive accuracy.

The integration of empirical and semi-empirical models for membrane thickness degradation has further refined the predictive framework, by applying linear regression to minimise reliance on experimental data. The combination of predicted voltage and membrane thickness data has facilitated RUL forecast, offering insights into PEM fuel cell health over extended operational periods.

The findings of this research show the effectiveness of the proposed methodology in managing the performance and reliability of PEM fuel cells. The application of STL, LSTM, and ESN models, coupled with empirical degradation modeling, demonstrates the potential for these techniques to enhance the predictive maintenance strategies for PEM fuel cells.

In summary, this thesis has provided a framework for PEM fuel cell degradation prediction, offering practical solutions and insights that can be applied to various operational scenarios. Future work could explore further refinements of these models and their application to different types of fuel cells and operating conditions.

Bibliography

[1] Adler, M., Peerlings, B., Boonekamp, T., van der Sman, E., Lim, N., Jongeling, A., and Pel, S. "The price of net-zero: Aviation investments towards destination 2050,". Technical report, SEO Amsterdam Economics and Royal Netherlands Aerospace Centre, Amsterdam, 3 2023.

[2] Fuel Cell and Hydrogen 2 Joint Undertaking. "Hydrogen roadmap Europe: a sustainable pathway for the European energy transition,". Technical report, Luxembourg, 2019. doi: 10.2843/341510. URL `https://www.clean-hydrogen.europa.eu/document/download/b4ea2b61-a7da-4484-a522-1b2232bff134_en?filename=Hydrogen%20Roadmap%20Europe_Report.pdf`.

[3] Stanton, I., Munir, K., Ikram, A., and El-Bakry, M. "Predictive maintenance analytics and implementation for aircraft: Challenges and opportunities," *Systems Engineering* Vol. 26, No. 2, 2023, pp. 216–237. ISSN 10981241 (ISSN). doi: 10.1002/sys.21651. URL `https://www.scopus.com/inward/record.uri?eid=2-s2.0-85145178898&doi=10.1002%2fsys.21651&partnerID=40&md5=aa7c3ead5b2713fe1615e684342cbbdc`.

[4] Madheswaran, D. K., Thangamuthu, M., Gnanasekaran, S., Gopi, S., Ayyasamy, T., and Pardeshi, S. S. "Powering the Future: Progress and Hurdles in Developing Proton Exchange Membrane Fuel Cell Components to Achieve Department of Energy Goals—A Systematic Review," *Sustainability (Switzerland)* Vol. 15, No. 22, 2023. ISSN 20711050 (ISSN). doi: 10.3390/su152215923. URL `https://www.scopus.com/inward/record.uri?eid=2-s2.0-85181910311&doi=10.3390%2fsu152215923&partnerID=40&md5=5718786f504c4c09a1fdcb235cd4f41a`.

[5] Kongkanand, A., Masten, D., Wang, C., Chen, J., Spendelow, J., James, B., and Huya-Kouadio, J. "Automotive fuel cell targets and status,". Technical report, U.S. Department of Energy, Washington DC, 8 2020. URL `https://www.hydrogen.energy.gov/docs/hydrogenprogramlibraries/pdfs/20005-automotive-fuel-cell-targets-status.pdf`.

[6] Yue, M., Li, Z., Roche, R., Jemei, S., and Zerhouni, N. "Degradation identification and prognostics of proton exchange membrane fuel cell under dynamic load," *Control Engineering Practice* Vol. 118, 2022. ISSN 09670661 (ISSN). doi: 10.1016/j.conengprac.2021.104959. URL `https://www.scopus.com/inward/record.uri?eid=2-s2.0-85117216245&doi=10.1016%2fj.conengprac.2021.104959&partnerID=40&md5=028fadf585551e5d60513716db192357`.

[7] Ebner, K. and Koops, L. "Potentials of prognostics and health management for polymer electrolyte fuel cells in aviation applications," *Aircraft Engineering and Aerospace Technology* Vol. 94, No. 9, 2022, pp. 1481–1490. ISSN 17488842 (ISSN). doi: 10.1108/AEAT-01-2022-0020. URL `https://www.scopus.com/inward/record.uri?eid=2-s2.0-85130118799&doi=10.1108%2fAEAT-01-2022-0020&partnerID=40&md5=d56a152957ca47688f3467aae4a345b3`.

[8] Hua, Z., Zheng, Z., Pahon, E., Péra, M. C., and Gao, F. A review on lifetime prediction of proton exchange membrane fuel cells system, 5 2022. ISSN 03787753.

[9] Polverino, P. and Pianese, C. "Model-based prognostic algorithm for online RUL estimation of PEMFCs,". In Sarrate, R., editor, *Conference on Control and Fault-Tolerant Systems, SysTol*, Vol. 2016-November, pp. 599–604. IEEE Computer Society, 2016. ISBN 21621195 (ISSN); 978-150900658-8 (ISBN). doi: 10.1109/SYSTOL.2016.7739814. URL `https://www.scopus.com/inward/record.uri?eid=2-s2.0-85002170889&doi=10.1109%2fSYSTOL.2016.7739814&partnerID=40&md5=bb852e53fc1a0c2ef8bb90675e5a6ff4`.

[10] Karpenko-Jereb, L., Sternig, C., Fink, C., and Tatschl, R. "Membrane degradation model for 3D CFD analysis of fuel cell performance as a function of time," *International Journal of Hydrogen Energy* Vol. 41, No. 31, 2016, pp. 13644–13656. ISSN 03603199 (ISSN). doi: 10.1016/j.ijhydene.2016.

05.229. URL https://www.scopus.com/inward/record.uri?eid=2-s2.0-84991813348&doi=10.1016%2fj.ijhydene.2016.05.229&partnerID=40&md5=700eb133a59003e0b5b3895cf6e07400.

[11] Jouin, M., Gouriveau, R., Hissel, D., Péra, M. C., and Zerhouni, N. ”Degradations analysis and aging modeling for health assessment and prognostics of PEMFC,” *Reliability Engineering & System Safety* Vol. 148, 4 2016, pp. 78–95. ISSN 0951-8320. doi: 10.1016/J.RESS.2015.12.003.

[12] Liu, H., Chen, J., Hissel, D., Lu, J., Hou, M., and Shao, Z. ”Prognostics methods and degradation indexes of proton exchange membrane fuel cells: A review,” *Renewable and Sustainable Energy Reviews* Vol. 123, 5 2020, page 109721. ISSN 1364-0321. doi: 10.1016/J.RSER.2020.109721.

[13] Liu, H., Chen, J., Hissel, D., Hou, M., and Shao, Z. ”A multi-scale hybrid degradation index for proton exchange membrane fuel cells,” *Journal of Power Sources* Vol. 437, 10 2019, page 226916. ISSN 0378-7753. doi: 10.1016/J.JPOWSOUR.2019.226916.

[14] Jahnke, T., Futter, G., Latz, A., Malkow, T., Papakonstantinou, G., Tsotridis, G., Schott, P., Gérard, M., Quinaud, M., Quiroga, M., Franco, A. A., Malek, K., Calle-Vallejo, F., Ferreira De Morais, R., Kerber, T., Sautet, P., Loffreda, D., Strahl, S., Serra, M., Polverino, P., Pianese, C., Mayur, M., Bessler, W. G., and Kompis, C. ”Performance and degradation of Proton Exchange Membrane Fuel Cells: State of the art in modeling from atomistic to system scale,” *Journal of Power Sources* Vol. 304, 2 2016, pp. 207–233. ISSN 0378-7753. doi: 10.1016/J.JPOWSOUR.2015.11.041.

[15] Liu, J., Li, Q., Chen, W., Yan, Y., Qiu, Y., and Cao, T. ”Remaining useful life prediction of PEMFC based on long short-term memory recurrent neural networks,” *International Journal of Hydrogen Energy*, 2019, pp. 5470–5480. ISSN 03603199 (ISSN). doi: 10.1016/j.ijhydene.2018.10.042. URL https://www.scopus.com/inward/record.uri?eid=2-s2.0-85055506236&doi=10.1016%2fj.ijhydene.2018.10.042&partnerID=40&md5=46ac787508c1d2834d7539d4fbefa313.

[16] Ming, W., Sun, P., Zhang, Z., Qiu, W., Du, J., Li, X., Zhang, Y., Zhang, G., Liu, K., Wang, Y., and Guo, X. ”A systematic review of machine learning methods applied to fuel cells in performance evaluation, durability prediction, and application monitoring,” *International Journal of Hydrogen Energy* Vol. 48, No. 13, 2023, pp. 5197–5228. ISSN 03603199 (ISSN). doi: 10.1016/j.ijhydene.2022.10.261. URL https://www.scopus.com/inward/record.uri?eid=2-s2.0-85146723435&doi=10.1016%2fj.ijhydene.2022.10.261&partnerID=40&md5=f687d1d6ee8ebf5d70bf71f89cbf7b57.

[17] Xia, Z., Wang, Y., Ma, L., Zhu, Y., Li, Y., Tao, J., and Tian, G. ”A Hybrid Prognostic Method for Proton-Exchange-Membrane Fuel Cell with Decomposition Forecasting Framework Based on AEKF and LSTM,” *Sensors* Vol. 23, No. 1, 2023. ISSN 14248220 (ISSN). doi: 10.3390/s23010166. URL https://www.scopus.com/inward/record.uri?eid=2-s2.0-85145968628&doi=10.3390%2fs23010166&partnerID=40&md5=46cb623035fbf14844141f0d025a6972.

[18] Zhao, J. and Li, X. ”A review of polymer electrolyte membrane fuel cell durability for vehicular applications: Degradation modes and experimental techniques,” *Energy Conversion and Management* Vol. 199, 2019. ISSN 01968904 (ISSN). doi: 10.1016/j.enconman.2019.112022. URL https://www.scopus.com/inward/record.uri?eid=2-s2.0-85072017961&doi=10.1016%2fj.enconman.2019.112022&partnerID=40&md5=fb895bbc0823bcf15019be56e51af9dc.

[19] Gouriveau, R., Hilairet, M., Hissel, D., Jemei, S., Jouin, M., Lechartier, E., Morando, S., Pahon, E., Pera, M. C., and Zerhouni, N. ”IEEE PHM 2014 data challenge: Outline, experiments, scoring of results, winners,”. In *Proc. IEEE Conf. Prognostics Health Management*, pp. 1–6, 2014. URL https://search-data.ubfc.fr/fclab/FR-18008901306731-2021-07-19_IEEE-PHM-Data-Challenge-2014.html#gen.

[20] Hua, Z., Zheng, Z., Pahon, E., Pera, M.-C., and Gao, F. ”Lifespan Prediction for Proton Exchange Membrane Fuel Cells Based on Wavelet Transform and Echo State Network,” *IEEE Transactions on Transportation Electrification* Vol. 8, No. 1, 2022, pp. 420–431. ISSN 23327782 (ISSN). doi: 10.1109/TTE.2021.3121179. URL https://www.scopus.com/inward/record.uri?eid=2-s2.0-85118254862&doi=10.1109%2fTTE.2021.3121179&partnerID=40&md5=9dc32b667b1606562a073b8217487661.

[21] Hua, Z., Zheng, Z., Pahon, E., Pera, M.-C., and Gao, F. ”Multi-Timescale Lifespan Prediction for PEMFC Systems under Dynamic Operating Conditions,” *IEEE Transactions on Transportation*

Electrification Vol. 8, No. 1, 2022, pp. 345–355. ISSN 23327782 (ISSN). doi: 10.1109/TTE.2021.3103921. URL https://www.scopus.com/inward/record.uri?eid=2-s2.0-85127531957&doi=10.1109%2fTTE.2021.3103921&partnerID=40&md5=1ed04a914d0de7b8d104d1d4fdd798d0.

[22] Hua, Z., Zheng, Z., Pahon, E., Péra, M.-C., and Gao, F. "Remaining useful life prediction of PEMFC systems under dynamic operating conditions," *Energy Conversion and Management* Vol. 231, 2021. ISSN 01968904 (ISSN). doi: 10.1016/j.enconman.2021.113825.

[23] Li, S., Luan, W., Wang, C., Chen, Y., and Zhuang, Z. "Degradation prediction of proton exchange membrane fuel cell based on Bi-LSTM-GRU and ESN fusion prognostic framework," *International Journal of Hydrogen Energy* Vol. 47, No. 78, 9 2022, pp. 33466–33478. ISSN 0360-3199. doi: 10.1016/J.IJHYDENE.2022.07.230.

[24] Larminie, J. and Dicks, A. *Fuel cell systems explained: Second edition.* Wiley, 2013, pp. 1–406. ISBN 978-111887833-0 (ISBN); 047084857X (ISBN); 978-047084857-9 (ISBN). doi: 10.1002/9781118878330. URL https://www.scopus.com/inward/record.uri?eid=2-s2.0-84949778632&doi=10.1002%2f9781118878330&partnerID=40&md5=caafe063f3f6bbd449beb5dd2513cfc2.

[25] Zhao, J. "Catalyst Layers in Polymer Electrolyte Membrane Fuel Cells: Formation, Characterization and Performance," PhD thesis, 2019. URL http://hdl.handle.net/10012/14425.

[26] Shahgaldi, S., Zhao, J., Alaefour, I., and Li, X. "Investigation of catalytic vs reactant transport effect of catalyst layers on proton exchange membrane fuel cell performance," *Fuel* Vol. 208, 2017, pp. 321–328. ISSN 00162361 (ISSN). doi: 10.1016/j.fuel.2017.07.035. URL https://www.scopus.com/inward/record.uri?eid=2-s2.0-85024100901&doi=10.1016%2fj.fuel.2017.07.035&partnerID=40&md5=3a5670a11e4a998798697456f538e562.

[27] Shahgaldi, S., Alaefour, I., Zhao, J., and Li, X. "Impact of ionomer in the catalyst layers on proton exchange membrane fuel cell performance under different reactant flows and pressures," *Fuel* Vol. 227, 2018, pp. 35–41. ISSN 00162361 (ISSN). doi: 10.1016/j.fuel.2018.04.076. URL https://www.scopus.com/inward/record.uri?eid=2-s2.0-85045749542&doi=10.1016%2fj.fuel.2018.04.076&partnerID=40&md5=3223995fb2d8994ec98b365a3478ead5.

[28] Zhao, J., Shahgaldi, S., Alaefour, I., Xu, Q., and Li, X. "Gas permeability of catalyzed electrodes in polymer electrolyte membrane fuel cells," *Applied Energy* Vol. 209, 2018, pp. 203–210. ISSN 03062619 (ISSN). doi: 10.1016/j.apenergy.2017.10.087. URL https://www.scopus.com/inward/record.uri?eid=2-s2.0-85032669981&doi=10.1016%2fj.apenergy.2017.10.087&partnerID=40&md5=c32ad0d54a072a6d4a490af41a9ea292.

[29] Park, S. and Popov, B. N. "Effect of cathode GDL characteristics on mass transport in PEM fuel cells," *Fuel* Vol. 88, No. 11, 2009, pp. 2068–2073. ISSN 00162361 (ISSN). doi: 10.1016/j.fuel.2009.06.020. URL https://www.scopus.com/inward/record.uri?eid=2-s2.0-67651091581&doi=10.1016%2fj.fuel.2009.06.020&partnerID=40&md5=0b81491bf943dbd1ff41314f5fc806ff.

[30] Wu, J., Yuan, X. Z., Martin, J. J., Wang, H., Zhang, J., Shen, J., Wu, S., and Merida, W. "A review of PEM fuel cell durability: Degradation mechanisms and mitigation strategies," *Journal of Power Sources* Vol. 184, No. 1, 2008, pp. 104–119. ISSN 03787753 (ISSN). doi: 10.1016/j.jpowsour.2008.06.006. URL https://www.scopus.com/inward/record.uri?eid=2-s2.0-48149094359&doi=10.1016%2fj.jpowsour.2008.06.006&partnerID=40&md5=a590360375f0603136f163cebd1ab3d9.

[31] Hu, M., Gu, A., Wang, M., Zhu, X., and Yu, L. "Three dimensional, two phase flow mathematical model for PEM fuel cell: Part I. Model development," *Energy Conversion and Management* Vol. 45, No. 11-12, 2004, pp. 1861–1882. ISSN 01968904 (ISSN). doi: 10.1016/j.enconman.2003.09.022. URL https://www.scopus.com/inward/record.uri?eid=2-s2.0-1642293482&doi=10.1016%2fj.enconman.2003.09.022&partnerID=40&md5=00e408bb8d8a1ee151c7c9ece4d48ac6.

[32] Hu, M., Zhu, X., Wang, M., Gu, A., and Yu, L. "Three dimensional, two phase flow mathematical model for PEM fuel cell: Part II. Analysis and discussion of the internal transport mechanisms," *Energy Conversion and Management* Vol. 45, No. 11-12, 2004, pp. 1883–1916. ISSN 01968904 (ISSN). doi: 10.1016/j.enconman.2003.09.023. URL https://www.scopus.com/inward/record.

uri?eid=2-s2.0-1642381423&doi=10.1016%2fj.enconman.2003.09.023&partnerID=40&md5=2a46fdf4b7cb6c7d9e358625f362fdfe.

[33] Li, X. and Sabir, I. "Review of bipolar plates in PEM fuel cells: Flow-field designs," *International Journal of Hydrogen Energy* Vol. 30, No. 4, 2005, pp. 359–371. ISSN 03603199 (ISSN). doi: 10.1016/j.ijhydene.2004.09.019. URL https://www.scopus.com/inward/record.uri?eid=2-s2.0-13444283580&doi=10.1016%2fj.ijhydene.2004.09.019&partnerID=40&md5=db62173e820a10b378151a9816418b15.

[34] Shen, Y. "Mechanical Degradation of Membrane Electrode Assemblies in Proton Exchange Membrane Fuel Cells," PhD thesis, 2017. URL http://hdl.handle.net/10012/11990.

[35] Yuan, X.-Z., Song, C., Wang, H., and Zhang, J. *Electrochemical impedance spectroscopy in PEM fuel cells: Fundamentals and applications*. Springer London, 2010, pp. 1–420. ISBN 978-184882845-2 (ISBN). doi: 10.1007/978-1-84882-846-9. URL https://www.scopus.com/inward/record.uri?eid=2-s2.0-84895371417&doi=10.1007%2f978-1-84882-846-9&partnerID=40&md5=43917c75684092524e4722cbef016c7e.

[36] Gubler, L., Kuhn, H., Schmidt, T. J., Scherer, G. G., Brack, H.-P., and Simbeck, K. "Performance and durability of membrane electrode assemblies based on radiation-grafted FEP-g-polystyrene membranes," *Fuel Cells* Vol. 4, No. 3, 2004, pp. 196–207. ISSN 16156846 (ISSN). doi: 10.1002/fuce.200400019. URL https://www.scopus.com/inward/record.uri?eid=2-s2.0-4344605180&doi=10.1002%2ffuce.200400019&partnerID=40&md5=39323e00ab8169074f7b2b6f22eceb69.

[37] Gittleman, C. S., Coms, F. D., and Lai, Y. H. "Membrane Durability: Physical and Chemical Degradation," *Polymer Electrolyte Fuel Cell Degradation*, 1 2012, pp. 15–88. doi: 10.1016/B978-0-12-386936-4.10002-8.

[38] Lee, C., Wang, X., Peng, J.-K., Katzenberg, A., Ahluwalia, R. K., Kusoglu, A., Komini Babu, S., Spendelow, J. S., Mukundan, R., and Borup, R. L. "Toward a Comprehensive Understanding of Cation Effects in Proton Exchange Membrane Fuel Cells," *ACS Applied Materials and Interfaces* Vol. 14, No. 31, 2022, pp. 35555–35568. ISSN 19448244 (ISSN). doi: 10.1021/acsami.2c07085. URL https://www.scopus.com/inward/record.uri?eid=2-s2.0-85135768059&doi=10.1021%2facsami.2c07085&partnerID=40&md5=24f90181c3c0a216e498932979cd312a.

[39] Borup, R., Meyers, J., Pivovar, B., Kim, Y. S., Mukundan, R., Garland, N., Myers, D., Wilson, M., Garzon, F., Wood, D., Zelenay, P., More, K., Stroh, K., Zawodzinski, T., Boncella, J., McGrath, J. E., Inaba, M., Miyatake, K., Hori, M., Ota, K., Ogumi, Z., Miyata, S., Nishikata, A., Siroma, Z., Uchimoto, Y., Yasuda, K., Kimijima, K.-I., and Iwashita, N. "Scientific aspects of polymer electrolyte fuel cell durability and degradation," *Chemical Reviews* Vol. 107, No. 10, 2007, pp. 3904–3951. ISSN 00092665 (ISSN). doi: 10.1021/cr050182l. URL https://www.scopus.com/inward/record.uri?eid=2-s2.0-35748941340&doi=10.1021%2fcr050182l&partnerID=40&md5=4202e567c207a403b580d04823a60073.

[40] Weber, A. Z. "Gas-Crossover and Membrane-Pinhole Effects in Polymer-Electrolyte Fuel Cells," *Journal of The Electrochemical Society* Vol. 155, No. 6, 2008, page B521. ISSN 1945-7111. doi: 10.1149/1.2898130. URL https://dx.doi.org/10.1149/1.2898130.

[41] De Bruijn, F. A., Dam, V. A. T., and Janssen, G. J. M. "Review: Durability and degradation issues of PEM fuel cell components," *Fuel Cells* Vol. 8, No. 1, 2008, pp. 3–22. ISSN 16156854 (ISSN). doi: 10.1002/fuce.200700053. URL https://www.scopus.com/inward/record.uri?eid=2-s2.0-54149117709&doi=10.1002%2ffuce.200700053&partnerID=40&md5=aaa54992ba4a35749cb3a7648d3e88ea.

[42] Chandesris, M., Vincent, R., Guetaz, L., Roch, J. S., Thoby, D., and Quinaud, M. "Membrane degradation in PEM fuel cells: From experimental results to semi-empirical degradation laws," *International Journal of Hydrogen Energy* Vol. 42, No. 12, 3 2017, pp. 8139–8149. ISSN 0360-3199. doi: 10.1016/J.IJHYDENE.2017.02.116.

[43] Sharma, R. and Andersen, S. M. "Quantification on Degradation Mechanisms of Polymer Electrolyte Membrane Fuel Cell Catalyst Layers during an Accelerated Stress Test," *ACS Catalysis* Vol. 8, No. 4, 2018, pp. 3424–3434. ISSN 21555435 (ISSN). doi: 10.1021/acscatal.8b00002. URL https://www.scopus.com/inward/record.uri?eid=2-s2.0-85045094077&doi=10.1021%2facscatal.8b00002&partnerID=40&md5=ebb2eedcaea3841c4a685fca8517ffe0.

[44] Moein-Jahromi, M., Kermani, M. J., and Movahed, S. ”Degradation forecast for PEMFC cathode-catalysts under cyclic loads,” *Journal of Power Sources* Vol. 359, 8 2017, pp. 611–625. ISSN 0378-7753. doi: 10.1016/J.JPOWSOUR.2017.05.102.

[45] Bi, W. and Fuller, T. F. ”Modeling of PEM fuel cell Pt/C catalyst degradation,” *Journal of Power Sources* Vol. 178, No. 1, 3 2008, pp. 188–196. ISSN 0378-7753. doi: 10.1016/J.JPOWSOUR.2007.12.007.

[46] St-Pierre, J. and Jia, N. ”Successful Demonstration of Ballard PEMFCS for Space Shuttle Applications,” *Journal of New Materials for Electrochemical Systems* Vol. 5, No. 4, 2002, pp. 263–271. ISSN 14802422 (ISSN). URL `https://www.scopus.com/inward/record.uri?eid=2-s2.0-0346387329&partnerID=40&md5=e50490002f4fb4ae51e4ce9dd28b7aaf`.

[47] Schulze, M., Wagner, N., Kaz, T., and Friedrich, K. A. ”Combined electrochemical and surface analysis investigation of degradation processes in polymer electrolyte membrane fuel cells,” *Electrochimica Acta* Vol. 52, No. 6, 2007, pp. 2328–2336. ISSN 00134686 (ISSN). doi: 10.1016/j.electacta.2006.05.063. URL `https://www.scopus.com/inward/record.uri?eid=2-s2.0-33846054152&doi=10.1016%2fj.electacta.2006.05.063&partnerID=40&md5=793ee5e989c26b92c1a9b34c2a80d8d3`.

[48] Owejan, J. E., Yu, P. T., and Makharia, R. ”Mitigation of carbon corrosion in microporous layers in PEM fuel cells,”. In *ECS Transactions*, Vol. 11, pp. 1049–1057, 2007. ISBN 19386737 (ISSN); 978-156677582-3 (ISBN); 978-156677567-0 (ISBN). doi: 10.1149/1.2781018. URL `https://www.scopus.com/inward/record.uri?eid=2-s2.0-45249091467&doi=10.1149%2f1.2781018&partnerID=40&md5=8ada08afa8e88a2ee0a7f0b6e289a3fe`.

[49] Nguyen, H. L., Han, J., Nguyen, X. L., Yu, S., Goo, Y.-M., and Le, D. D. ”Review of the durability of polymer electrolyte membrane fuel cell in long-term operation: Main influencing parameters and testing protocols,” *Energie* Vol. 14, No. 13, 2021. ISSN 19961073 (ISSN). doi: 10.3390/en14134048. URL `https://www.scopus.com/inward/record.uri?eid=2-s2.0-85110276919&doi=10.3390%2fen14134048&partnerID=40&md5=c2a40cbc1ffb7e66cb71e6ae1f873594`.

[50] Hua, Z., Zheng, Z., Pahon, E., Pera, M.-C., and Gao, F. ”Health Indicators for PEMFC Systems Life Prediction under Both Static and Dynamic Operating Conditions,”. In *IECON Proceedings (Industrial Electronics Conference)*, Vol. 2020-October, pp. 3963–3968. IEEE Computer Society, 2020. ISBN 978-172815414-5 (ISBN). doi: 10.1109/IECON43393.2020.9254916.

[51] 2013-2016: ANR PROGELEC PROPICE: Prognostics et Health Management de systèmes Piles à Combustible de type PEMFC. URL `https://anr.fr/Project-ANR-12-PRGE-0001`.

[52] Sharaf, O. Z. and Orhan, M. F. ”An overview of fuel cell technology: Fundamentals and applications,” *Renewable and Sustainable Energy Reviews* Vol. 32, 4 2014, pp. 810–853. ISSN 1364-0321. doi: 10.1016/J.RSER.2014.01.012.

[53] Morgan, J. M. and Datta, R. ”Understanding the gas diffusion layer in proton exchange membrane fuel cells. I. How its structural characteristics affect diffusion and performance,” *Journal of Power Sources* Vol. 251, 4 2014, pp. 269–278. ISSN 0378-7753. doi: 10.1016/J.JPOWSOUR.2013.09.090.

[54] Mao, L., Jackson, L., and Jackson, T. ”Investigation of polymer electrolyte membrane fuel cell internal behaviour during long term operation and its use in prognostics,” *Journal of Power Sources* Vol. 362, 9 2017, pp. 39–49. ISSN 0378-7753. doi: 10.1016/J.JPOWSOUR.2017.07.018.

[55] Franco, A. ”Modelling and analysis of degradation phenomena in polymer electrolyte membrane fuel cells,” *Polymer Electrolyte Membrane and Direct Methanol Fuel Cell Technology*, 1 2012, pp. 291–367. doi: 10.1533/9780857095473.2.291.

[56] Yuan, X. Z., Zhang, S., Ban, S., Huang, C., Wang, H., Singara, V., Fowler, M., Schulze, M., Haug, A., Andreas Friedrich, K., and Hiesgen, R. ”Degradation of a PEM fuel cell stack with Nafion® membranes of different thicknesses. Part II: Ex situ diagnosis,” *Journal of Power Sources* Vol. 205, 5 2012, pp. 324–334. ISSN 0378-7753. doi: 10.1016/J.JPOWSOUR.2012.01.074.

[57] Pei, P., Chang, Q., and Tang, T. ”A quick evaluating method for automotive fuel cell lifetime,” *International Journal of Hydrogen Energy* Vol. 33, No. 14, 2008, pp. 3829–3836. ISSN 03603199 (ISSN). doi: 10.1016/j.ijhydene.2008.04.048. URL `https://www.scopus.com/inward/record.uri?eid=2-s2.0-48949115544&doi=10.1016%2fj.ijhydene.2008.04.048&partnerID=40&md5=327871f887574ac8779f0649902ba063`.

[58] Robin, C., Gérard, M., Quinaud, M., d'Arbigny, J., and Bultel, Y. ”Proton exchange membrane fuel cell model for aging predictions: Simulated equivalent active surface area loss and comparisons with durability tests,” *Journal of Power Sources* Vol. 326, 9 2016, pp. 417–427. ISSN 0378-7753. doi: 10.1016/J.JPOWSOUR.2016.07.018.

[59] Wang, X., Li, W., Chen, Z., Waje, M., and Yan, Y. ”Durability investigation of carbon nanotube as catalyst support for proton exchange membrane fuel cell,” *Journal of Power Sources* Vol. 158, No. 1, 7 2006, pp. 154–159. ISSN 0378-7753. doi: 10.1016/J.JPOWSOUR.2005.09.039.

[60] Yuan, X. Z., Zhang, S., Wang, H., Wu, J., Sun, J. C., Hiesgen, R., Friedrich, K. A., Schulze, M., and Haug, A. ”Degradation of a polymer exchange membrane fuel cell stack with Nafion® membranes of different thicknesses: Part I. In situ diagnosis,” *Journal of Power Sources* Vol. 195, No. 22, 11 2010, pp. 7594–7599. ISSN 0378-7753. doi: 10.1016/J.JPOWSOUR.2010.06.023.

[61] Wong, K. H. and Kjeang, E. ”Mitigation of chemical membrane degradation in fuel cells: Understanding the effect of cell voltage and iron ion redox cycle,” *ChemSusChem* Vol. 8, No. 6, 2015, pp. 1072–1082. ISSN 18645631 (ISSN). doi: 10.1002/cssc.201402957. URL `https://www.scopus.com/inward/record.uri?eid=2-s2.0-84924942469&doi=10.1002%2fcssc.201402957&partnerID=40&md5=fdf7b78f0bc5a0f628f4f378d96e31c6`.

[62] Xu, Y. ”A Review of Machine Learning With Echo State Networks,”. Technical report, 2020. URL `https://www.researchgate.net/profile/Yuanchao-Xu/publication/340167246_Machine_Learning_With_Echo_State_Networks/links/5f1744f0299bf1720d56fb32/Machine-Learning-With-Echo-State-Networks.pdf`.

[63] Sahajpal, K., Rana, K. P. S., and Kumar, V. ”Accurate long-term prognostics of proton exchange membrane fuel cells using recurrent and convolutional neural networks,” *International Journal of Hydrogen Energy* Vol. 48, No. 78, 2023, pp. 30532–30555. ISSN 03603199 (ISSN). doi: 10.1016/j.ijhydene.2023.04.143. URL `https://www.scopus.com/inward/record.uri?eid=2-s2.0-85158106768&doi=10.1016%2fj.ijhydene.2023.04.143&partnerID=40&md5=50fb5c3fd7af2f694aee8a0953afde0f`.

[64] Elsheikh, A., Yacout, S., and Ouali, M. S. ”Bidirectional handshaking LSTM for remaining useful life prediction,” *Neurocomputing* Vol. 323, 1 2019, pp. 148–156. ISSN 0925-2312. doi: 10.1016/J.NEUCOM.2018.09.076.

[65] Behera, S., Misra, R., and Sillitti, A. ”Multiscale deep bidirectional gated recurrent neural networks based prognostic method for complex non-linear degradation systems,” *Information Sciences* Vol. 554, 4 2021, pp. 120–144. ISSN 0020-0255. doi: 10.1016/J.INS.2020.12.032.

[66] Schiller, U. D. and Steil, J. J. ”Analyzing the weight dynamics of recurrent learning algorithms,” *Neurocomputing* Vol. 63, No. SPEC. ISS., 2005, pp. 5–23. ISSN 09252312 (ISSN). doi: 10.1016/j.neucom.2004.04.006. URL `https://www.scopus.com/inward/record.uri?eid=2-s2.0-12144261601&doi=10.1016%2fj.neucom.2004.04.006&partnerID=40&md5=e4b01268f6bf37362f2a5f666694d9d3`.

[67] Jaeger, H. ”The “echo state” approach to analysing and training recurrent neural networks-with an erratum note,” *Bonn, Germany: German National Research Center for Information Technology GMD Technical Report* Vol. 148, No. 34, 2001, page 13.

[68] Jaeger, H., Lukoševičius, M., Popovici, D., and Siewert, U. ”Optimization and applications of echo state networks with leaky- integrator neurons,” *Neural Networks* Vol. 20, No. 3, 4 2007, pp. 335–352. ISSN 0893-6080. doi: 10.1016/J.NEUNET.2007.04.016.

[69] Lukoševičius, M. ”A practical guide to applying echo state networks,” *Lecture Notes in Computer Science (including subseries Lecture Notes in Artificial Intelligence and Lecture Notes in Bioinformatics)* Vol. 7700 LECTURE NO, 2012, pp. 659–686. ISSN 03029743 (ISSN); 978-364235288-1

(ISBN). doi: 10.1007/978-3-642-35289-8{_}36. URL https://www.scopus.com/inward/record.uri?eid=2-s2.0-84872502995&doi=10.1007%2f978-3-642-35289-8_36&partnerID=40&md5=b6f6f3dc73bb8b31af7adca4d96b81b7.

[70] Morando, S., Jemei, S., Hissel, D., Gouriveau, R., and Zerhouni, N. "ANOVA method applied to proton exchange membrane fuel cell ageing forecasting using an echo state network," *Mathematics and Computers in Simulation* Vol. 131, 2017, pp. 283–294. ISSN 03784754 (ISSN). doi: 10.1016/j.matcom.2015.06.009. URL https://www.scopus.com/inward/record.uri?eid=2-s2.0-84940054512&doi=10.1016%2fj.matcom.2015.06.009&partnerID=40&md5=28be257e92f01b2229fa78baed100380.

[71] Ben Taieb, S., Sorjamaa, A., and Bontempi, G. "Multiple-output modeling for multi-step-ahead time series forecasting," *Neurocomputing* Vol. 73, No. 10-12, 6 2010, pp. 1950–1957. ISSN 0925-2312. doi: 10.1016/J.NEUCOM.2009.11.030.

[72] Gouriveau, R. and Zerhouni, N. "Connexionist-systems-based long term prediction approaches for prognostics," *IEEE Transactions on Reliability* Vol. 61, No. 4, 2012, pp. 909–920. ISSN 00189529 (ISSN). doi: 10.1109/TR.2012.2220700. URL https://www.scopus.com/inward/record.uri?eid=2-s2.0-84870563115&doi=10.1109%2fTR.2012.2220700&partnerID=40&md5=c02eb5b533d4f86a7e43c4018d7115ea.

[73] Sorjamaa, A. and Lendasse, A. "Time Series Prediction using DirRec Strategy,". In *ESANN 2006 Proceedings - European Symposium on Artificial Neural Networks*, pp. 143–148. d-side publication, 2006. ISBN 2930307064 (ISBN); 978-293030706-0 (ISBN). URL https://www.scopus.com/inward/record.uri?eid=2-s2.0-85028212829&partnerID=40&md5=5d7e8379828f4b122123ffc3d63c7d6e.

[74] Rodriguez, H., Medrano, M., Rosales, L. M., Penunuri, G. P., and Flores, J. J. "Multi-step forecasting strategies for wind speed time series,". In *2020 IEEE International Autumn Meeting on Power, Electronics and Computing, ROPEC 2020*. Institute of Electrical and Electronics Engineers Inc., 2020. ISBN 978-172819953-5 (ISBN). doi: 10.1109/ROPEC50909.2020.9258743. URL https://www.scopus.com/inward/record.uri?eid=2-s2.0-85097992034&doi=10.1109%2fROPEC50909.2020.9258743&partnerID=40&md5=988fc1c0f19d8bbfb0a080266d24d852.

[75] Benaggoune, K., Yue, M., Jemei, S., and Zerhouni, N. "A data-driven method for multi-step-ahead prediction and long-term prognostics of proton exchange membrane fuel cell," *Applied Energy* Vol. 313, 5 2022. ISSN 03062619. doi: 10.1016/j.apenergy.2022.118835.

[76] Collier, A., Wang, H., Zi Yuan, X., Zhang, J., and Wilkinson, D. P. "Degradation of polymer electrolyte membranes," *International Journal of Hydrogen Energy* Vol. 31, No. 13, 10 2006, pp. 1838–1854. ISSN 0360-3199. doi: 10.1016/J.IJHYDENE.2006.05.006.

[77] A. B. LaConti, M. Hamdan, and R. C. McDonald. Mechanisms of membrane degradation. Handbook of Fuel Cells: Fundamentals, Technology, and Applications, Vol. 3. Wiley, Chichester, 2003, Chaps. 49, pp. 647–662.

[78] Hinaje, M., Raël, S., Noiying, P., Nguyen, D. A., and Davat, B. "An equivalent electrical circuit model of proton exchange membrane fuel cells based on mathematical modelling," *Energies* Vol. 5, No. 8, 2012, pp. 2724–2744. ISSN 19961073 (ISSN). doi: 10.3390/en5082724. URL https://www.scopus.com/inward/record.uri?eid=2-s2.0-84865783705&doi=10.3390%2fen5082724&partnerID=40&md5=85a260bcbde11a0ac4f6082810815840.

[79] Gu, X., Hou, Z., and Cai, J. "Data-based flooding fault diagnosis of proton exchange membrane fuel cell systems using LSTM networks," *Energy and AI* Vol. 4, 2021. ISSN 26665468 (ISSN). doi: 10.1016/j.egyai.2021.100056. URL https://www.scopus.com/inward/record.uri?eid=2-s2.0-85107662426&doi=10.1016%2fj.egyai.2021.100056&partnerID=40&md5=2b92b9e20420182a8c878e9226905548.

[80] Hua, Z. "Lifespan Prediction of Proton Exchange Membrane Fuel Cell System," PhD thesis, Université Bourgogne Franche-Comté, 12 2021. URL https://theses.hal.science/tel-03793342.